Fall 1995

Investigation into fracture behavior and longevity of pneumatically fractured fine-grained formations

Heathe Ann Hall
New Jersey Institute of Technology

Copyright Warning & Restrictions

The copyright law of the United States (Title 17, United States Code) governs the making of photocopies or other reproductions of copyrighted material.

Under certain conditions specified in the law, libraries and archives are authorized to furnish a photocopy or other reproduction. One of these specified conditions is that the photocopy or reproduction is not to be "used for any purpose other than private study, scholarship, or research." If a, user makes a request for, or later uses, a photocopy or reproduction for purposes in excess of "fair use" that user may be liable for copyright infringement,

This institution reserves the right to refuse to accept a copying order if, in its judgment, fulfillment of the order would involve violation of copyright law.

Please Note: The author retains the copyright while the New Jersey Institute of Technology reserves the right to distribute this thesis or dissertation

Printing note: If you do not wish to print this page, then select "Pages from: first page # to: last page #" on the print dialog screen

INFORMATION TO USERS

This manuscript has been reproduced from the microfilm master. UMI films the text directly from the original or copy submitted. Thus, some thesis and dissertation copies are in typewriter face, while others may be from any type of computer printer.

The quality of this reproduction is dependent upon the quality of the copy submitted. Broken or indistinct print, colored or poor quality illustrations and photographs, print bleedthrough, substandard margins, and improper alignment can adversely affect reproduction.

In the unlikely event that the author did not send UMI a complete manuscript and there are missing pages, these will be noted. Also, if unauthorized copyright material had to be removed, a note will indicate the deletion.

Oversize materials (e.g., maps, drawings, charts) are reproduced by sectioning the original, beginning at the upper left-hand corner and continuing from left to right in equal sections with small overlaps. Each original is also photographed in one exposure and is included in reduced form at the back of the book.

Photographs included in the original manuscript have been reproduced xerographically in this copy. Higher quality 6" x 9" black and white photographic prints are available for any photographs or illustrations appearing in this copy for an additional charge. Contact UMI directly to order.

UMI

A Bell & Howell Information Company
300 North Zeeb Road, Ann Arbor MI 48106-1346 USA
313/761-4700 800/521-0600

ABSTRACT

INVESTIGATION INTO FRACTURE BEHAVIOR AND LONGEVITY OF PNEUMATICALLY FRACTURED FINE-GRAINED FORMATIONS

This study investigates volume changes in fine-grained soil formations and their effect on pneumatically induced fractures. Pneumatic fracturing is an enhancement technology for *in situ* remediation of hazardous waste sites, which increases the formation permeability by creating fractures. A number of formation properties and environmental conditions which affect fracture aperture were identified in this study.

Laboratory experiments were performed with control devices to investigate idealized fracture flow under linear and radial flow geometries. These tests exhibited cubic law behavior, and gas compressibility was seen as a measurable effect. A horizontal infiltrometer device was successfully developed to induce and control volume changes in natural soils with an artificial discrete fracture by moisture addition and removal. Tests performed with Woodbury clay showed that changes in fracture aperture were reversible, and that porous media flow was instrumental in aperture behavior.

A new concept of a "secondary active zone" is introduced which describes the zone of increased activity along the fracture boundary soils. A classification model is presented for assessing volume change potential of fine-grained formations based on their physical, chemical, and mineralogical properties. The model also recommends treatment alternatives for pneumatically fractured sites including hydraulic control, chemical stabilization, and fracture propping.

INVESTIGATION INTO FRACTURE BEHAVIOR AND LONGEVITY OF PNEUMATICALLY FRACTURED FINE-GRAINED FORMATIONS

by
Heather Ann Hall

A Thesis
Submitted to the Faculty of
New Jersey Institute of Technology
in Partial Fulfillment of the Requirements for the Degree of
Master of Science in Environmental Science

Department of Chemical Engineering, Chemistry, and Environmental Science

October 1995

APPROVAL PAGE

INVESTIGATION INTO FRACTURE BEHAVIOR AND LONGEVITY OF PNEUMATICALLY FRACTURED FINE-GRAINED FORMATIONS

Heather Ann Hall

Dr. John R. Schuring, Thesis Advisor — Date
Professor of Civil and Environmental Engineering, NJIT

Dr. Richard Trattner, Committee Member — Date
Associate Chairman and Professor of Environmental Science, NJIT

Dr. Paul C. Chan, Committee Member — Date
Professor of Civil and Environmental Engineering, NJIT

BIOGRAPHICAL SKETCH

Author: Heather Ann Hall

Degree: Master of Science in Environmental Science

Date: October 1995

Undergraduate and Graduate Education:

- Master of Science in Environmental Science
  New Jersey Institute of Technology
  Newark, New Jersey, 1995

- Bachelor of Arts in Geology-Biology
  Colby College
  Waterville, Maine, 1990

Major: Environmental Science

Publications:

Hall, H.A. and R.E. Nelson. 1990. Paleoenvironmental Analysis of Subfossil Coleoptera (Beetles) from Sandy River Terrace Sediments in Starks, Maine. *Maine Geologist*, 16(2): 5.

This thesis is dedicated
to my parents, Janet and Martin Hall,
for their love, support and encouragement

ACKNOWLEDGMENT

I wish to express my sincere gratitude and appreciation to my advisor, Dr. John Schuring for his inspiration, encouragement, and guidance throughout this research. His efforts in fostering my technical, management, leadership, and communication skills have been invaluable.

I thank Dr. Richard Trattner and Dr. Paul Chan for serving as members of the committee, and for their careful review and suggestions.

I also acknowledge friends and pneumatic fracturing colleagues Tom Boland, Sean McGonigal, Suresh Puppala, Joe DiBernardo, Laurence Thoraval, Brian Sielski, Hugo Fernandez, and Verdane Simeon. Thanks also to Conan Fitzgerald from Accutech Remedial Systems.

To Jack Gidney, John Eimuss, and John Grisgavage for their assistance and resources in fabrication of parts for the experimental portion of this research, I am indebted. I also thank Clint Brockway for his help in all aspects of this research.

In addition, I express my appreciation to the Center for Environmental Engineering and Science, the Department of Chemical Engineering, Chemistry, and Environmental Science, and the Department of Civil and Environmental Engineering at New Jersey Institute of Technology which made this research possible.

Finally, I wish to acknowledge my family and close friends who provided unconditional love and support throughout the pursuit of this degree.

TABLE OF CONTENTS

TABLE OF CONTENTS
(Continued)

Chapter **Page**

TABLE OF CONTENTS
(Continued)

TABLE OF CONTENTS
(Continued)

TABLE OF CONTENTS
(Continued)

Chapter **Page**

LIST OF TABLES

LIST OF FIGURES

LIST OF FIGURES
(Continued)

LIST OF FIGURES
(Continued)

LIST OF SYMBOLS

A	=	area (L^2)
b_a	=	actual aperture given by thickness of sheet metal spacers (L)
b_c	=	calculated effective aperture (L)
b_i	=	aperture of a fracture segment (L)
g	=	acceleration due to gravity (L/θ^2)
i	=	hydraulic gradient (L/L)
K	=	hydraulic conductivity (L/θ)
l_i	=	length of a fracture segment (L)
L_1, L_2	=	linear distance from extraction point, $L_2>L_1$ (L)
n	=	aperture exponent, b^n (dimensionless)
P_1, P_2	=	absolute air pressures at distance from extraction point, $P_2>P_1$ (L)
P_{abs}	=	absolute pressure (L)
P_{atm}	=	atmospheric pressure (L)
P_g	=	gauge pressure (L)
P_o	=	absolute gauge operating pressure (L)
P_s	=	absolute standard pressure (L)
Q_o	=	flow at operating conditions (L^3/θ)
Q_s	=	flow at standard conditions (70°F and 1 atm) (L^3/θ)
Re	=	Reynolds number (dimensionless)

LIST OF SYMBOLS
(Continued)

R_1, R_2	=	radial distance from extraction point, $R_2 > R_1$ (L)
T_s	=	standard temperature (T)
T_o	=	operating temperature (T)
μ	=	dynamic viscosity of fluid ($F\text{-}\theta/L^2$ or $M/L\text{-}\theta$)
V	=	flow velocity (L/θ)
ν	=	kinematic viscosity of fluid (L^2/θ)
w	=	fracture width (L)
ϕ	=	potential function (L)
γ_a	=	specific weight of air (F/L^3)
γ_w	=	specific weight of water (F/L^3)

CHAPTER 1

INTRODUCTION

1.1 Background

As a result of expansion of the petroleum and chemical industries since the late nineteenth century, significant amounts of hazardous waste have been generated. Releases of these chemicals to the environment have occurred as a result of shortsighted disposal practices. Recognizing needs for proper management, treatment and disposal of waste and for remediation of contaminated sites, the legislature enacted the Resource Conservation and Recovery Act (RCRA) and the Comprehensive Environmental Response, Compensation, and Liability Act (CERCLA) in 1976 and 1980, respectively.

As of March 1995, the number of hazardous waste sites being investigated by the U.S. Environmental Protection Agency (EPA) under CERCLA alone rose to 14,156, as listed on the Comprehensive Environmental Response, Compensation, and Liability Act Information System. Over 1,290 of these have been placed on CERCLA's National Priorities List as sites that pose the greatest risks to human health and the environment.

Dealing with the growing number of sites requiring cleanup is becoming a financial burden to industry and the public. Elevated costs result from strict regulatory requirements and a lack of remediation technologies appropriate for dealing with the complexity of these sites. As a result, extended time periods are required to attain cleanup levels if they can be met at all.

In 1986, CERCLA was amended by the Superfund Amendments and Reauthorization Act (SARA). SARA addressed these shortcomings by encouraging the development of innovative treatment technologies. In addition, as part of the 1995 reauthorization of CERCLA, legislation is being reviewed to further increase federal spending on development of innovative technologies, and to remove current barriers in their testing and verification (Rubin and Powers, 1994).

The influx of spending on innovative technologies is being funneled to those which deal with contamination on site and in place, termed "in situ" technologies, because of their inherent cost effectiveness. Although in situ technologies are becoming a preferred method of treatment, site conditions often hinder their effectiveness. In particular, geologic formations of low permeability, including fine-grained soils and rock, are problematic because fluid flow rates are insufficient for the application of most primary remediation technologies.

To overcome this difficulty, a process called pneumatic fracturing was developed at the Hazardous Substance Management Research Center (HSMRC) at New Jersey Institute of Technology (NJIT). The process increases formation permeability by injection of air at high pressures and flows which creates fractures in the soil and rock matrices. The increase in permeability enhances the rate of cleanup when coupled with other technologies such as vapor extraction, bioremediation, and thermal treatment.

Pneumatic fracturing is similar in concept to hydraulic fracturing (hydrofracing) which has been used in the petroleum and water well industries for decades. The principal difference is that pneumatic fracturing utilizes air or other gas as the fracturing fluid, while hydraulic fracturing injects water or other liquid agents for fracture

propagation. In addition, pneumatic fracturing generally relies on self-propping of the fractures created by injection, while hydraulic fracturing typically uses a granular agent (e.g., sand) to prop the fractures.

One advantage of pneumatic fracturing over hydraulic fracturing is that it does not introduce liquids into the formation which leads to detrimental migration of contaminants, especially when operating in the vadose zone. Pneumatic fracturing is also desirable because it relies on open self-propped fractures which can transmit significantly more fluid than sand-filled fractures. This is due to the relationship between flow and width of the fracture opening, or aperture, described by the cubic law, where flow rate through a planar fracture is proportional to the cube of the aperture for a given gradient in head.

Although open fractures offer an advantage to propped fractures in the remediation of contaminated sites, there is increased risk that volume changes of the formation will occur over time leading to changes in the fracture aperture. Even a slight reduction in aperture will significantly affect flow and contaminant removal rates. In contrast, a slight increase in aperture will lead to significant enhancement. Of particular importance is the possibility of fracture closure or "healing" with time.

Predicting the potential for changes in fracture aperture and controlling these changes are essential to the commercial success of the technology. In addressing these issues, it is important to recognize that low permeability is generally a result of the presence of high proportions of fine-grained particles, particularly clays, which are susceptible to shrinking and swelling as a result of changes in ambient conditions.

1.2 Objectives and Scope

Although pneumatic fracturing is a relatively young technology, questions related to fracture viability and longevity are becoming increasingly important as the technology matures. The problem is complex since pneumatic fracturing is being applied to sites with a wide variety of conditions. In addition, long term data are somewhat limited, and no prior investigations of fracture longevity are available in the literature.

The goal of this study is therefore to gain an understanding of the influence of volume change on fracture behavior and longevity in low permeability formations. The specific objectives of this research are as follows:

(1) Perform a comprehensive literature review of formation properties and environmental conditions which affect volume change.

(2) Design and fabricate new laboratory devices including:

a) Control devices to investigate idealized fracture flow using smooth parallel plates of linear and radial flow geometries.

b) Horizontal infiltrometer devices to permit investigation of volume change phenomena in natural soil. Calibration tests will be conducted on a natural clay soil using moisture as the major variable.

(3) Develop a classification model of volume change mechanisms to assess fracture behavior and viability at pneumatically fractured sites. Included will be recommended treatment alternatives for controlling fracture aperture and optimizing longevity.

(4) Develop recommendations for future studies based on the results of this research.

CHAPTER 2

BACKGROUND

2.1 Review of Pneumatic Fracturing Technology

2.1.1 Technology History

The pneumatic fracturing process was developed and patented by the Hazardous Substance Management Research Center (HSMRC) at New Jersey Institute of Technology (NJIT). The process was designed to improve the effectiveness of in situ technologies in moderate and low permeability formations, and to deliver liquid or granular supplements into geologic formations to enhance the rate and efficiency of cleanup. Research on pneumatic fracturing began in Spring 1988, and since that time has involved laboratory studies, field studies, theoretical modeling, and computer modeling.

2.1.1.1 Laboratory Studies. Initial laboratory studies investigated the potential for fracturing fine-grained soils using compressed air. Bench scale tests were conducted by Papanicolaou (1989) and Shah (1991) using plastic tanks filled with fine-grained soil which had been mixed with a surrogate contaminant of known concentration. Soil vapor extraction (SVE) was then simulated on the fractured soils and the results were compared to SVE tests performed on unfractured soils. Removal efficiencies for the fractured condition were consistently 170% to 360% higher than the unfractured condition.

As the pneumatic fracturing system developed, laboratory studies were expanded to address fluid flow characteristics and mass transport rates through a discrete fracture with known dimensions. Ng (1991) conducted tests to model the removal of a contaminant from pre-fracture and post-fracture soils in the vadose zone. These laboratory studies proved that improved mass flow rate in fractured soil was attributable to enhanced subsurface air flow.

Bench scale studies have also focused on the integration of pneumatic fracturing with other innovative in situ remediation technologies. Studies have been performed on bioremediation (Fitzgerald, 1993); fracturing with injection of nutrient pellets to support bioremediation (Rahman, 1994); use of surfactants to enhance desorption of contaminants (Rahman, 1994); fracturing and injection of graphite/glass frit starter path material to enhance in situ vitrification of a coarse-grained formation (NJIT and ARS, 1994; McGonigal, 1995); integration with air sparging to enhance removal of volatile organic compounds (Ososkov, in progress); and integration of pneumatic fracturing with ultrasound to enhance contaminant desorption (Fernandez, in progress).

2.1.1.2 Field Studies. In 1989, the technology began its transition from laboratory bench scale to full field scale, where the technology was successfully demonstrated at a number of "clean" and contaminated sites (Schuring et al., 1991; Schuring and Chan, 1992). The initial field demonstrations yielded critical data for evaluating theoretical aspects of pneumatic fracturing, and have provided feedback for improvements in design of the technology.

In August 1992, the technology was evaluated by the U.S. Environmental Protection Agency (EPA) under the Superfund Innovative Technology Evaluation (SITE) program. The demonstration took place at an industrial site contaminated with volatile organics in the vadose zone. As a result of the application of pneumatic fracturing, air flow and contaminant removal rates increased by more than 600% (EPA, 1993).

In Spring 1993, HSMRC licensed the technology to Accutech Remedial Systems (ARS) of Keyport, New Jersey in its first commercial venture. Since commercialization, a number of both public and private sector sites in the United States and Canada have been successfully fractured. Field applications have included integration of pneumatic fracturing with numerous remediation technologies. A summary of the sites pneumatically fractured to date is provided as Table 2.1. As seen from the table, the majority were performed in vadose zone clay and silts with vapor extraction of volatiles.

2.1.1.3 Theoretical Modeling. Theoretical modeling has paralleled field studies since their inception. King (1993) developed an understanding of the mechanics of pneumatic fracturing in soil and rock formations and presented a model to predict fracture initiation and maintenance pressures. An investigation and development of a model to describe flow of compressible fluids in discrete fractures was undertaken by Nautiyal (1994), and model analysis of contaminant transport using a dual porosity approach was performed by Ding (1995). An inquiry into fracture propagation and transport of liquid and granular supplements in the discrete fracture is currently underway (Puppala, in progress). This work will expand on initial work performed by McGonigal (1995), who modeled the transport of granular media in a fractured coarse-grained formation.

Table 2.1 Summary of Sites Pneumatically Fractured to Date

Location	Date	Textural Description (USCS Classification)	Fracturing Depth (ft)	Hydrogeologic Zone	Contaminant Type	Coupled Technology
Frelinghuysen, NJ	1990-93	sandy silt and clay (CL, ML)	5-10	vadose	clean	SVE (30" H_2O vacuum)
Richmond, VA	1990	silty clay, clayey silt (CH, MH)	7-11	vadose	chlorinated solvent	SVE (27" H_2O vacuum)
Newark, NJ	1991	sandstone	9-17	vadose	clean	SVE (20" H_2O vacuum)
Roseland, NJ	1991	clayey sand, silty sand (SC, SM)	4-7	vadose/saturated	chlorinated solvent	SVE (30" H_2O vacuum)
Hillsborough, NJ	1992-93	siltstone	9-16	vadose/ perched	chlorinated solvent	SVE (136" H_2O vacuum) w/hot gas injection*
Newark, NJ	1992	fine-grained soil	4-7	vadose	petroleum VOCs	SVE
East Brunswick, NJ	1992	siltstone	unknown	vadose/saturated	clean	water reinjection*
Marcus Hook, PA	1992-93	clayey silt, silty clay (CL, ML)	3-8	vadose/ perched	petroleum VOCs	SVE (20" H_2O vacuum) w/bioremediation
East Orange, NJ	1993	sand/sandy silt (SM, ML)	5-13	vadose	VOCs	SVE (30" H_2O vacuum)*
Santa Clara, CA	1993	silty/sandy clay (CH)	4-15	vadose	chlorinated solvent	SVE (136" H_2O vacuum)*
Oklahoma City, OK	1993	silty clay (CL)	6-9	vadose/perched/ saturated	petroleum VOCs and chlorinated solvent	SVE (140" H_2O vacuum) w/free product recovery*
Huntsville, AL	1994	coarse-grained soil	25-37	saturated	VOCs	pump and treat*
Shreveport, LA	1994	fine-grained soil	7-22	vadose/saturated	chlorinated solvent	SVE*
Toronto, Canada	1994	clayey silt	4-12	vadose	petroleum VOCs	SVE*
Highland Park, NJ	1994	siltstone and limestone	9-24	vadose	petroleum VOCs and chlorinated solvent	SVE*
Piketon, OH	1994	silty clay	8-23	vadose/saturated	clean	groundwater pumping*
Richland, WA	1995	sandy gravel (GP)	14	vadose	clean (pilot for radioactive wastes)	in situ vitrification
Flemington, NJ	1995	siltstone	in progress	vadose/saturated	chlorinated solvent	bioremediation*

*Involved Pneumatic Fracturing Extraction (PFE) by Accutech Remedial Systems, Keyport, NJ
SVE soil vapor extraction; VOCs volatile organic compounds

2.1.1.4 Computer Modeling. Data and models from laboratory studies, field studies, and theoretical modeling is now being assimilated into a comprehensive computer model (Sielski, in progress). This user-friendly, interactive model programmed in Microsoft Visual Basic will be used to screen potential sites, predict enhancements to formation permeability and mass removal rates, and establish preliminary design considerations for fracturing. Elements of site screening and correlation, fracture propagation, fracture flow and transport, and supplemental media injection will be incorporated.

2.1.2 Process Description

Pneumatic fracturing utilizes air as an injection media to create fracture networks which increase the permeability of the formation. Because pressures exceed the natural in situ stresses of the formation and flow rates exceed the natural permeability of the formation, the formation fractures in response to the injected air. The resultant fracture network converts the primary fluid flow mechanism from diffusion to convection, thus allowing for increased fluid flow rates through the formation. Figure 2.1 is a schematic of the pneumatic fracturing concept in fine-grained soils.

Pneumatic fracturing is performed by injection of high pressure air or other gas through the patented "HQ injector" which is lowered into the borehole. Two packers are inflated to seal off a two foot interval of the borehole. A source of high pressure air is connected to the injector through a system of hoses and an injection manifold, and pressures and flow rates are controlled by a set of precision switches, valves, and regulators.

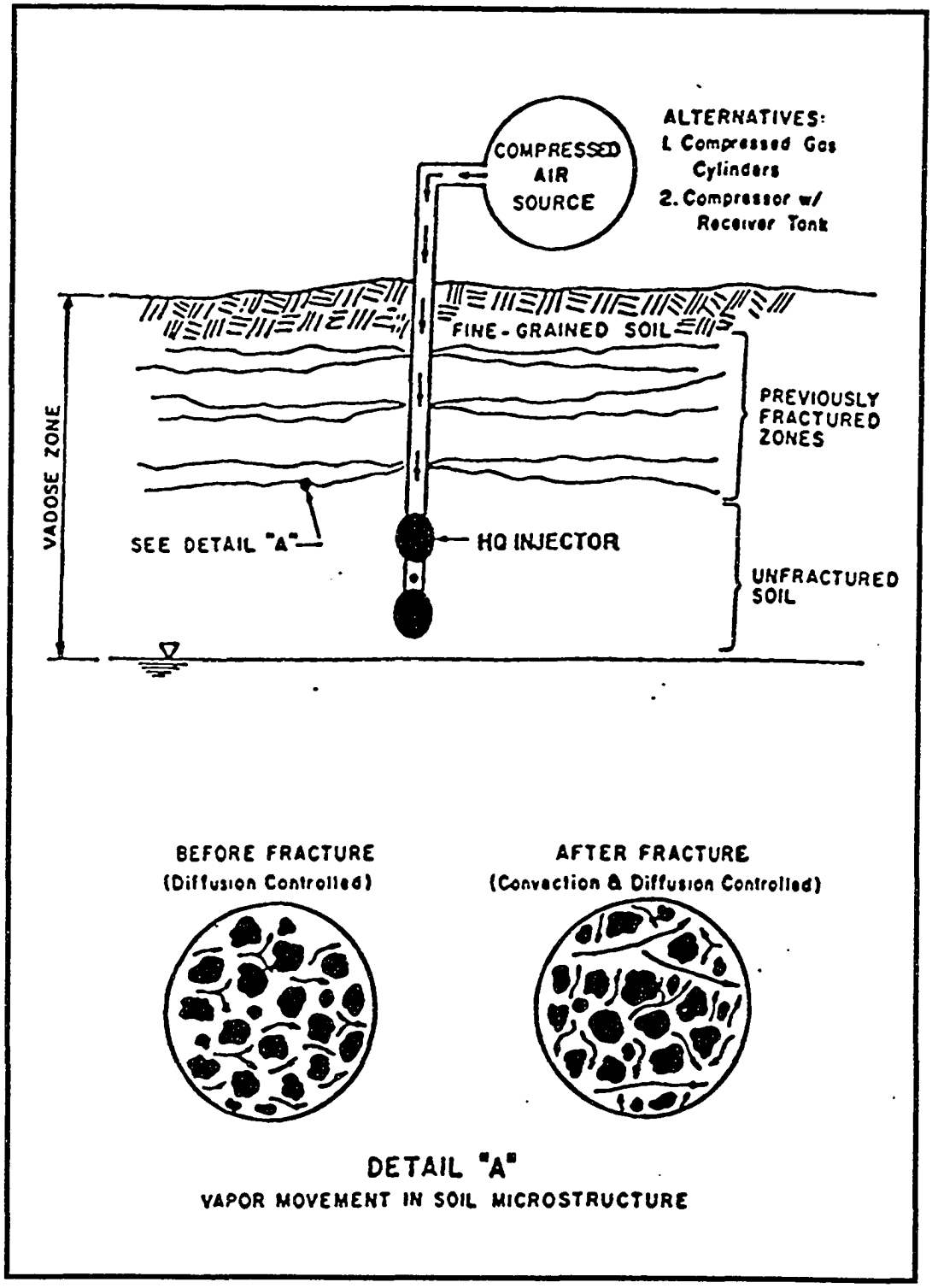

Figure 2.1 Concept of Pneumatic Fracturing in Fine-Grained Formations. From Schuring and Chan (1992).

In general, fractures can be satisfactorily propagated in fine-grained formations with pressures of 300 to 500 lb/in^2 (PSI) and flow rates of 1,000 to 2,000 ft^3/min (CFM). Pneumatically induced fractures continue to propagate until the fluid loss rate equals the injection flow rate, which typically result in radii of 10 to 25 ft in fine-grained formations. An average injection duration is 30 seconds or less, but can be maintained in a dilated state for longer periods to permit the injection of supplemental media.

Following injection, the packers are deflated and the injector is moved vertically within the borehole to perform subsequent fracture injections. Once a fracture network has been created throughout the contaminated area, other primary remediation technologies are applied. Integration of these primary technologies with pneumatic fracturing results in increased treatment rates and removal efficiencies.

A variety of field monitoring equipment are used to evaluate the effectiveness of the pneumatic fracturing process. During fracture injections, a pressure transducer in placed in the borehole near the HQ injector and is used for determination of fracture initiation pressures. In addition, pressure gauges are positioned at outlying monitoring wells to monitor fracture connectivity within the formation. Heave of the ground resulting from the injection is monitored using electronic biaxial tiltmeters.

Following injection, post-fracture pneumatic conductivities are determined by inducing flow through the formation and measuring the flow rate with a manifold of variable area flow meters. These results are then compared to pre-fracture results to determine permeability enhancements. Finally, a borehole video camera allows for direct visual observations of the formation.

2.2 Factors Affecting Formation Volume Changes

Inherent in the prediction of fracture longevity is an understanding of the mechanisms of volume change. Shrinking and swelling, which accompany formations containing clay, are believed to have a significant effect on fracture apertures with time. This section will begin with a background discussion of the expansive nature of clay soils (2.2.1) and the effect of clay mineralogy and structure on volume change (2.2.2). This will be followed by a description of secondary formation properties which establish the propensity of a clay soil to volume change (2.2.3). Finally, there is discussion of environmental conditions, which when varied, may lead to volume changes (2.2.4). The primary and secondary factors considered in this section are summarized in Figure 2.2.

2.2.1 Expansive Behavior of Clay Soils

The universal property of all expansive soils is the presence of clay. Clay will significantly influence properties by coating and preventing direct interparticle contact of the granular constituents, even when present in small quantities. For water contents usually encountered in practice, 15 to 40 percent, clay will dominate soil behavior even if it constitutes as little as one-third of the soil solids (Mitchell, 1993). It should be noted that volume change is not limited to soil formations, but may also be substantial in argillaceous rock formations such as shale, especially under highly weathered conditions.

Expansive formations, defined as those with a propensity for volume change, comprise approximately 20%-30% of the formations in the United States (Krohn and Slosson, 1980), as shown in Figure 2.3. The expansive nature of different regions can be attributed to the following: highly overconsolidated clays and weathered shales in North

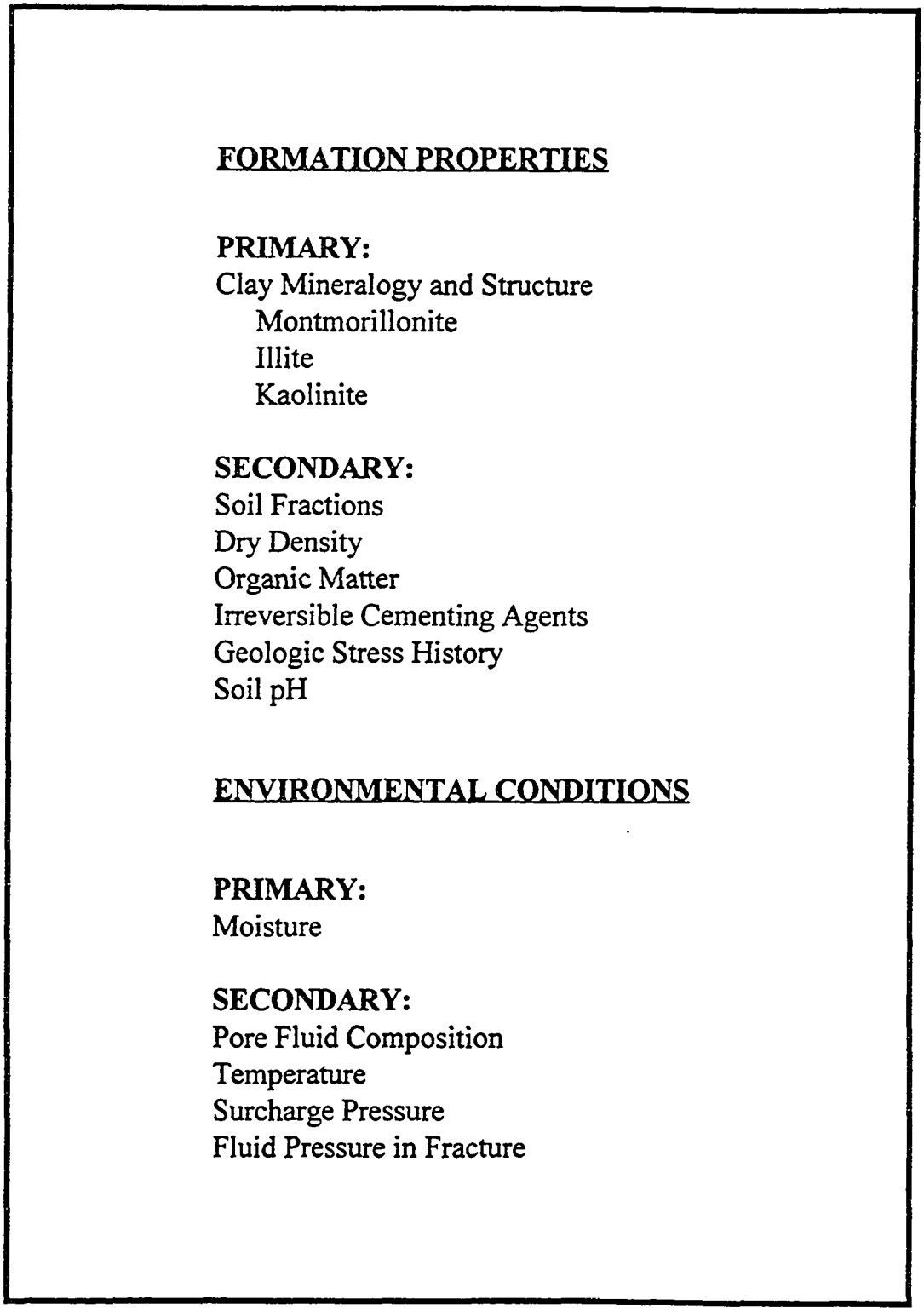

Figure 2.2 Factors Affecting Volume Changes in Fine-Grained Formations.

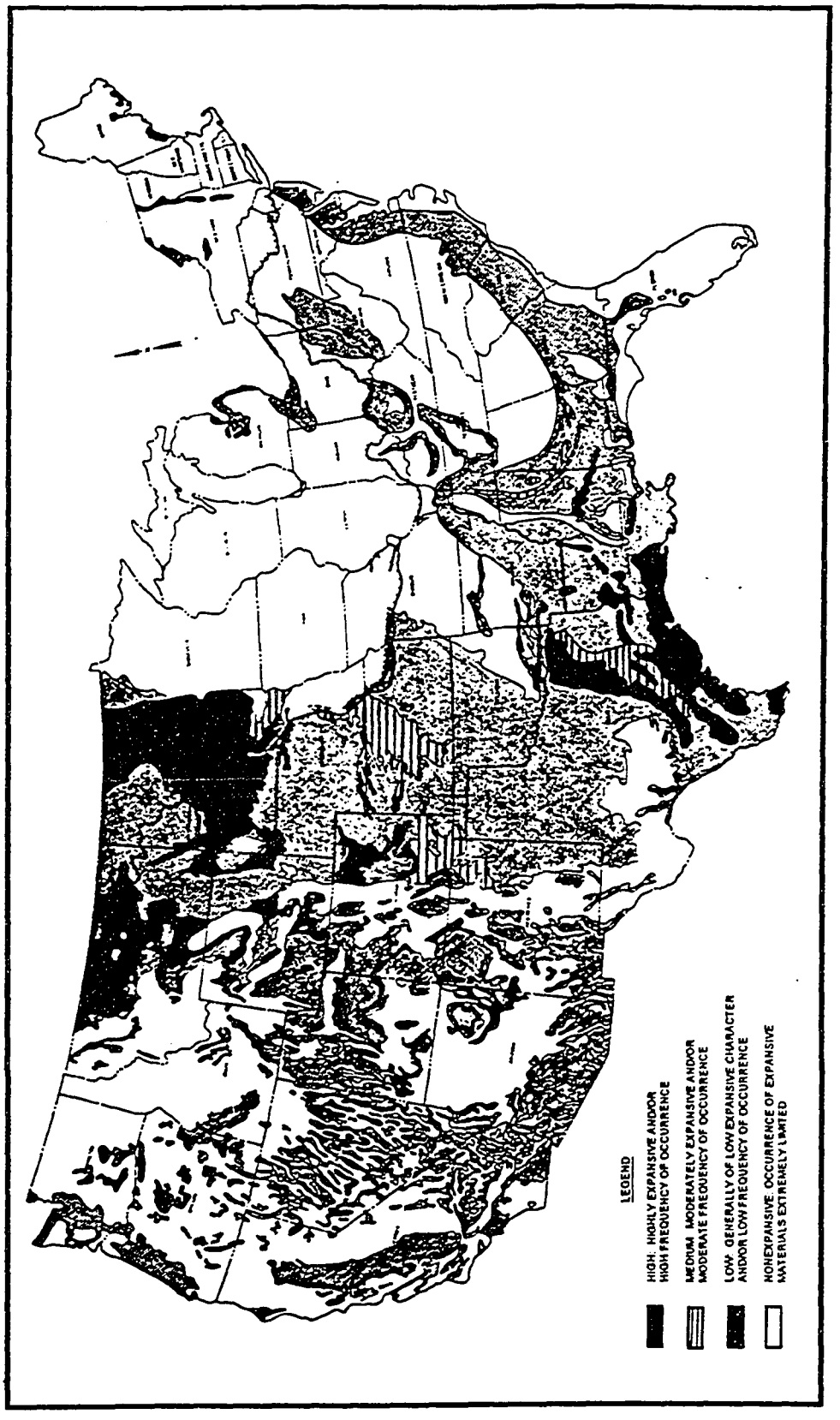

Figure 2.3 U.S. Occurrence and Distribution of Potentially Expansive Materials. From Nelson and Miller (1992).

Dakota, South Dakota, Montana, Wyoming, and Colorado; overconsolidated, desiccated soils in central and western Texas and western Oklahoma; seasonal fluctuations in moisture content in eastern Oklahoma, Texas, Florida, Gulf States and Great Lakes; Cretaceous shales in Minnesota; and desiccated alluvial, colluvial, and volcanic soils in California (Nelson and Miller, 1992).

2.2.2 Clay Mineralogy and Structure

The clay mineralogy of a formation is the primary factor influencing volume change because it dictates the nature of interaction between the soils and their surroundings. This section describes the basic properties of clay minerals, followed by a discussion of each of the three most common clay minerals. References for this section include Grim (1962), Mitchell (1993), Newman (1987), and Gillott (1987).

Clay minerals are composed of layers of tetrahedra and octahedra with various arrangements and types of interlayer bonding. Spaces in those tetrahedra and octahedra are typically occupied by cations other than those of the ideal structure. This substitution, termed isomorphous substitution, gives clay particles a net negative charge, as cations of lower valence replace those of higher valence. To preserve electrical neutrality, cations, termed exchangeable cations, are then attracted to the mineral and undergo hydration by surrounding water molecules.

The negatively charged surface and distribution of positive ions in solution adjacent to the clay mineral surface are together termed the diffuse double layer (Bohn et al., 1985). Swelling is caused by double diffuse layers which overlap between particles resulting in the generation of interparticle repulsive forces, or swelling pressures.

Increases in the thickness of the double diffuse layer are dependent on the clay mineral structure, amount and type of isomorphous substitution, and amount and type of exchangeable cations. In general a thicker double diffuse layer is associated with lower cation concentrations and/or the presence of cations with lower valence (Mitchell, 1993). Thus, for soils with similar clay mineralogy, more swelling would occur in the soils with exchangeable sodium (Na^{+}) cations than in soils with exchangeable calcium (Ca^{+2}) or magnesium (Mg^{+2}) cations.

Two indices of surface reactivity are generally indicative of changes in the double diffuse layer. The first is specific surface, the surface area of the mineral, and the second is cation exchange capacity (CEC), the ability of an adsorbed ion to be replaced with one existing in the pore water. Clay mineralogy, organic composition, and particle size distribution are responsible for variations in levels of surface reactivity. Generally, the greater the specific surface and CEC, the greater the potential for volume change.

The most common clay minerals are the hydrous aluminum silicates which include kaolinites, illites, and montmorillonites. The structures of each mineral group are illustrated in Figure 2.4, and a summary of the characteristics and conditions for formation of each mineral is presented in Table 2.2.

Montmorillonites are characterized by their extensive isomorphous substitution and weak interlayer bonding. As a result, cations can penetrate both between unit cell layers and on surface particles. Energy from hydration of these cations overcomes the attractive forces of layer interaction resulting in complete layer separation. The characteristic expanding lattice of montmorillonite can result in 2,000% volumetric

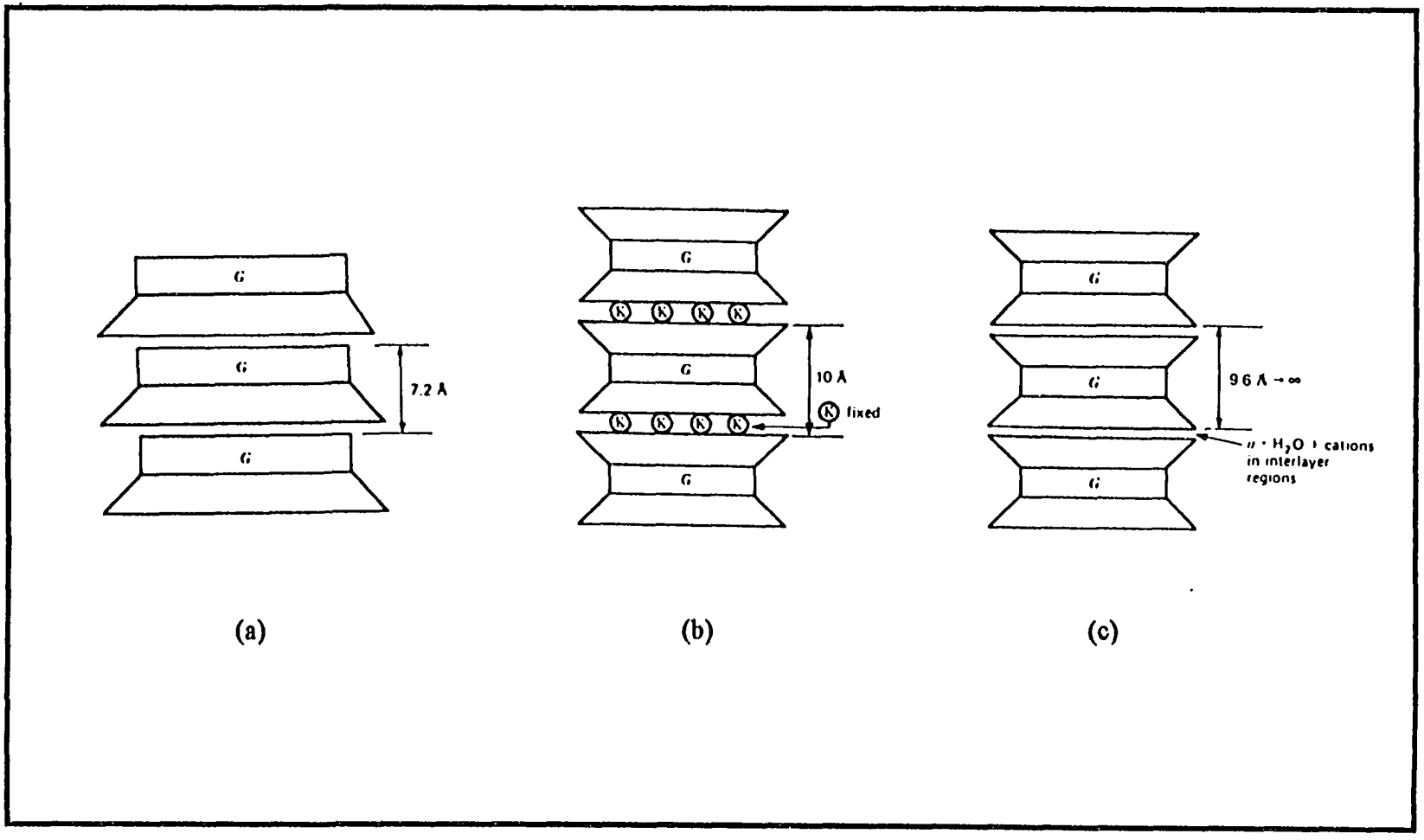

Figure 2.4 Schematic Diagrams of Structures of Most Common Hydrous Aluminum Silicates. (a) Kaolinite. (b) Illite. (c) Montmorillonite. From Mitchell (1993).

Table 2.2 Clay Mineral Characteristics and Conditions for Formation

Clay Mineral	Structural Properties		Surface Reactivity		Formation Conditions	
	Isomorphous Substitution	Interlayer Bonding	CEC (meq/100g)	Specific Surface (m^2/g)	Parent Material	Climate
Mont-morillonite	extensive	van der Waals bonds (very weak) expandable lattice	80-150	50-120 (primary) 700-840 (secondary)	Rocks high in alkaline earth (Ca^{+2}, Mg^{+2}), basic and intermediate igneous, volcanic ash, and derivatives containing ferromagnesium minerals and calcic plagioclase	Where evaporation exceeds precipitation, and where there is poor leaching, such as arid and semi-arid areas
Illite	extensive	K bonds (strong) fixed lattice	10-40	65-100	The presence of potassium is essential, igneous or metamorphic rocks and their derivatives; alteration of muscovite to illite is also a significant source	Similar to montmorillonite formation
Kaolinite	little	hydrogen bonding (strong) fixed lattice	3-15	10-20	Forms from feldspars and micas by acid leaching of acidic (SiO_2-rich) granitic rocks	Where precipitation is high and there is good drainage to ensure leaching of cations (calcium and iron)

Modified from Mitchell (1993)

swelling (Tourtelot, 1973), and can generate swelling pressures up to 30,000 lb/in^2 (PSI) (Dawson, 1953). These properties make montmorillonite the most expansive of all the clay minerals. Figure 2.5 shows the distribution of montmorillonite in near-outcrop bedrock formations in the United States.

Of the three minerals, illites are second to montmorillonite in potential for volume change. Illites also undergo extensive isomorphous substitution, but do not possess an expanding lattice like that of montmorillonite. This is because charge deficiencies are balanced by potassium, which are so strongly held by interlayer bonding that the spacing between layers remains fixed. Illites exhibit volume change because of their common interstratification with other minerals, the most common of which is illite-montmorillonite which can result in 15-100% volumetric swelling (Tourtelot, 1973). Swelling may also occur by adsorption of water and cations between illite sheets.

Kaolinites are the least expansive of the three minerals. Little isomorphous substitution occurs, and the strong hydrogen bonds between layers limit any expansion between unit cell layers. Cation exchange in kaolinite is dominated by broken bonds or unsatisfied valencies on the surfaces of the mineral. Kaolintes are typically considered to be nonexpansive because water and cations are limited to adsorption between sheets.

Aside from mineralogy, the development of preferred orientations is also important in determining the propensity of a soil to volume change. Clay structure, also known as soil fabric, is defined by two basic arrangements, flocculent and dispersed. A flocculent microstructure, typical of marine deposits, is characterized by random orientations and a dispersed microstructure, typical of fresh-water deposits, is characterized by parallel orientations (Lambe, 1953). Schematics of these two soil

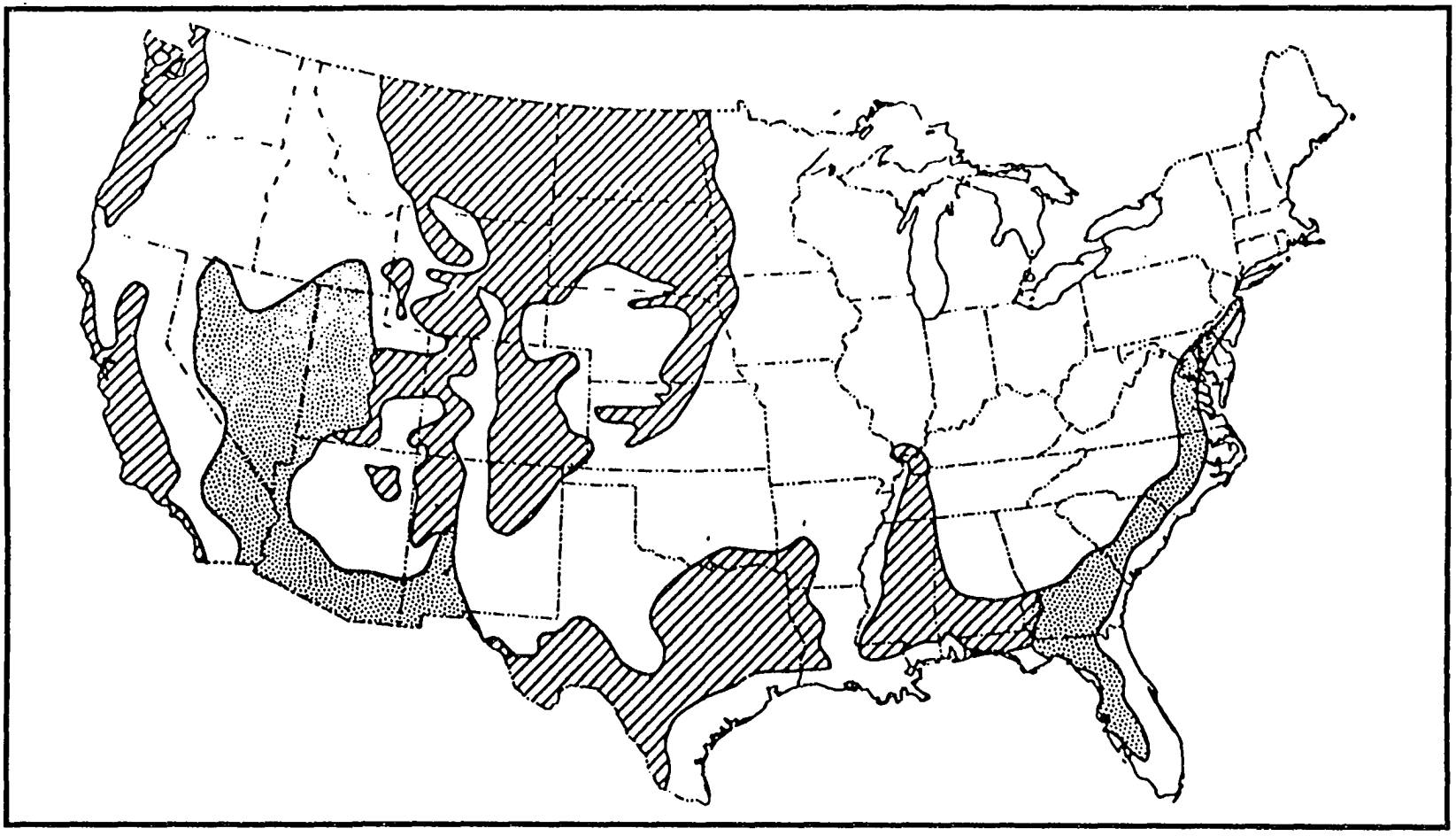

Figure 2.5 U.S. Distribution of Montmorillonite in Near-Outcrop Bedrock Formations. Diagonal pattern: regionally abundant in continuous geologic formations. Dotted pattern: locally abundant in variable or discontinuous geologic formations. No pattern: minor constituent in bedrock formations but may be locally abundant in surficial deposits and soils. From Kinney (1966).

fabrics are provided as Figure 2.6. Soils with flocculent fabrics are more likely to be expansive than those with dispersed fabrics because of easier relative particle movements, and the increased capillary stresses resulting from the smaller average pore sizes (Mitchell, 1993).

2.2.3 Other Formation Properties Affecting Volume Change

This section outlines other characteristics of a formation which can be used as indicators of volume change potential. In general, these are considered as secondary characteristics and are not expected to be as significant as clay mineralogy and structure. These properties include (1) soil fractions; (2) density; (3) organic content; (4) irreversible cementing agents; (5) geologic stress history; and (6) pH.

2.2.3.1 Soil Fractions. Swelling of soils is highly dependent on the proportion of clay minerals to nonclay minerals and the resultant grain size distribution of the formation. The nonclay minerals may be composed of bulky shaped inorganic or organic particles, such as sand and gravel or allophane. In general, there is an inverse linear relationship between swell and the fraction of inert material; as amount of inert material increases there is a decrease in swell. Komornik and Livneh (1969) determined that the reduction in swell that occurs with an increase in inert material was due to a decrease in the dry density when the soils were compacted with the same level of effort. The effect of secondary mechanical interactions between the inert particles, as a result of soil compression due to volume changes, becomes more significant the coarser the gradation, the more angular the particles, and the more uniform the soils (Mitchell, 1993).

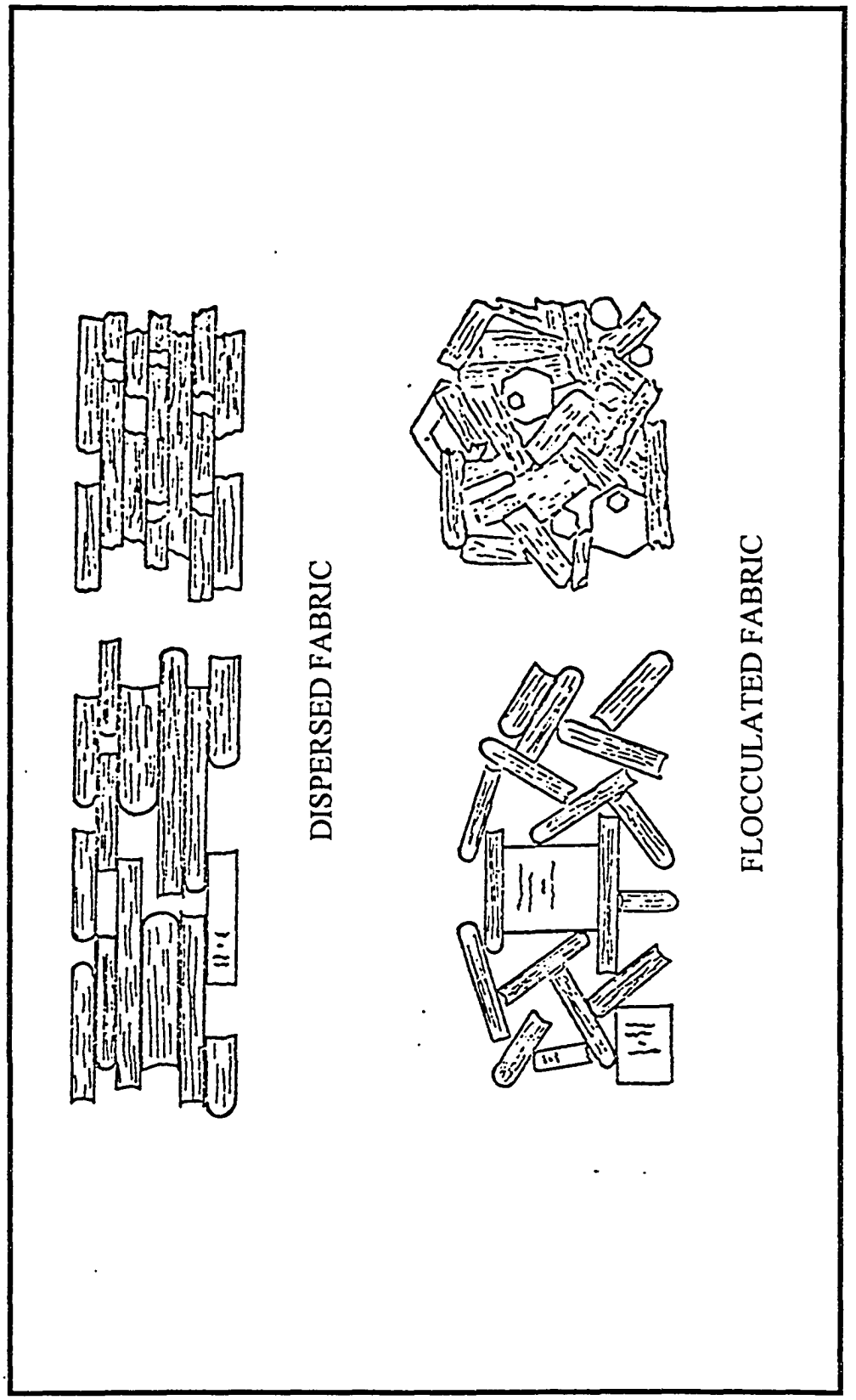

Figure 2.6 Flocculated and Dispersed Soil Fabrics. From Compton (1970).

2.2.3.2 Dry Density. Soils of higher dry density will swell more than those of lower dry density. As individual clay particles swell by absorbing water, expansion occurs into the voids of the looser soil before increasing the volume of the soil mass. In the denser soil, there are fewer voids and the soil mass has to swell to accommodate the volume change in the particles (Donaldson, 1969). In addition, at higher densities, there is a higher degree of particle interaction which results in higher repulsive potential between particles. The effect of density on volume changes of clay soils is illustrated in Figure 2.7.

2.2.3.3 Organic Matter. The presence and type of organic matter, namely the percent nonhumic and humic fractions, also affect the susceptibility of a formation to volume change. The presence of organic matter has been shown to produce high cation exchange capacities, high plasticity, and high shrinkage (Grim, 1962). The effects of organic carbon on plasticity were determined by Odell et al. (1960) in comparison with the influence of percent clay and the percent montmorillonite. Data showed that increasing the organic content by only 1-2% may increase liquid and plastic limits by as much as an equivalent increase of 10-20% particles finer than 2μm or in the percent montmorillonite.

In inorganic soils, 65-70% of the organic matter consists of the humic fraction, although both fractions are important in establishing the degree to which changes may occur. The nonhumic fraction includes those with still recognizable physical and chemical characteristics. In soils with a high nonhumic fraction, high shrinkage is expected, although it is unclear if appreciable swelling is anticipated (Mitchell, 1993).

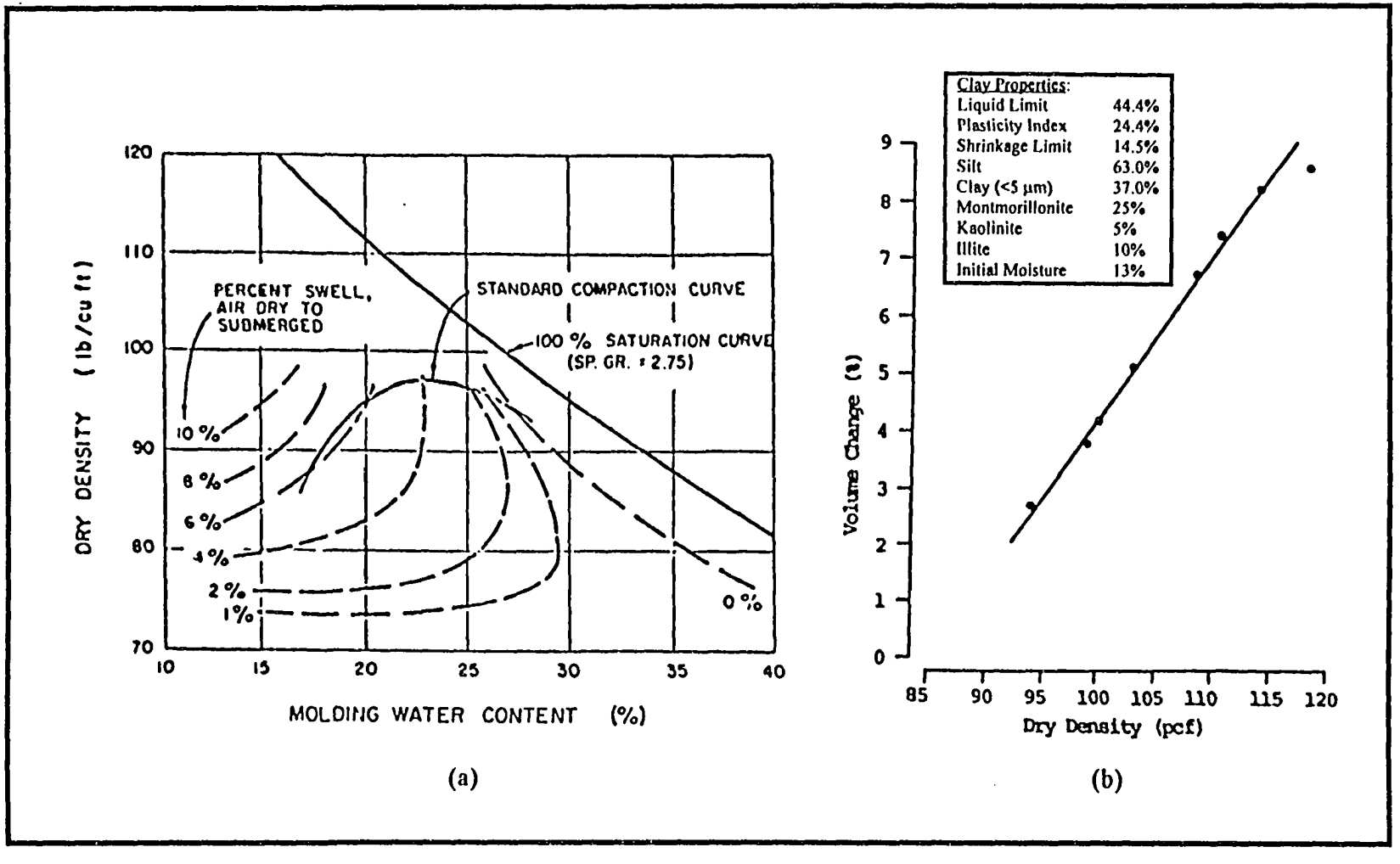

Figure 2.7 Effect of Varying Density on Volume Change of Clay Soil. (a) From Holtz and Gibbs (1956). (b) From Chen (1973).

The humic fraction is characterized by a highly complex chemical nature and strong interactions with clay minerals. High humic fractions will affect double layer thickness although the effect is dependent on the nature of the chemical interactions between these molecules and the clay minerals. In addition, the humic fraction may form complexes with metals and organics that increase the concentrations of these constituents in pore water to levels that exceed their calculated solubilities (Page et al., 1986).

2.2.3.4 Irreversible Cementing Agents. Irreversible cementing agents are those which cannot regain their original properties, and affect volume change by both mechanical and physico-chemical interactions with clay minerals. Carbonates and oxides commonly coat clay mineral aggregates and physically restrict swelling by binding particles together.

Hydroxy interlayering, which occurs from the physico-chemical interaction of irreversible cementing agents with clay minerals, serves to bind expandable clay mineral unit layers to reduce swelling (Mitchell, 1973a). Interlayering of hydroxy-Al is common in montmorillonite and illite and is favored by pH<6.0, low concentrations of organic matter and frequently varying water content. Hydroxy-Fe evidently plays the same role as hydroxy-Al only at a lower pH, and hydroxyl-Mg is the principal interlayering component in alkaline soils (Coleman and Thomas, 1964; Sposito, 1989). The degree of interlayering in soils is usually small (10-20%), but is enough to fix the unit layers inhibiting layer expansion. More uniform interlayering and stronger bonds between the hydroxide and the silicate surface occur with Al-OH interlayering than interlayering with Fe-OH or Mg-OH. CEC and specific surface are greatly reduced by interlayer formation.

2.2.3.5 Geologic Stress History. The geologic stress history of a formation is also of particular significance to volume change. As changes occur in interparticle forces in fine-grained soils, deformation is dependent on both past and present states of stress. Under equal void ratios, overconsolidated formations are more expansive than normally consolidated formations when effective stress is lessened (Mitchell, 1993). Overconsolidated formations are those which have been loaded to a maximum pressure and then unloaded to a lower confining pressure, while normally consolidated formations are those which have been subjected only to an increase in pressure.

2.2.3.6 Soil pH. pH is one of the most indicative measurements of the chemical properties of the soil. Soil pH can indicate something about the base saturation, the relative bonding of ions to exchange sites, and the activity of microorganisms. Soils of different pH values will react differently to changes in ambient environmental conditions. Three major pH groups were identified by Thomas (1967): a pH <4 generally indicates the presence of free acids from the oxidation of sulfides; a pH <5.5 suggests the likely occurrence of exchangeable aluminum; and a pH from 7.8 to 8.2 indicates the presence of calcium carbonate.

The most important effect of pH is on the ionization of aluminum and the presence of hydroxy interlayering. At low pH, hydroxy aluminum holds a positive charge and moves from within the clay mineral structure into exchange positions binding clay mineral unit layers and reducing swell. As the pH rises, an increase in swell potential occurs because the hydroxy aluminum precipitates as bulk $Al(OH)_3$.

2.2.4 Environmental Conditions Affecting Volume Change

Environmental conditions are defined as those parameters which are subject to change over the time frame of site remediation. Changes in soil behavior due to varying environmental conditions will occur only within the range prescribed by the formation properties. The most important environmental influence, moisture, is first described followed by a discussion of the effects of changes which may occur by variations in pore fluid composition, temperature, surcharge pressure, and fluid pressure in the fracture.

2.2.4.1 Moisture. Variation in moisture content is the primary environmental factor affecting volume change, specifically with respect to the initial water content and the pattern of moisture changes with time. Since swelling results from surface hydration, cation hydration, and osmotic pressure effects, the lower the initial water content, the higher the swell. At low water contents the double layer is depressed, the osmotic pressure (or soil suction) is high, and a greater amount of water will be imbibed, when available, causing corresponding volume changes. Figure 2.8 shows the effect of moisture content and saturation on volume changes of a clay soil under constant density.

The pattern of soil moisture changes is determined primarily by the relationship between evaporation and precipitation. Where there is a marked separation between a wet season and a hot, dry season, there is also marked seasonal variation in soil moisture content, and shallow water tables show considerable seasonal fluctuations (Donaldson, 1969). In areas where the seasonal changes are less drastic, such as desert areas where evaporation consistently exceeds precipitation, water tables are very deep or nonexistent

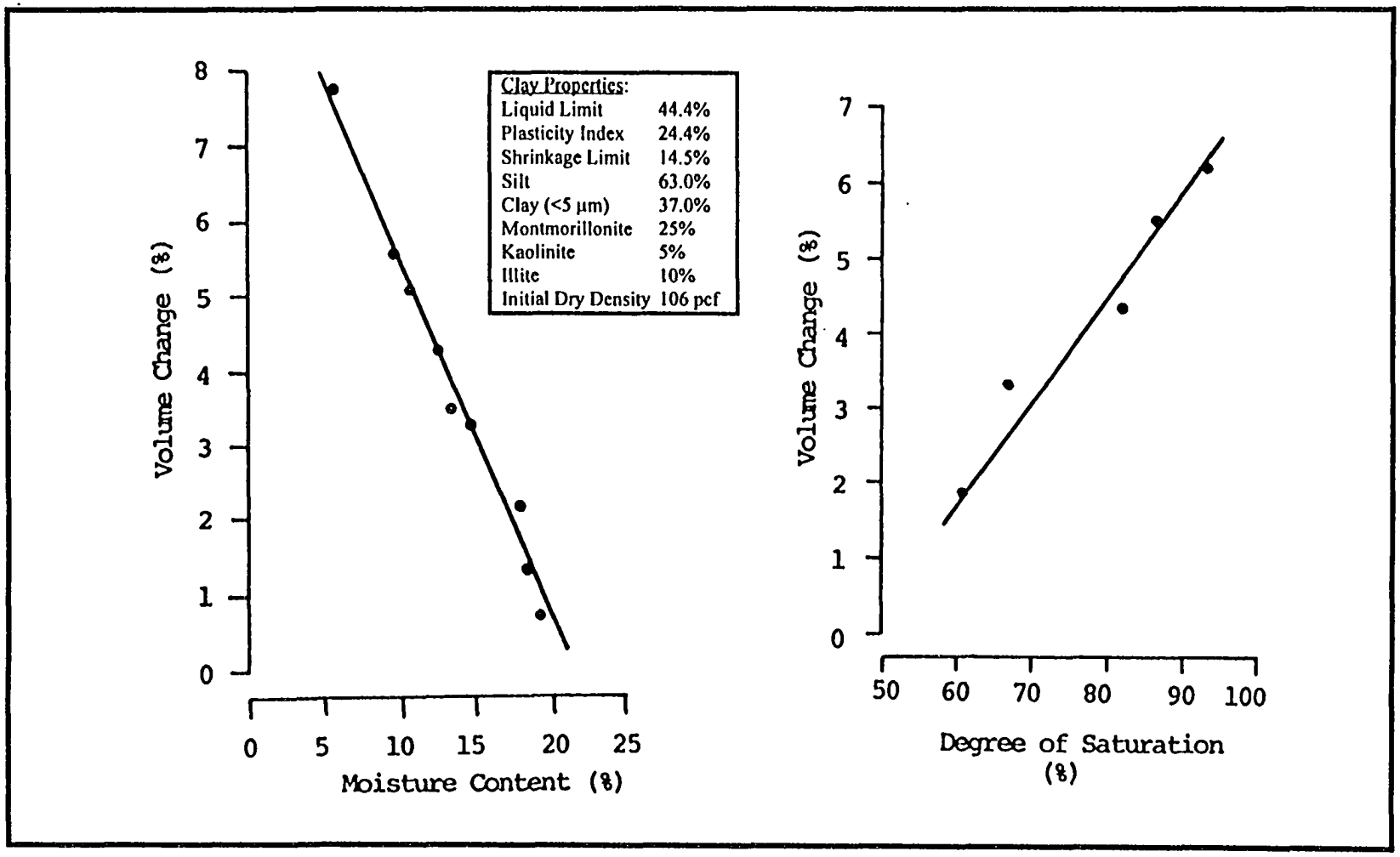

Figure 2.8 Effect of Varying Moisture Content and Degree of Saturation on Volume Change of Clay Soil. From Chen (1973).

and the moisture content of the soil remains virtually constant. Similarly, when the soils are kept wet throughout the year, little or no volume change may occur.

The rating factor which considers both precipitation and evaporation has been established for various climatic regions in the United States as shown in Figure 2.9. Each contour line relates to a frequency distribution for precipitation. The lower numbered contours reflect areas where climate changes are likely to be severe (i.e., periods of rainfall mixed with periods of drought) and the higher numbered contours correspond to generally wetter and less severe areas (Krohn and Slosson, 1980). These ratings may be utilized to determine potential expansiveness of geographic areas to which pneumatic fracturing may be applied.

It is noted that soil moisture may also be artificially altered. For example, ground covers, irrigation, leaking underground pipes and tanks, and remediation activities all can affect soil moisture content. These factors are discussed in greater detail in Chapter 6.

2.2.4.2 Pore Fluid Composition. Changes in pore fluid composition may occur from migration of chemical contamination in the groundwater or pore water by infiltrating surface water. The effects on volume change may be pronounced for changes in soluble salt concentration, type and amount of exchangeable ions, and contamination by organic compounds. Generally, any change in pore solution chemistry that depresses or expands the thickness of double layer leads to shrinkage or swelling, respectively. Mitchell (1973a) and Morgenstern and Balasubramonian (1980) verified that pore fluid changes cause swell in montmorillonite clay and clay-shale, respectively.

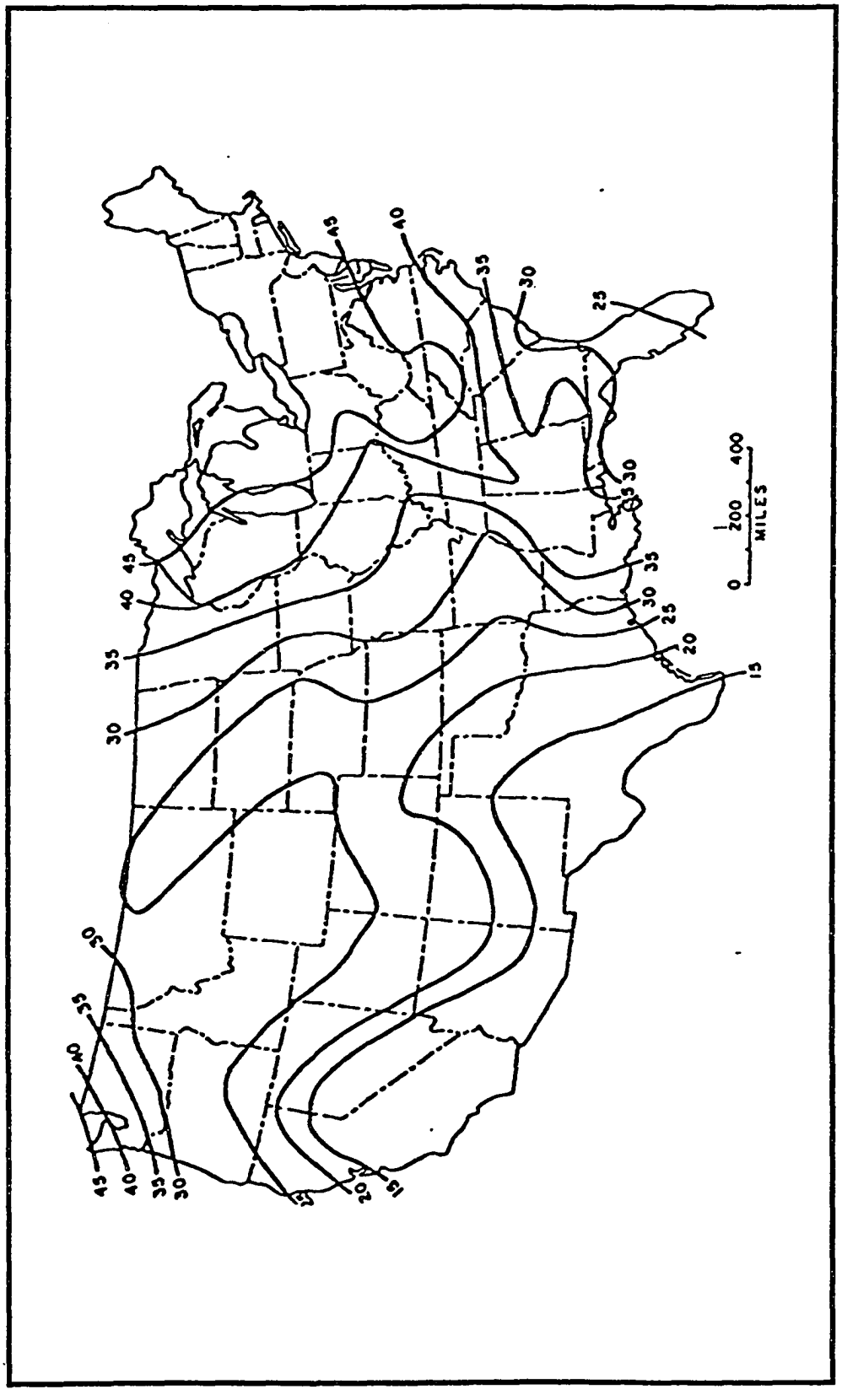

Figure 2.9 U.S. Climatic Ratings Based on Frequency Distribution for Precipitation. From Krohn and Slosson (1980).

Increased electrolyte concentrations (salt solution) will cause depression of the double layer, the amount dependent upon the moisture content. The influence of salts are pronounced at high moisture contents, of considerable significance at moisture contents near the plastic limit, and insignificant at moisture contents near the shrinkage limit (Thomson and Ali, 1969).

Replacement of pore water by cations of increased valence will also depress the double layer. Even small amounts of di- or trivalent cations can have a significant effect on the double layer, as multivalent cations are preferentially adsorbed. In addition, ions of the same valency which are least hydrated have the greatest power of replacement and are replaced with the greatest difficulty (Wiegner, 1935). These include K, Na, and Li followed by Ca and Mg in order of decreasing hydrated radii (Soil Science Society of America, 1977).

Replacement of pore water with organic compounds typically present at pneumatic fracturing sites (e.g., petroleum and chlorinated solvents) is generally expected to decrease swell because dielectric constants and dipole moments are lower than equivalent values for water. Similarly, high concentrations of organic compounds with higher dielectric constants and dipole moments than water may provide sufficient competition for adsorption sites leading to increased swell.

It should be noted that interactions between salts, ions, and organics and the soil are highly complex and are specific to the clay mineral and molecule types and concentrations. Extensive work has been performed on the interaction of chemicals with

clays and such work should be consulted for chemical specific cases. Some references of the effects of cations and organics on clays include: Park et al. (1991), Stockmeyer (1991), Edil et al. (1991), Czurda and Wagner (1991), Storey and Peirce (1989), Liljestrand et al. (1992), Barone et al. (1992), DiCola (1986), and Rebhun et al. (1992).

2.2.4.3 Temperature. Changes in temperature are responsible for differential volume changes resulting from expansion or reduction in mineral solids and pore water, and for changes in the form of reversible cementing agents. Volume changes associated with the first mechanism are more common, but are expected to be smaller in magnitude than those associated with the second mechanism.

The temperature sensitive nature of the pore water and soil particles creates a condition analogous to unloading which suggests an increase in volume change. As the temperature increases, pore pressure are increased and effective stresses are decreased. Yaalon in Mitchell (1973b) showed that daily temperature changes and the amplitude of those changes (difference between maximum and minimum air temperatures) are related to vertical heave. Figure 2.10 shows this relationship compiled from 160 events.

Drop in temperatures also causes reversible cementing agents to crystallize, including water (freezing) and sodium sulfate salt (32°C to 4°C). Salt heave is a significant volume change mechanism but is limited to arid regions with high concentrations of sodium sulfate, such as those in southern Nevada and southeastern California (Blaser and Arulanandan, 1973).

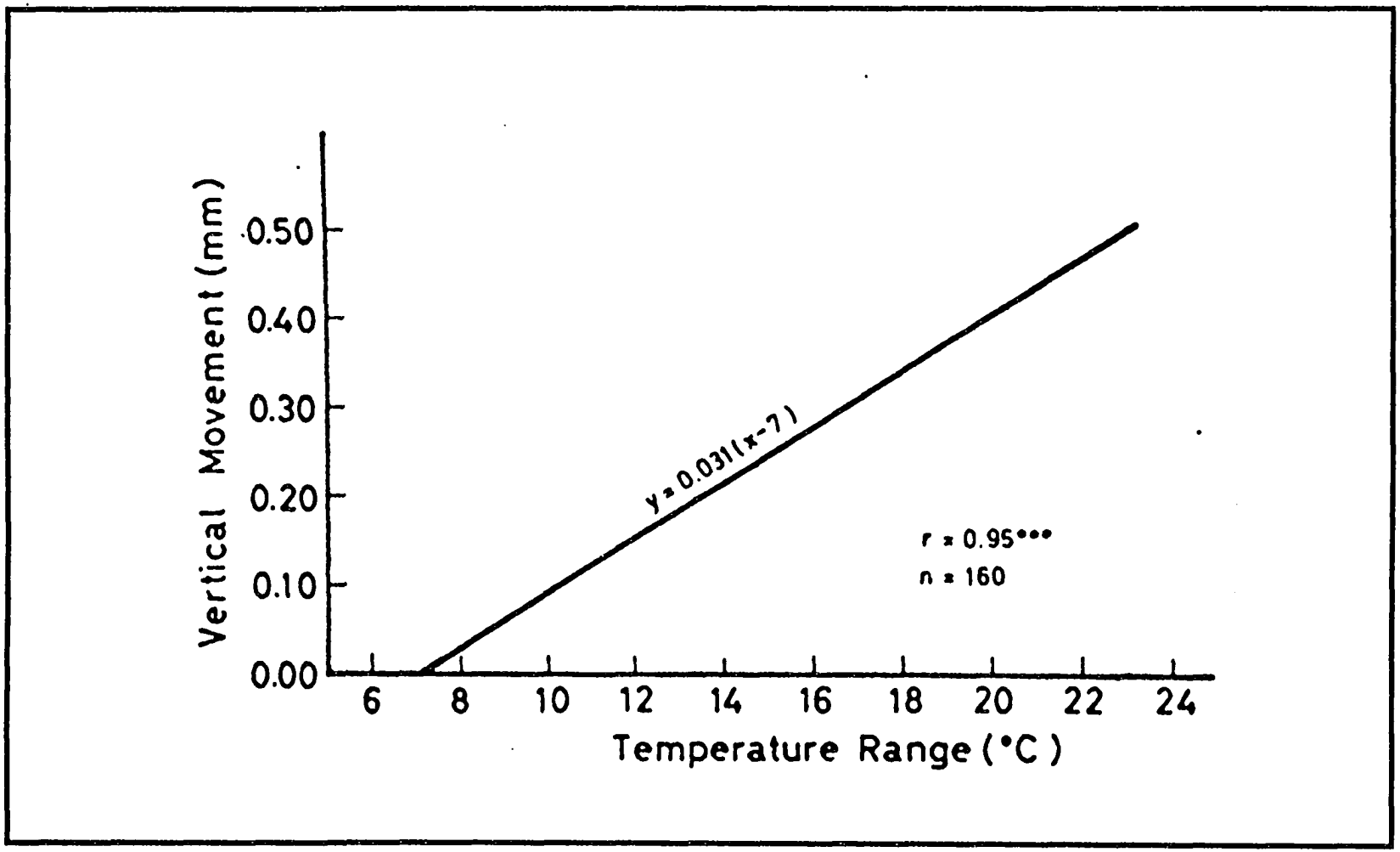

Figure 2.10 Effect of Diurnal Temperature Range on Vertical Heave of Undisturbed Soil. From Mitchell (1973b).

2.2.4.4 Surcharge Pressure. The restraining pressure on the soil under normal conditions comprises the overburden weight and applied loads due to a buildings or other surface structures. If the force of the load equals or exceeds the force of the swelling pressure of the formation, which averages 10,000 lb/ft^2 (PSF), no volumetric expansion will occur. However, if the swelling pressure does equal or exceed the force of the overburden soil or weight applied to the ground surface, volume change may occur. Figure 2.11 illustrates the effect of varying pressure on volume change of a clay for constant density and moisture conditions. It is noted that this principle applies to surface heave and does not necessarily reflect changes which may occur to the fracture aperture. Additional discussion on the addition and removal of surcharge pressure is provided in Chapter 6.

2.2.4.5 Fluid Pressures in Fracture. Gale (1975) determined that changes in pressure exerted on a fracture results in changes to the aperture. Positive pressure will generally increase apertures and negative pressures will decrease apertures. The deformation that may occur as a result of these pressure changes could be a significant percentage of the initial fracture aperture. Using an instrument termed the "fracture deformation gauge," Gale determined with well injection tests that for a fracture located 29 ft below ground surface in deformable rock, a decrease in fluid pressure of 20 lb/in^2 (PSI) gave a fracture closure of 5×10^{-5} ft. The same fracture opened to 3×10^{-4} ft from a 20 lb/in^2 (PSI) increase in fluid pressure.

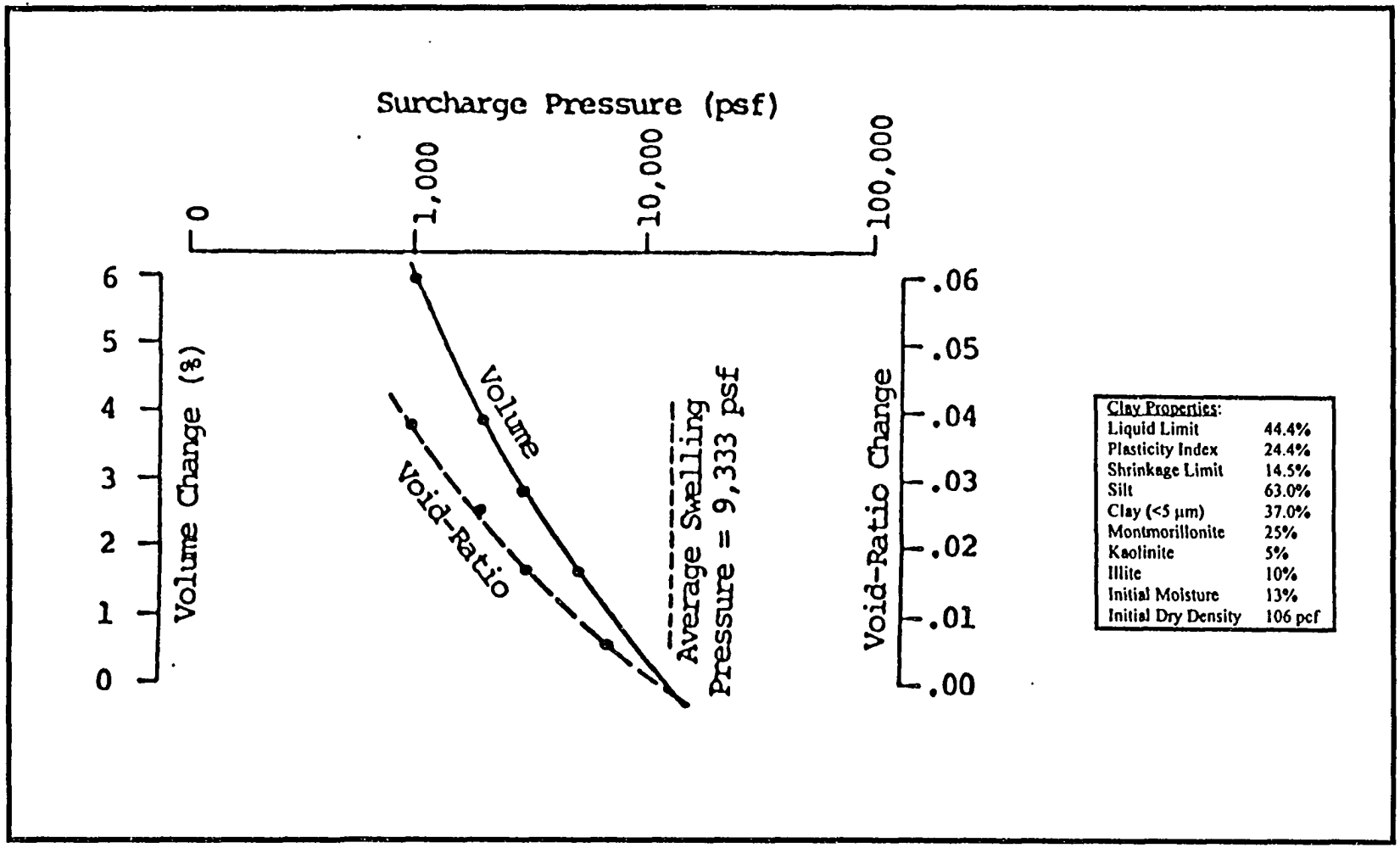

Figure 2.11 Effect of Varying Pressure on Volume Change of Clay Soil. From Chen (1973).

2.2.5 Summary

In summary, the development of expansive soil conditions is believed to be dependent on the fulfillment of two conditions. The first is that the formation must be susceptible to volume change based on its physical and chemical properties, and the second is that there must be a shift in ambient environmental conditions to initiate the change. Thus, properties of the formation generally define the range over which volume changes may occur, and environmental conditions dictate the degree to which these changes may occur. The factors affecting volume change developed in the previous sections are summarized in Tables 2.3 and 2.4.

2.3 Qualitative Volume Change Prediction

Engineering classification tests and the empirical relationships developed from these tests are the most commonly used qualitative indicators of volume change potential. These tests, which have been used primarily in the foundation and pavement engineering disciplines, are numerous and varied, and simultaneous results are typically considered.

2.3.1 Engineering Classification Tests

The engineering properties of primary significance in addressing the potential of a formation for volume changes are Atterberg limits and soil activity. This section provides a discussion of these and other tests used as indicators of volume change. A summary of the most common engineering classification tests is presented in Table 2.5.

Table 2.3 Summary of Formation Properties Affecting Volume Change

Soil Property	Component	Effect on Volume Change	Data Type	Determination
Mineralogy	Clay Mineral	Of common clay minerals, montmorillonite is the most expansive, followed by illite (from interstratification with montmorillonite), and then kaolinite	Qualitative (limited quantitative)	lab tests** or literature
Soil Fractions	Amount of Clay Minerals	There is increased potential for volume change as percentage of clay minerals vs. nonclay components increases	Quantitative	lab tests** or literature
	Grain Size Distribution	Grain size distribution determines the range of soil density. A decreased density will cause a reduction in volume change potential.	Quantitative	lab tests*
Bulk Dry Density	--	The higher the density the greater the volume change	Quantitative	site/lab tests* or literature
Surface Reactivity	CEC	The higher the CEC the greater the volume change	Quantitative	tests*
	Specific Surface	The higher the specific surface the greater the swelling	Quantitative	tests**
Organic Matter	Nonhumics	High nonhumic fraction are associated with high shrinkage	Quantitative/ Qualitative	tests* observation
	Humics	Associated with volume change, dependent on interactions		
Irreversible Cementing Agents	Aggregate Cementation	Increased cementation will restrict volume changes	Qualitative	observation or literature
	Hydroxy Interlayering	Formation of hydroxy interlayering will restrict volume changes	Qualitative	lab tests* with interpretation
Stress History	Consolidation State	Overconsolidated states are more expansive than normally consolidated states	Quantitative/ Qualitative	site tests or literature
Soil Structure	Fabric	Flocculated fabrics are more expansive than dispersed fabrics	Qualitative	lab tests**
pH	--	Indicator of chemical and microbiological properties of soil; used to determine presence of hydroxy interlayering which may reduce swell.	Quantitative	lab tests*

* These laboratory tests are readily available by commercial laboratories.

** These laboratory tests are available commercially, but are limited to isolated suppliers and are typically special requests.

Note: Refer to Table 5.1 for a summary of specific laboratory test methods.

Table 2.4 Summary of Environmental Conditions Affecting Volume Change

Condition	Components	Effect on Volume Change	Data Type	Determination
Moisture	Initial Moisture	The lower the moisture, the more expansive the soil where a water source is present	Quantitative	lab tests*
	% Saturation	Volume change increases as water content increases; vadose zone is more expansive than saturated zone	Quantitative	lab tests*
	Evaporation & Precipitation	Areas with periods of rainfall mixed with periods of drought (low climatic ratings) are most expansive	Quantitative	climate (see Figure 2.9)
	Construction Influences	Covered areas have steady increased moisture, less swell. Moisture/desiccation from drainage, heated areas of buildings, leaking USTs, etc	Qualitative	observation
	Evapo-transpiration	Desiccation from vegetation increases expansiveness where water source is present	Qualitative	observation
Pore Fluid Composition	Salts	Increased salt content causes decrease in swelling	Quantitative	lab tests*
	Ions	Increased valence and size causes a swell decrease	Quantitative	lab tests*
	Organics	Chemicals with lower dipole moments or dielectric constants will depress swelling relative to water	Qualitative Quantitative	literature (properties) lab tests* (type and concentration)
Temperature	Air	Increased temp., increased volume, increased swell	Quantitative	*in situ* site tests
	Salts	Reduction in temperature can lead to crystallization of sodium sulfate, and increase volume change	Qualitative/ Qualitative	lab tests* or literature
Surcharge Pressure	Overburden, Structures or Equipment	Decrease or increase in pressure will decrease or increase volume change; high sensitivity in shallow areas	Quantitative/ Qualitative	depth of fracturing and observation
Fracture Fluid Pressure	Remediation technology	Change in fluid pressure can increase (higher pressure) or decrease fracture size (lower pressure)	Quantitative	on site tests

* These laboratory tests are readily available by commercial laboratories.

Note: Refer to Table 5.1 for a summary of specific laboratory test methods.

Table 2.5 Engineering Tests Used as Qualitative Indicators of Swelling Potential

Test	Properties Investigated	Parameters Determined
Atterberg Limits	Plasticity, consistency	
Liquid Limit (LL)	Upper limit water content of soil plasticity	PI = LL-PL = PI
Plastic Limit (PL)	Lower limit water content of soil plasticity	$LL = \frac{w - LL}{LL - PL} = LI$
Shrinkage Limit (SL)	Lower limit water content of soil shrinkage	R = shrinkage ratio L_s = linear shrinkage
Soil Activity	Distribution of fine-grained particle sizes in relation to plasticity	$\text{Activity} = \frac{PI}{\%\ \text{finer}\ 2\mu m}$
Free Swell Test	Swell upon wetting of unconsolidated, unconfined sample of air dried soil	$\text{Free swell} = \frac{(V_{wet} - V_{dry})}{(V_{dry} \cdot 100)}$
Potential Volume Change (PVC) Meter	One-dimensional swell and pressure of compacted, remolded sample under semi-strain controlled conditions	SI (Swell Index) (lb/ft^2) PVC (Potential Volume Change)
Expansion Index (EI) Test	One-dimensional swell under 1 psi surcharge of sample compacted to initial 50% saturation	Expansion Index (EI)
California Bearing Ratio (CBR) Test	One-dimensional swell under surcharge pressure of compacted, remolded samples on partial wetting	Percent Swell CBR (%)
Coefficient of Linear Extensibility (COLE) Test	Linear strain of a natural soil clod when dried from 5 psi to oven dry suction	COLE and LE (%)

Modified from Nelson and Miller (1992)

2.3.1.1 Atterberg Limits. The Atterberg limits define moisture content boundaries between states of consistency of fine-grained soils (Atterberg, 1911). Figure 2.12 presents a schematic of the four distinct states of consistency depending on water content. The boundaries of these states are defined as the shrinkage limit (SL), the plastic limit (PL) and the liquid limit (LL). The majority of volume changes occur where water contents are between the SL and the PL, the difference between which is defined as the shrinkage index (SI). The range in moisture content over which the soil is plastic is defined by the plasticity index (PI), the difference between the liquid limit and the plastic limit. Typical ranges in Atterberg limits for kaolinite, illite, and montmorillonite are summarized in Table 2.6.

Table 2.6 Atterberg Limits of Common Clay Minerals

Mineral	LL (%)	PL (%)	SL (%)
Kaolinite	30-100	25-40	25-29
Illite	60-120	35-60	15-17
Montmorillonite	100-900	50-100	8.5-15

From Nelson and Miller (1992)

2.3.1.2 Soil Activity. Activity has also been used as an index property to determine the swelling potential of expansive clays. Skempton (1953) defined activity (A_c) as follows:

$$A_c = \frac{\text{plasticity index}}{\%\ \text{finer than } 2\mu m} \qquad (2.1)$$

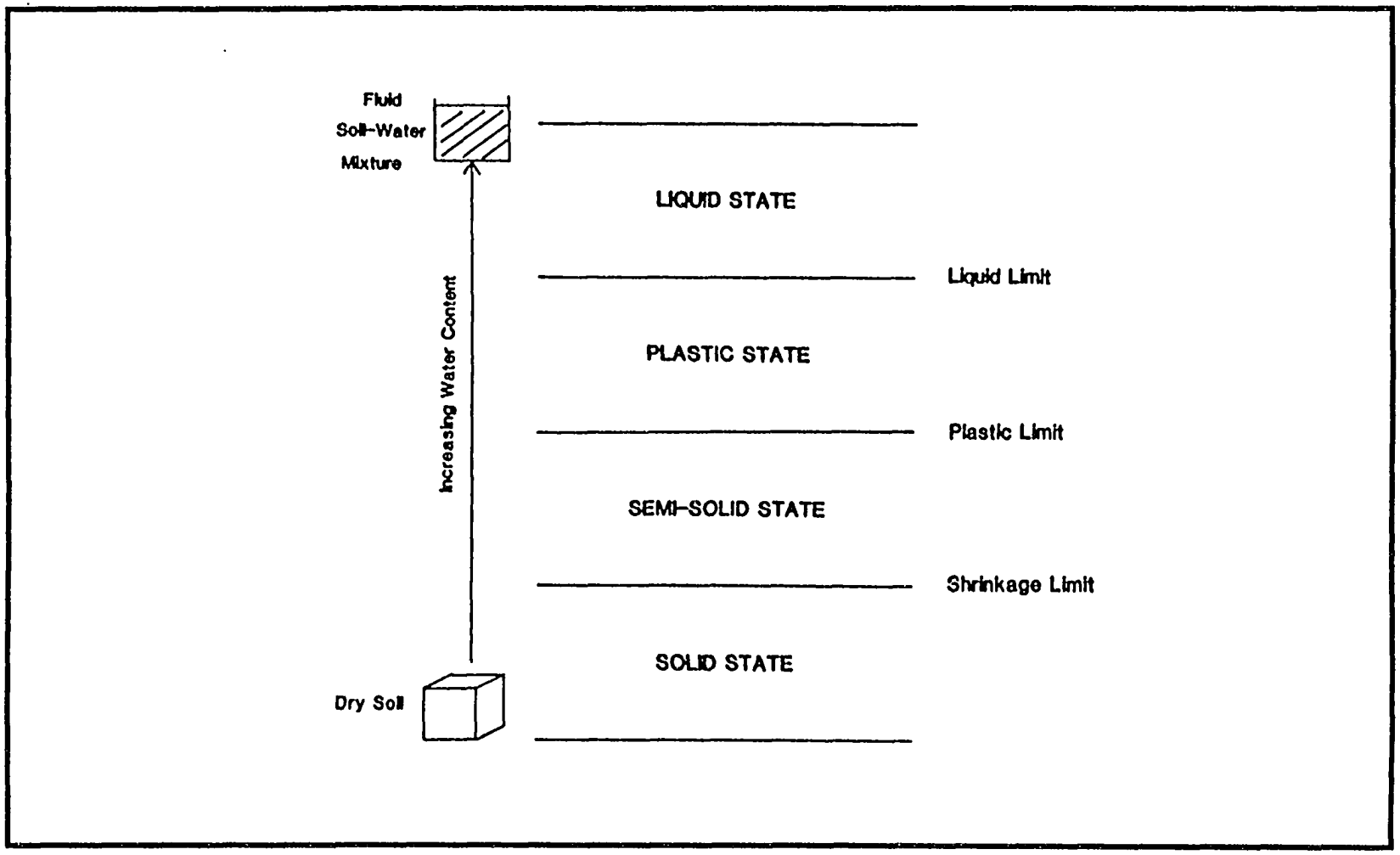

Figure 2.12 States of Consistency and Atterberg Limits of Fine-Grained Soils. From Lambe and Whitman (1969).

For most clays, a plot of plasticity index versus clay content yields a straight line passing through the origin. The slope of the line give for each clay gives the activity (Mitchell, 1993). Typical activity values for clay minerals are presented in Table 2.7,

Table 2.7 Activities of Common Clay Minerals

Mineral	Activity
Kaolinite	0.33-0.46
Illite	0.9
Montmorillonite (Ca)	1.5
Montmorillonite (Na)	7.2

From Skempton (1953)

Another term used in volume change prediction developed Pearring (1963) and Holt (1969) is cation exchange activity, CEA_c, defined as:

$$CEA_c = \frac{\text{activity}}{\%\ \text{finer than } 2\mu m} \qquad (2.2)$$

2.3.1.3 Other. Other classification tests exist, but discussion is limited to Table 2.5 as these are typically not performed during environmental site investigations, and results would not be available for pneumatically fractured formations. These include free-swell test (Holtz and Gibbs, 1956), potential volume change meter (Lambe, 1960), expansion index test (UBC No. 29-2), California bearing ratio test (Yoder and Witczak, 1975; Kassiff et al., 1969), and COLE test (Brasher et al., 1966).

2.3.2 Empirical Relationships

The relationships between engineering properties and swelling potentials have been developed from experiments by a variety of investigators. The majority of the classification schemes utilize formation properties alone, including percent clay, Atterberg limits, activity, cation exchange activity, and density in the form of standard penetration resistance (SPR). The only environmental component used is in situ soil suction, a measure of the soil's affinity for water. In an evaluation of seventeen of the published criteria for predicting potential swell, Snethen et al. (1977) showed that liquid limit and plasticity index along with soil suction are the best indicators of potential swell.

Swelling potential has generally been defined with qualitative ratings such as "low," "medium," "high," and sometimes "very high," the magnitude of which refers to the relative capacity for expansion of different soils. Table 2.8 summarizes these classifications. In addition, Figure 2.13 presents classifications which use the relationships of percent clay, cation exchange activity, and activity in the estimation of volume change potential.

Based on these classifications, expansive soils are generally characterized by high plasticity indices, high liquid limits, low shrinkage limits, high activities, high colloid contents, and high densities. However, it is emphasized that the relationships presented are only indicators, and the actual expansion that will occur in the field may vary considerably. These classifications are useful only to indicate potentially expansive conditions and to identify the need for further predictive testing (Nelson and Miller, 1992).

Table 2.8 Summary of Expansive Soil Engineering Classifications by Various Investigators

Property	Volume Change Potential				Reference
	Low	Moderate	High	Very High	
Activity	<0.75	0.75-1.25	>1.25	--	Skempton (1953)
PI (%)	0-15	10-35	20-55	35+	Chen (1988)
SI (%)	0-2	20-30	30-60	>60	Ranganatham and Satyanarayana (1965)
PI (%)	<12	12-23	23-32	>32	Raman (1967)
SI (%)	<15	15-30	30-40	>40	
% Volume Change	<0.5	0.5-1.5	>1.5	--	Altmeyer (1955)
SL (%)	>12	10-12	<10	--	
% Volume Change	<10	10-20	20-30	>30	Holtz and Gibbs (1956)
%<0.0001 mm	<15	13-23	20-31	>28	
PI (%)	<18	15-28	25-41	>35	
SL (%)	>15	10-16	7-12	<11	
% Volume Change	<0.5	0.5-1.5	>1.5	--	Snethen et al. (1977)
LL (%)	<50	50-60	>60	--	
PI (%)	<25	25-35	>35	--	
μ_{nat} (tsf)	<0.5	0.5-1.5	>1.5	--	
% Volume Change	<10	10-20	20-30	>30	Chen (1965)
%<No. 200	<30	30-60	60-95	>95	
LL (%)	<30	30-40	40-60	>60	
SPR (blows/ft)	<10	10-20	20-30	>30	

Modified from Nelson and Miller (1992)

Note: The definition of volume change varies between investigators and results are reported according to the respective investigators definition μ_{nat} soil suction at natural moisture content; SPR standard penetration resistance; -- not applicable.

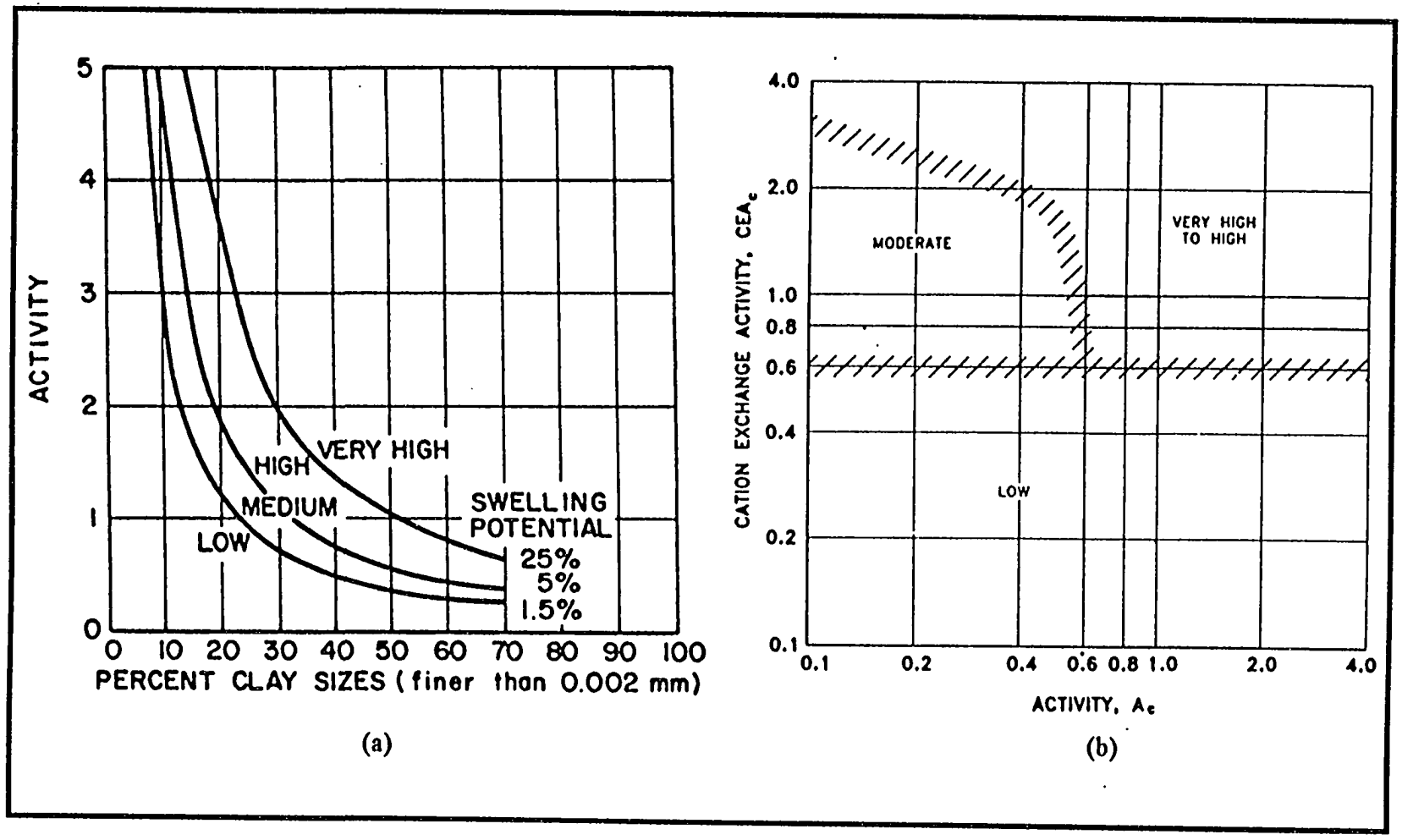

Figure 2.13 Graphical Classification Charts for Rating Expansion Potential. (a) From Seed et al. (1962). (b) McKeen and Hamburg (1981); Hamburg (1985).

2.4 Discrete Fracture Fluid Flow Modeling

This section provides a summary of fluid flow modeling as applied to discrete fracture flow of incompressible and compressible fluids. The two geometric arrangements traditionally modeled, linear and radial, are first described (2.4.1) followed by a presentation of the equations describing fracture flow (2.4.2).

2.4.1 Linear and Radial Flow Geometries

Fluid flow in fracture systems has been traditionally modeled by analyzing the fluid flow between two smooth parallel plates, known commonly as the "parallel plate analogy" (Wilson and Witherspoon, 1970; Louis, 1969; Snow, 1965). By varying the point of extraction, two configurations of the parallel plate analogy are established, termed the linear and radial flow geometries. The linear case represents flow through a fracture bounded on two sides, with extraction occurring linearly from one end. The radial flow geometry represents extraction from a center point in the fracture thus inducing a radial flow configuration. Schematics of both flow geometries are provided in Figure 2.14.

2.4.2 Fluid Flow Equations

The basic parallel plate flow model is derived from the fundamental equations which describe fluid mechanics, the Navier-Stokes equations. This inherently nonlinear set of partial differential equations has no general solution, and only a small number of exact solutions have been found. Poiseuille developed a functional relationship for describing

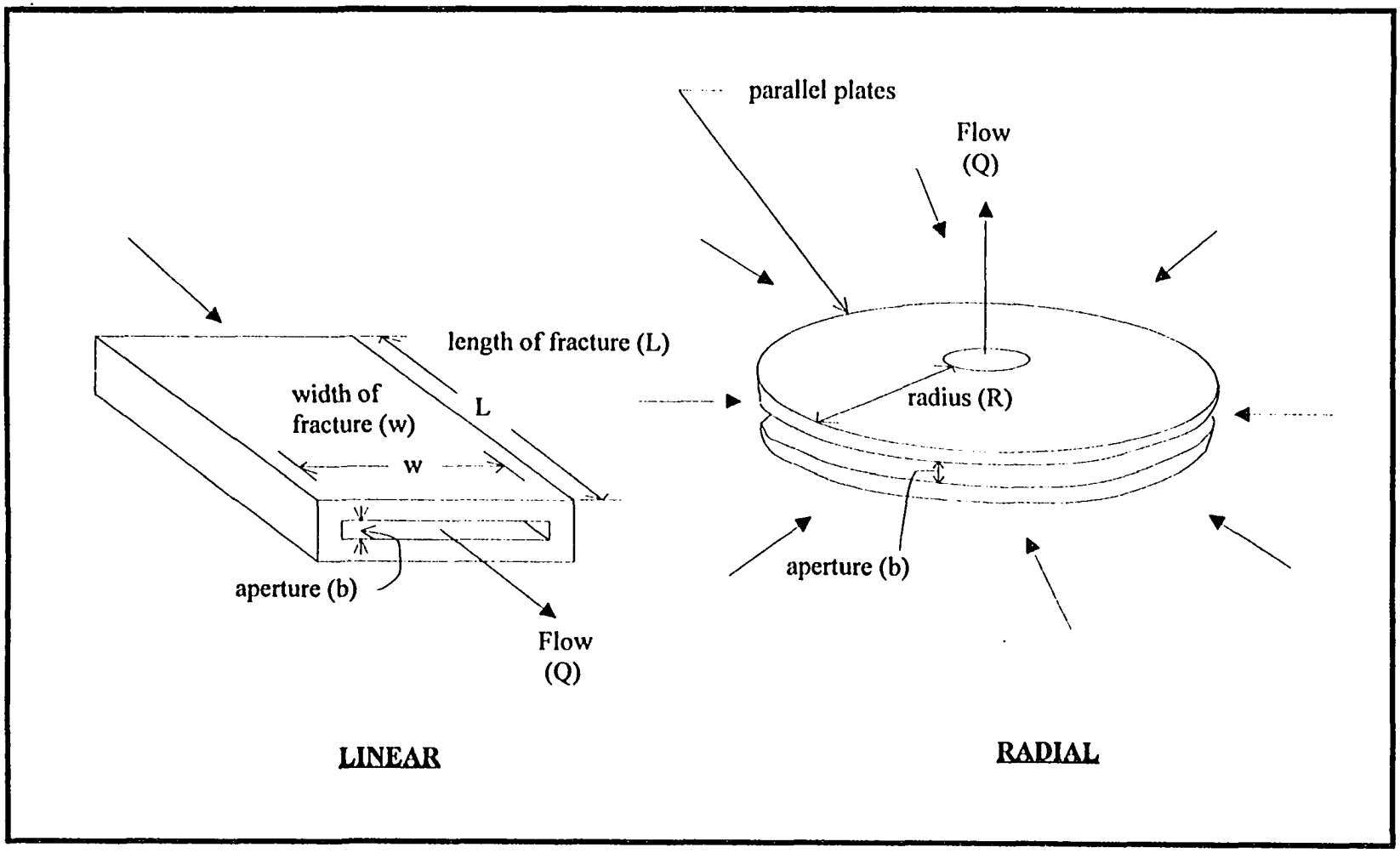

Figure 2.14 Schematic of Linear and Radial Flow Geometries.

single phase laminar flow of a viscous incompressible fluid. By combining this result with Darcy's law and utilizing an average flow velocity, relationships describing flow in a fracture can be derived. The equations describing flow of incompressible and compressible fluids in discrete fractures are presented below.

2.4.2.1 Incompressible Fluid Flow. Assuming laminar flow and an incompressible fluid, the volumetric flow rate per unit cross-sectional area of the fracture occurring radially towards an extraction point, Q, can be described as,

$$Q = -\frac{(P_2 - P_1)\cdot\pi\cdot g\cdot b^3}{6\cdot\nu\cdot\ln\left(\frac{R_2}{R_1}\right)} \tag{2.3}$$

where b is the fracture aperture, v is the kinematic viscosity, and P_1 and P_2 are pressures measured at radial distances R_1 and R_2, respectively, from the extraction point. This relationship is known as the "cubic law" because the flow rate is a function of the cube of the aperture. Deriving a similar equation for a linear flow geometry, the volumetric flow rate can be described as,

$$Q = -\frac{(P_2 - P_1)\cdot g\cdot b^3\cdot w}{12\cdot\nu\cdot(L_2 - L_1)} \tag{2.4}$$

where L_1 and L_2 are linear distances from the extraction point. Derivation of the equation for radial flow geometry is provided in Nautiyal (1994), and derivation of the equation for the linear flow geometry is provided in Appendix A.

2.4.2.2 Compressible Fluid Flow. The equations describing steady-state flow of viscous fluids can be redefined to address incompressible fluids as described by Sullivan and Hertel (1940), Muskat (1946), Langfelder et al. (1968) and Ziegler (1976). In describing the flow of a gas in a discrete fracture under isothermal conditions, Nautiyal (1994) accounted for compressibility effects by replacing the pressure gradient term, P_2-P_1, with

$$\frac{P_2^2 - P_1^2}{2 \cdot P_1} \tag{2.5}$$

Equations 2.3 and 2.4 can thus be extended to flow of laminar compressible fluids under isothermal conditions for the radial and linear flow geometries as follows,

$$Q = -\frac{\left(P_2^2 - P_1^2\right) \cdot \pi \cdot g \cdot b^3}{\left(2 \cdot P_1\right) \cdot 6 \cdot \nu \cdot \ln\left(\frac{R_2}{R_1}\right)} \tag{2.6}$$

$$Q = -\frac{\left(P_1^2 - P_2^2\right) \cdot g \cdot b^3 \cdot w}{\left(2 \cdot P_1\right) \cdot 12 \cdot \nu \cdot \left(L_2 - L_1\right)} \tag{2.7}$$

Derivation of the equation for the radial flow geometry is provided in Nautiyal (1994), and derivation of the equation for the linear flow geometry is provided in Appendix A.

CHAPTER 3

EXPERIMENTAL APPROACH

Based on the review of clay mineral behavior in Chapter 2, it is expected that volume changes will affect the aperture of pneumatically induced fractures. This chapter describes a series of bench scale studies performed to investigate volume change in the laboratory. These experiments include control tests to investigate idealized fracture flow (3.1), as well as horizontal infiltrometer tests using natural soil (3.2).

The experiments were designed to emulate as closely as possible the actual field conditions encountered at pneumatic fracturing sites. A summary of the experimental conditions chosen for the bench scale experiments are presented in Table 3.1, which also briefly describes the justification for each.

3.1 Control Tests

The control tests were designed to simulate ideal conditions by inducing air flow between smooth parallel plates. These devices allowed for investigation of the relationship between flow rate, pressure and aperture described by the cubic law. Such results are essential for later interpretation of the horizontal infiltrometer experiments involving fractures in natural soil. This section describes the setup and operation of the two flow geometries investigated, linear and radial.

Table 3.1 Experimental Conditions

Condition Chosen	Other Options	Justification	Control Devices	Horizontal Infiltrometer
Fine-grained soil	Coarse-grained soil or rock formation	Fine-grained formations are the most susceptible to volume changes, and are most common formations to which pneumatically fracturing is applied	--	X
Natural soil	Fabricated soil	Use of natural soil most closely models in-situ conditions and the complexities associated with natural conditions	--	X
Low to moderate soil expansiveness	Nonexpansive or highly expansive	Soil of average expansiveness was chosen as the most appropriate for calibration of the new device	--	X
Remolded sample	Intact sample	Remolded soil was chosen to simulate flocculated soil fabric, which is the most expansive fabric type; remolded samples also allow greater experimental flexibility	--	X
Extraction of air under vacuum	Water as extraction fluid	Air was chosen to simulate vacuum extraction, the most common technology coupled with pneumatic fracturing; typical field vacuum source levels were chosen	X	X
Unsaturated conditions	Saturated conditions	Chosen to simulate vadose zone conditions, which are most expansive and most commonly encountered at pneumatically fractured sites	--	X
Variations in moisture content	Secondary factors	Moisture is the primary environmental condition affecting volume change, and was chosen also for its ease of use and non-hazardous properties	--	X
Aperture thickness	--	Chosen to simulate those commonly obtained by the pneumatic fracturing process	X	X
Radial flow geometry	--	Most closely simulates field condition, yet difficult to experimentally model with soil	X	--
Linear flow geometry	--	Linear case easily modeled in soil; fluid flow models verified to support horizontal infiltrometer work	X	X

X applies; -- does not apply

3.1.1 Setup of Linear Control Tests

A linear flow geometry was established by setting two equidimensional rectangular plates parallel to one another, separated and bounded on two sides with spacers to control aperture width. A circular manifold was attached to one end of the rectangular plates, which established an end seal and allowed for connection to a flow manifold and vacuum source. A schematic of the setup of this device, termed the linear control device, is provided in Figure 3.1.

All parallel plates and circular manifolds were fabricated from 0.5 in. thick acrylic plastic and were 4 in. wide. Three different setups were constructed with lengths of 6 in., 12 in., and 24 in. to provide experimental variation. The aperture spacers were constructed of aluminum sheet metal, each with a width of 0.5 in. In order to investigate variable apertures, spacers were fabricated using sheet metal of three thicknesses: 0.015 in., 0.025 in., and 0.032 in. Figure 3.2 summarizes the dimensions of the plates, circular manifolds, and sheet metal spacers for the linear control devices.

The device was assembled by applying high vacuum grease to each side of the sheet metal spacers, and positioning them along the outer edges of one of the plates. The matching plate was then mounted on the sheet metal, and the device was secured with 2 in. clamps along its length. The number of clamps varied with the size of the plate: six clamps were used for the plates with lengths of 6 in., 8 for the plates with lengths of 12 in., and 10 for the plates with lengths of 24 in.

The circular manifold was sealed with a rubber bell reducer (4 in. to 2 in.) secured with hose clamps. A Magnehelic vacuum pressure gauge (manufactured by Dwyer Instruments, Inc.) was mounted at the extraction point to monitor pressure differentials.

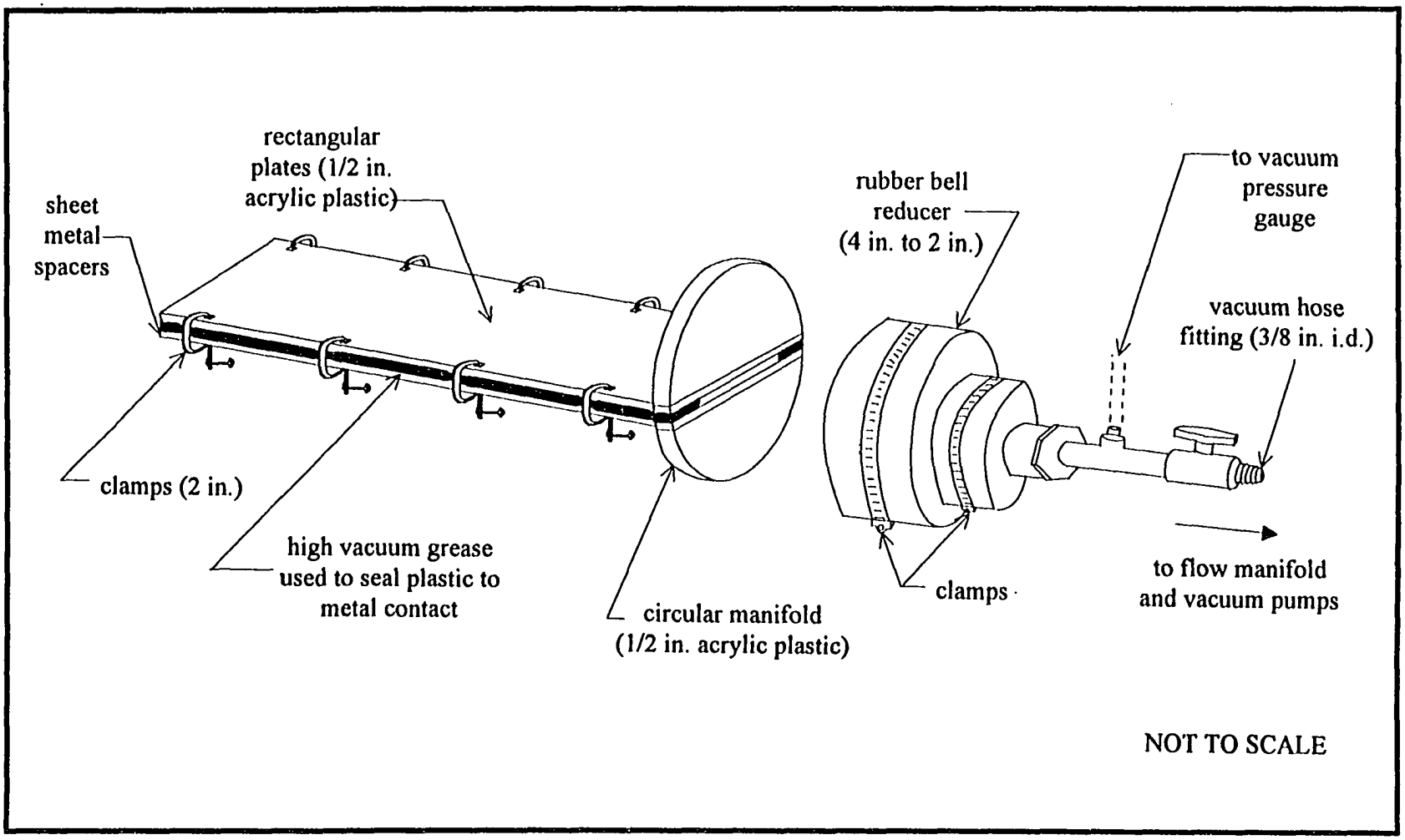

Figure 3.1 Setup Schematic of Linear Control Device.

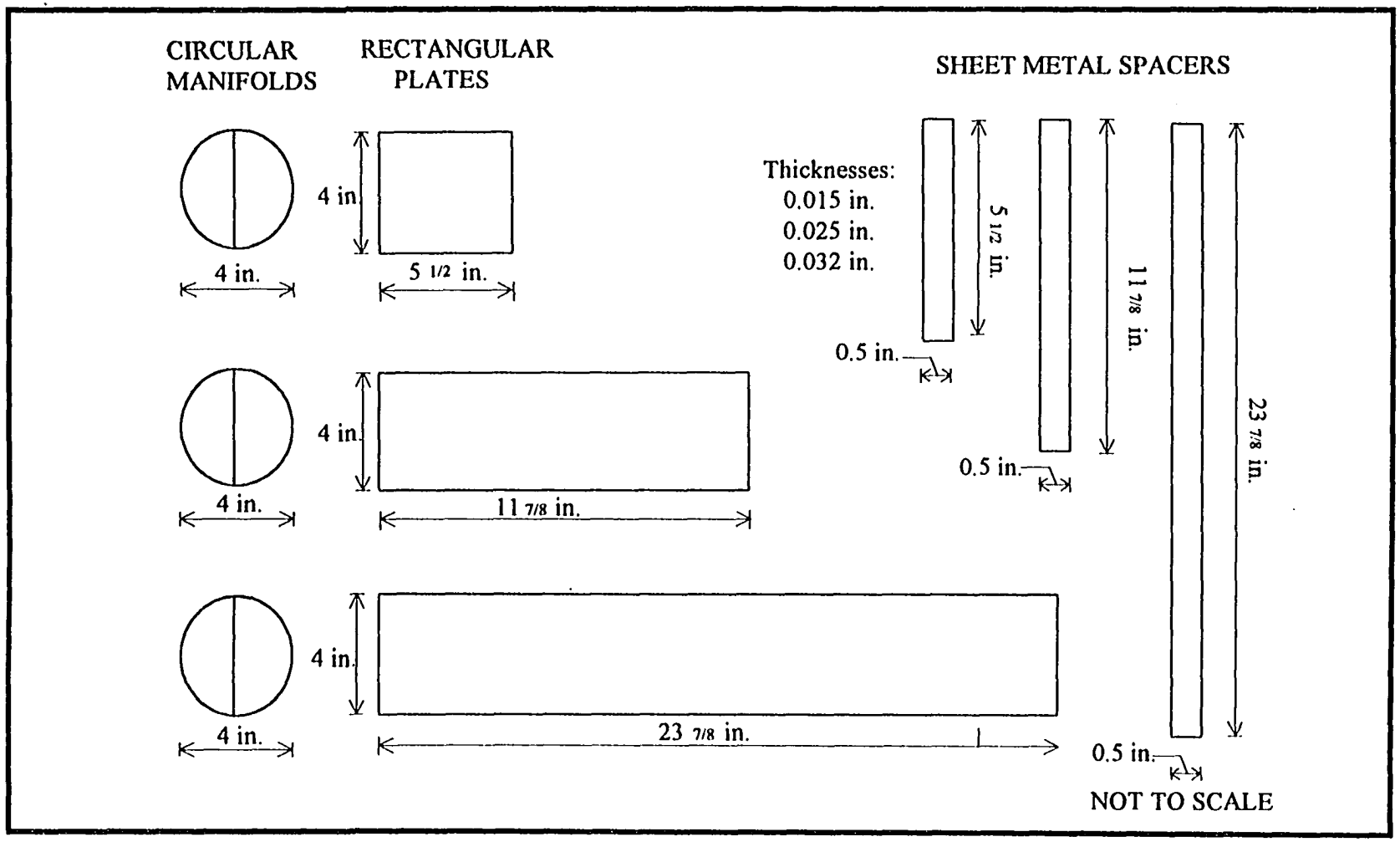

Figure 3.2 Dimensions of Plates, Circular Manifolds, and Sheet Metal Spacers for Linear Control Devices.

A rubber vacuum hose (3/8 in. diameter) connected the device to a flow manifold and vacuum source, which consisted of two pumps arranged in series. The flow manifold was composed of a calibrated electronic mass flow meter, equipped with a thermocouple for internal correction to standard temperature conditions, and a series of variable area flow meters (rotameters), as illustrated in Figure 3.3.

3.1.2 Setup of Radial Control Tests

A radial flow geometry was established by setting two equidimensional circular plates parallel to one another, separated with sheet metal spacers to control aperture width. The extraction point was located at the center of the upper plate, thereby inducing a radial flow configuration. A schematic of the setup of this device, termed the radial control device, is shown in Figure 3.4.

Three sets of circular parallel plates were fabricated from 0.5 in. thick acrylic plastic, with diameters of 6 in., 12 in., and 24 in. One edge was rounded and the other was left square to permit investigation of minor entrance losses. A 0.25 in. threaded hole was drilled at the center of the top plate. Aluminum sheet metal spacers were fabricated into wing-shaped pieces to minimize aerodynamic drag and pressure loss, and were made in three different thicknesses: 0.015 in., 0.025 in., and 0.032 in. A schematic of the plates and sheet metal spacers for the radial control devices is shown in Figure 3.5.

The device was assembled by placing the sheet metal spacers between the plates, arranged in a manner to maximize open fracture space yet still provide adequate aperture support. The device was secured with 2 in. clamps along the circumference of the plates, and was mounted on a pedestal to remove any flow restrictions. A Magnehelic vacuum

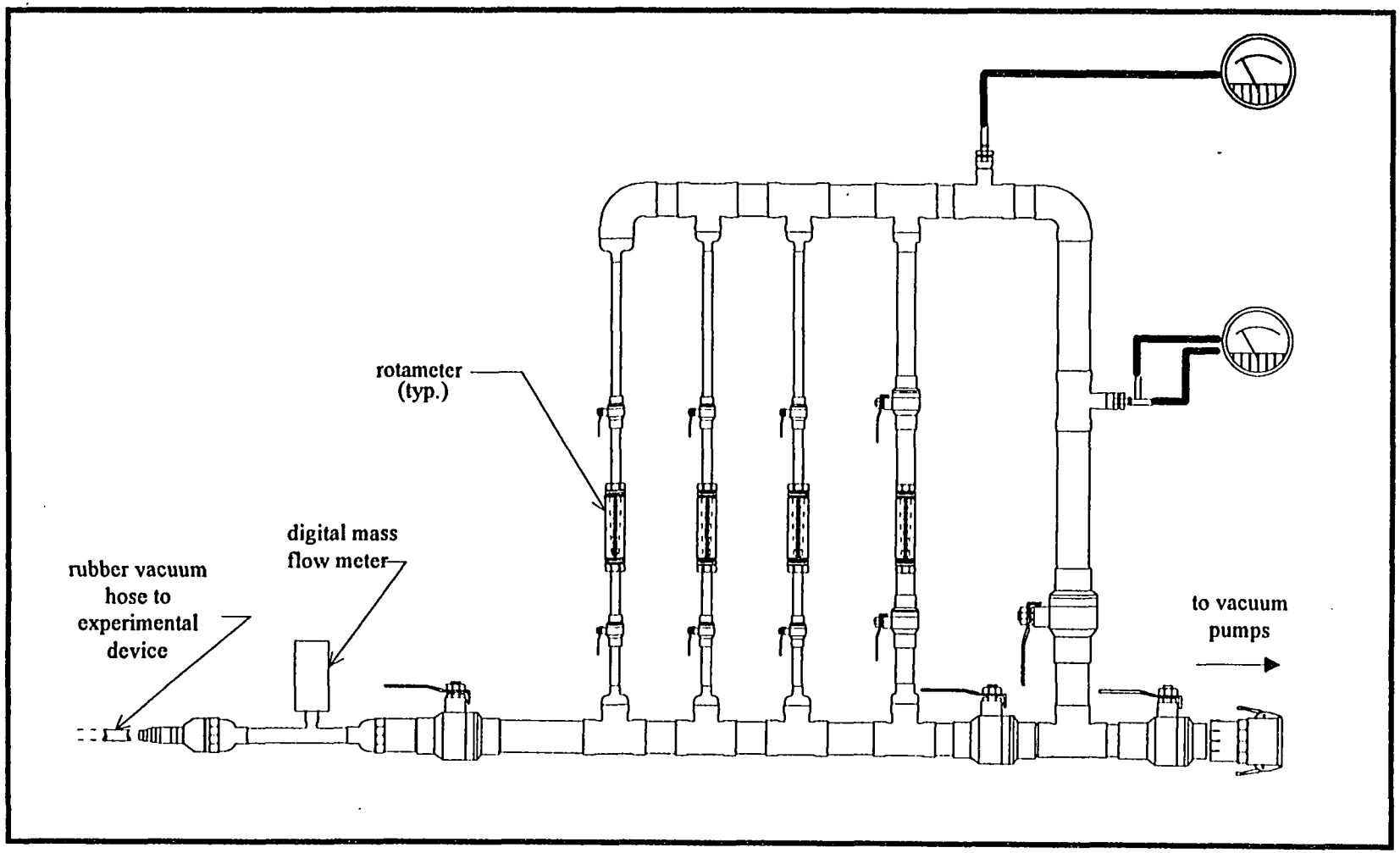

Figure 3.3 Schematic Diagram of Flow Manifold System.

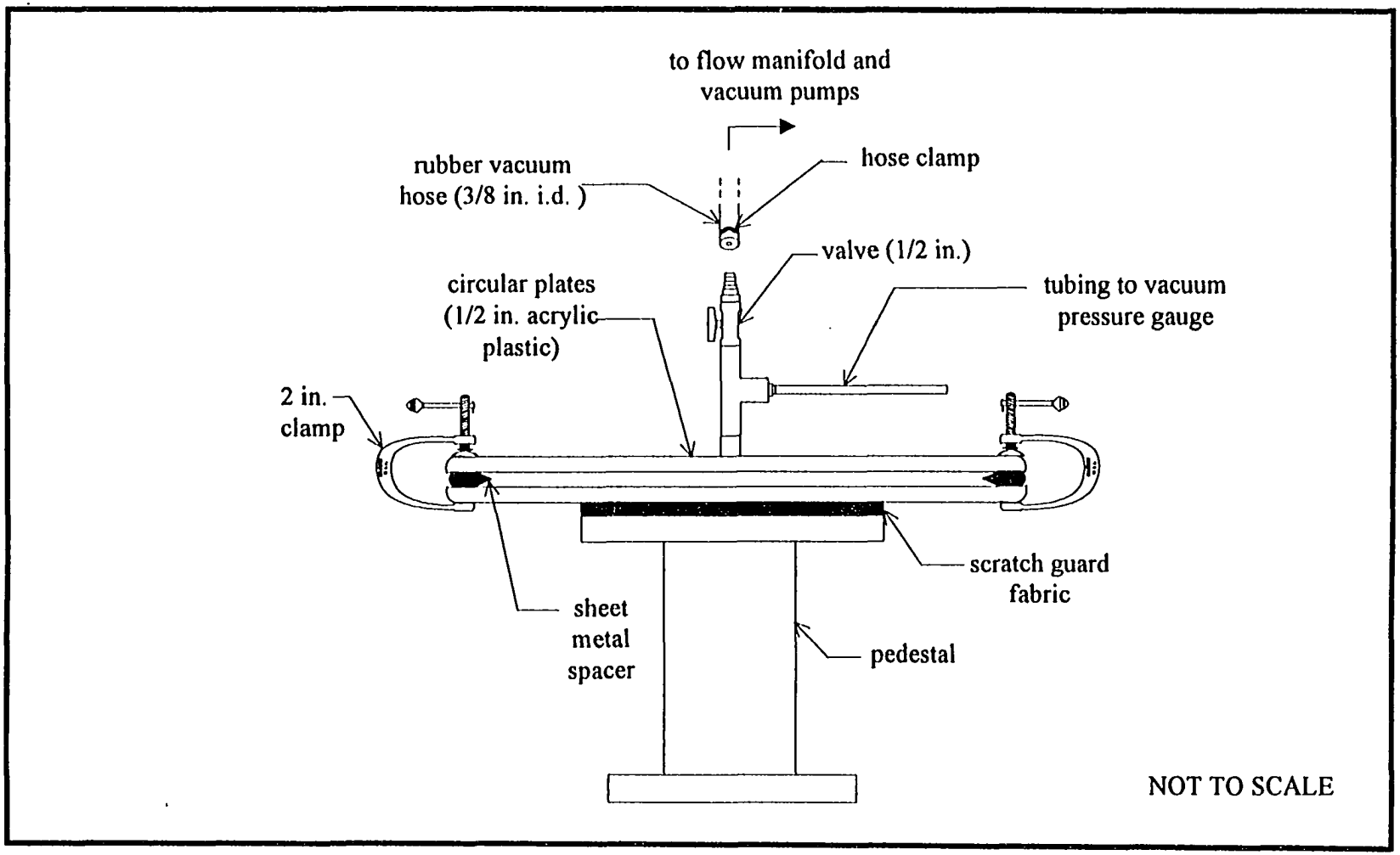

Figure 3.4 Setup Schematic of Radial Control Device.

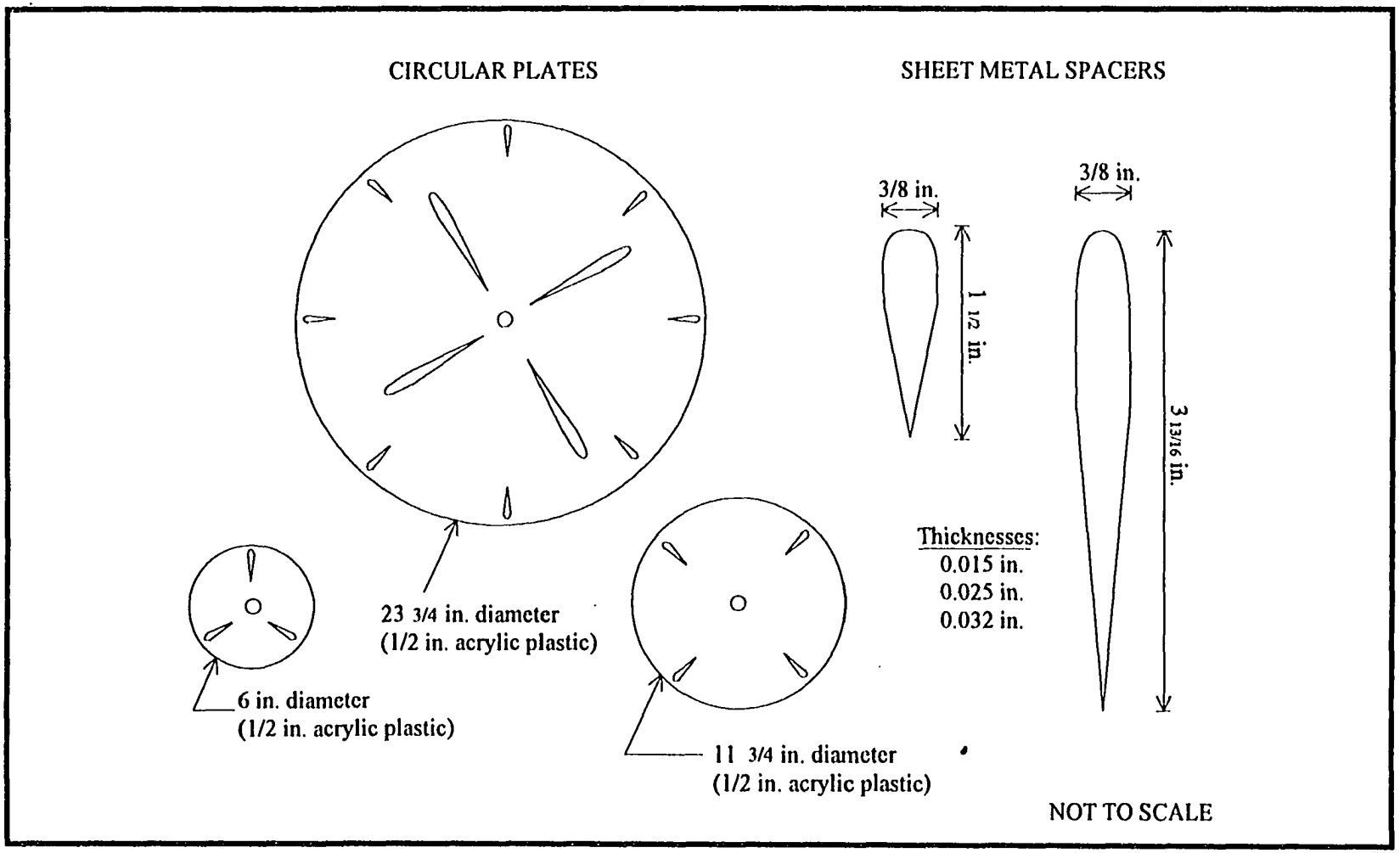

Figure 3.5 Schematic of Plates and Sheet Metal Spacers for Radial Control Devices.

pressure gauge was mounted at the extraction point to monitor pressure differentials. The device was connected to the flow manifold and vacuum pumps, which were previously described for the linear control devices, via a rubber vacuum hose (3/8 in. diameter).

3.1.3 Operation

Prior to an experimental run, the control devices were tested for vacuum tightness. Flow was then induced between the plates using a source vacuum capable of obtaining negative pressures up to 100 in. water. All tests were run under a passive inlet condition, with the inlet end open to the atmosphere. As the pressure differential was adjusted, flow rates and pressures at the extraction point were measured and recorded. In addition, temperature and atmospheric pressure were measured to permit adjustment of measured flow rates to conditions of standard temperature and pressure.

3.2 Horizontal Infiltrometer Tests

Two different horizontal infiltrometer devices were designed and fabricated to study flow through a fracture created in natural soil. The soil used for these tests contained a high percentage of clay to permit investigation of the mechanism of volume change. Experiments were performed by increasing or decreasing the moisture content of the soil through the fracture, and then monitoring the changes in fracture flow rate as an indicator of aperture change. This section presents a discussion of the soil used for the experiments (3.2.1), the setup of the rigid, confined horizontal infiltrometer (3.2.2), the setup of the semi-confined horizontal infiltrometer (3.2.3), and the operation of the devices (3.2.4). The experiments reported in this thesis are limited to development and calibration testing.

It is intended that additional experiments be conducted as part of future studies, as described in Chapter 6.

3.2.1 Test Soil

3.2.1.1 Selection. Based on a survey of local commercial clay pits, the Woodbury Formation was chosen as the most suitable soil for the calibration experiments. According to clay mineralogy and Atterberg limit data presented by DiCola (1986), this clay is expected to be the most active of the local soils. Physical and chemical tests were performed on Woodbury soil samples to verify this potential, and results are presented in the next section. In addition, the Woodbury Formation is homogenous in composition, and a large supply was easily available.

Approximately three hundred pounds of Woodbury Formation soil was collected from a clay pit located in Hightstown, Mercer County, New Jersey, from a band of clays, silts, and sands in the Coastal Plain Physiographic Province. The soil was obtained from a unit approximately 100 feet thick and approximately 40 feet below ground surface which was being excavated for use as a landfill liner. The soil was stored in plastic bags prior to preparation to minimize moisture loss.

3.2.1.2 Description. The Woodbury Formation is a thick, massive, silty, micaceous clay with thin, locally abundant lenses of glauconite (Fe-rich illite) sand. Siderite concretions ($FeCO_3$) up to several inches in length are common, and minor amounts of lignite are present. Depositional conditions during the Cretaceous favored restrictions in leaching allowing for the accumulation of ions necessary for montmorillonite formation, which is

the predominant clay mineral of the Woodbury (DiCola, 1986). Illite and kaolinite are the subordinate clay minerals, as determined by x-ray diffraction work of DiCola (1986).

A number of characterization tests were performed in the NJIT laboratory on samples of the Woodbury used in this research. These tests included mechanical sieve analysis, hydrometer test, specific gravity, organic content, and Atterberg liquid and plastic limits. Additional tests were performed by outside laboratories including NTH Consultants in Elkton, PA (Atterberg shrinkage limit) and Servi-Tech Laboratories in Dodge City, KS (soil salinity analysis and cation exchange capacity (CEC)). A proctor test had been performed by Demetracopoulos et al. (1985) on Woodbury specimens, and these results were adopted for this study. The physical properties of the Woodbury are summarized in Table 3.2. A grain size distribution curve and the moisture-density relationship are presented in Figures 3.6 and 3.7, respectively.

When these properties are compared to the empirical and physico-chemical relationships presented in Chapter 2, the Woodbury Formation is considered to have low to moderate volume change potential. Additional discussion of factors influencing the volume change potential of the Woodbury Formation is provided in Chapter 6.

3.2.1.3 Preparation. The soil was reduced to pieces less than 4.75 mm by manually breaking down blocks and passing through a No. 4 sieve to ensure even moisture distribution and uniform compaction. The soil moisture was elevated to the target moisture content by spraying and hand mixing until a uniform distribution was evident.

Table 3.2 Properties of the Woodbury Formation

PHYSICAL TESTS[a]								
Grain Size Distribution	**Atterberg Limits**	**Specific Gravity**	**USCS**	**Munsell Color**	**Standard Proctor Test**	**Natural Moisture Content**	**Natural K (cm/sec)**	**Organic Content (wt%)**
sand (fine): 4% %<75μm: 96% %2-75μm: 58% %<2μm: 38% %<1μm: 30%	LL: 44.3% PL: 25.7% SL: 18.0% PI: 18.6% SI: 7.7%	2.78	CL	Wet: very dark grey (gley scale N3/); Dry: grey (5Y 6/1)	Optimum Moisture: 18.9 wt% Density: 109.2 lb/ft^3	28.0 wt%	1 X 10^{-7}	7.61
CHEMICAL TESTS[b]								
Agricultural Soil Designation	**Exchangeable Basic Cations (ppm)**	**Soluble Salts (mmho/cm)**	**ECe (mmho/ cm)**	**Extractable Salt (@ 66-68% H_2O saturation-ppm)**	**Soil pH**	**CEC (meq/ 100g)**	**Sodium Adsorption Ratio (SAR)**	**Exchangeable Na Percentage (ESP)**
Saline/ Non-sodic	Ca: 2,270 Mg: 786 K: 14 Na: 5	5.49	71.0	Ca: 657 B: 0.0 Mg: 1,316 K: 6.0 Na: 15 Cl: 23 S: 9,608	1:1 soil-water: 2.2; Saturated paste: 2.0	29.04 by Na-acetate 71.4 by summation	0.1	0.0
WOODBURY EXPANSIVE SOIL RATINGS, % VOLUME CHANGE, AND METHOD REFERENCE								
Ac: 0.5 **CEA_c: 0.8**	**A_c: 0.5** **% clay (<2μm): 38%**	**A_c: 0.5**	**PI: 18.6%**	**SI: 7.7%**	**PI: 18.6%** **SI: 7.7%**	**SL: 18.0%**	**%<1μm: 30%** **PI: 18.6%** **SL: 18.0%**	**%<75μm: 96%, LL: 44.3%; SPR: 20-30 blows/ft (estimated)**
Moderate	Low 1.5%	Low	Moderate	Low	Low-Moderate <12-23%	Low <0.5%	Low-Moderate <10%	High 20-30%
McKeen and Hamburg (1981); Hamburg (1985)	Seed et al. (1962)	Skempton (1953)	Chen (1988)	Ranganatham and Satyanarayana (1965)	Raman (1967)	Altmeyer (1955)	Holtz and Gibbs (1956)	Chen (1965)

[a] Proctor test results were adopted from Demetacopolous et al. (1986); SL test was performed by NTH Consultants; hydraulic conductivity result was adopted from personal communication with B&J Warren and Sons (1994); all other tests were performed at NJIT laboratories.

[b] Chemical tests were performed by Servi-Tech Laboratories; Results represent an average of two samples submitted following the preparation step.

LL-liquid limit, PL-plastic limit, SL-shrinkage limit, PI-plasticity index, SI-shrinkage index, USCS-Unified Soil Classification System, K-hydraulic conductivity, ECe-electrical conductivity, CEC-cation exchange capacity, Ac-Activity, CEA_c-cation exchange activity, SPR-standard penetration resistance

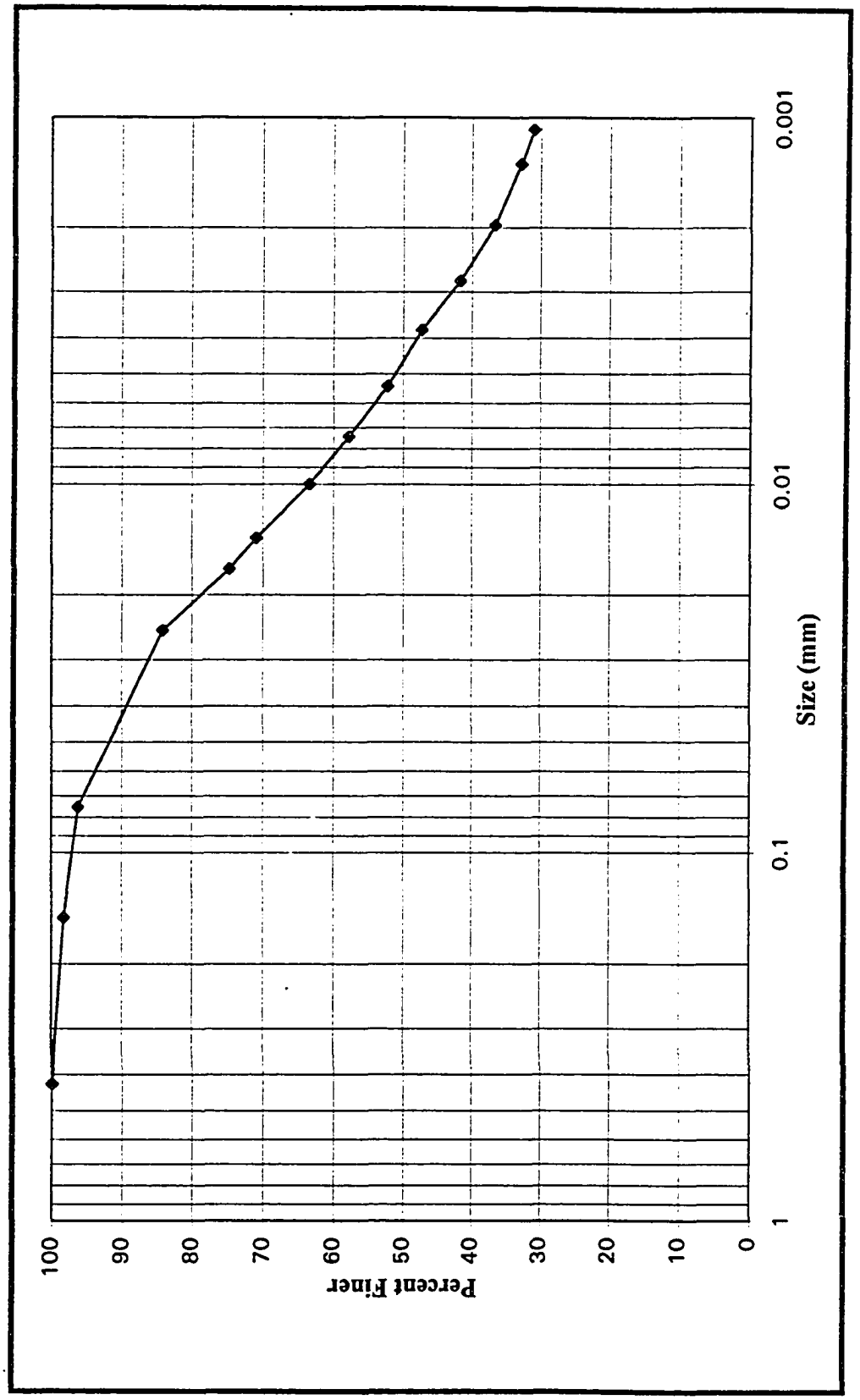

Figure 3.6 Grain Size Distribution of Woodbury Formation.

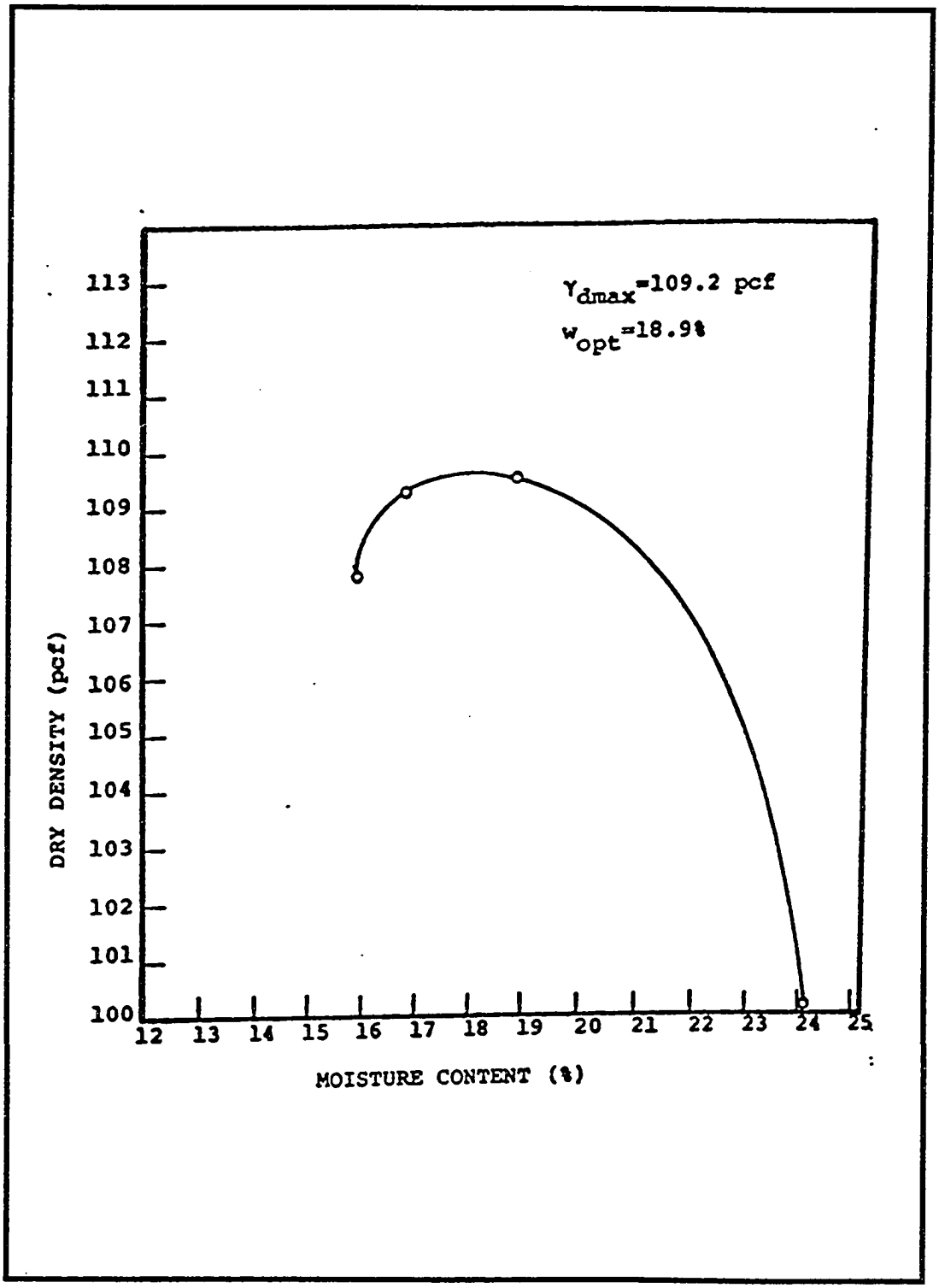

Figure 3.7 Moisture-Density Relationship for the Woodbury Formation. From Demetracopoulos et al. (1985).

Prepared batches were stored in plastic bags in an environmental chamber maintained at 60% humidity, and were allowed to equilibrate by diffusion for at least one week prior to use. Moisture contents were determined in triplicate prior using ASTM procedures.

3.2.2 Setup of Rigid, Confined Horizontal Infiltrometer Tests

The first attempt to model fracture flow through a natural soil utilized a rigid, Proctor mold cylinder. Soil was compacted into the cylinder around a metal plate which was then removed to create an open fracture. The ends of the cylinder were equipped with filters, allowing the fracture full access to flow. The cylinder was enclosed by steel end plates, sealed with neoprene gaskets and high vacuum grease, and secured by four tie rods and nuts. Holes in each of the end plates served as the inlet and extraction points. A schematic of the setup of the rigid, confined device is provided in Figure 3.8.

The filters fit tightly in each end of the cylinder and were composed of a No. 200 screen (0.075 mm) on one side and 1/16 in. diameter holes on the other. The filter was filled with gravel to provide a high permeability, high porosity substrate to maximize air flow. A schematic of the cylinder, end plates and filters are provided in Figure 3.9.

Limitations of the device were numerous and varied, resulting in design and fabrication of a second device, as described in the next section. During experimental runs, drying caused considerable soil shrinkage and transverse soil cracking, thus limiting the device to increasing moisture applications only. In addition, packing was difficult and time-consuming, and filters often caused deformation of the fracture resulting in abandonment and repacking.

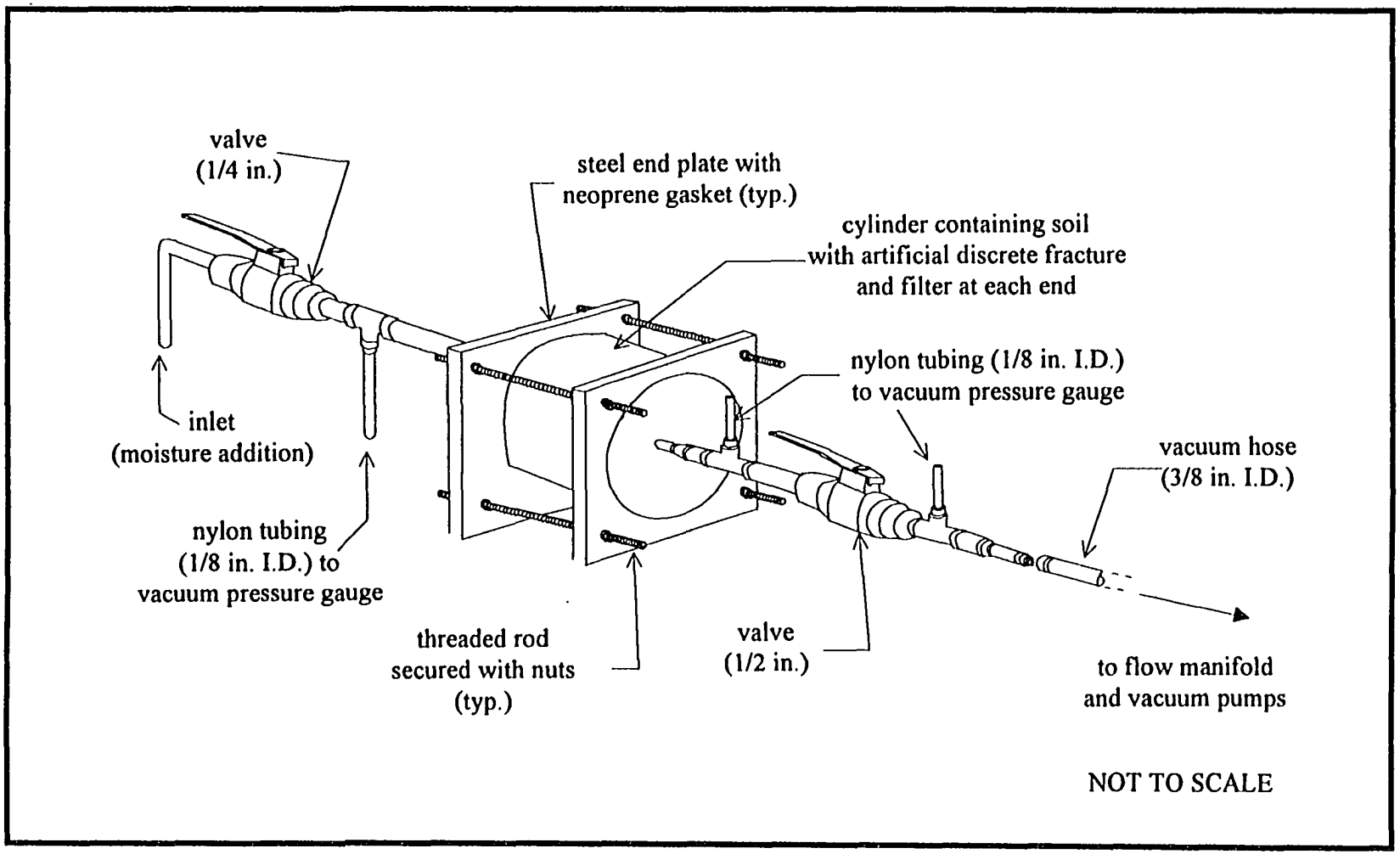

Figure 3.8 Setup Schematic of Rigid, Confined Horizontal Infiltrometer Device.

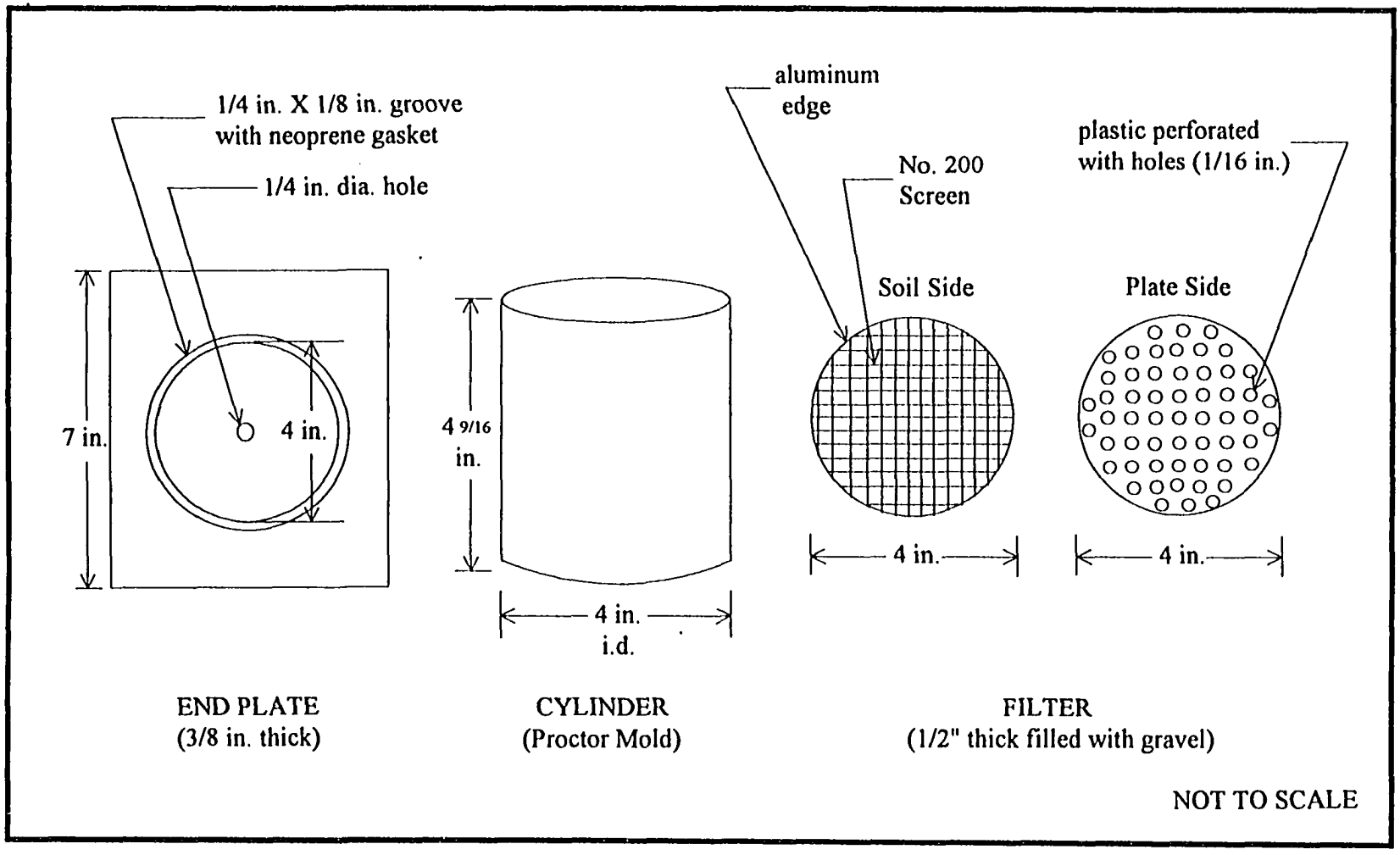

Figure 3.9 Plate, Cylinder, and Filter Dimensions for Rigid, Confined Horizontal Infiltrometer Device.

3.2.3 Setup of Semi-Confined Horizontal Infiltrometer Tests

A second horizontal infiltrometer device was designed to overcome the limitations experienced with the rigid, confined horizontal infiltrometer. The new device, termed the "semi-confined horizontal infiltrometer" was designed with lateral confinement only, with provisions for its addition and removal as needed. The new device utilized a larger soil sample to isolate the boundaries of the fracture from outside influences. The length of the fracture was also increased to promote laminar flow conditions. A schematic of the setup of the semi-confined horizontal infiltrometer is shown in Figure 3.10.

The device consisted of an aluminum box (12 in. wide, 16 in. long, and 4 in. high) with notches (4 in. wide by 3 in. high) cut at the ends of the box. Pieces of plywood (16 in. length) were used as lateral confinement spacers along the length of each side of the box. Three sets of removable wedges were placed along the length of the box, and when unbolted allowed for easy removal of lateral confinement.

The test soil was packed into the box between the plywood spacers and wedges around a metal strip. The strip was then removed to create an open fracture. Two copper pipe sections (3 in. diameter and width), sharpened on one end, were then driven into the soil around the fracture at the end notches. The natural clay soil provided a tight seal around the pipe. A series of fittings were then attached to each pipe. These included valves for vacuum tightness checks, quick disconnect fittings to allow for the addition of moisture, and fittings to attach Magnehelic vacuum pressure gauges.

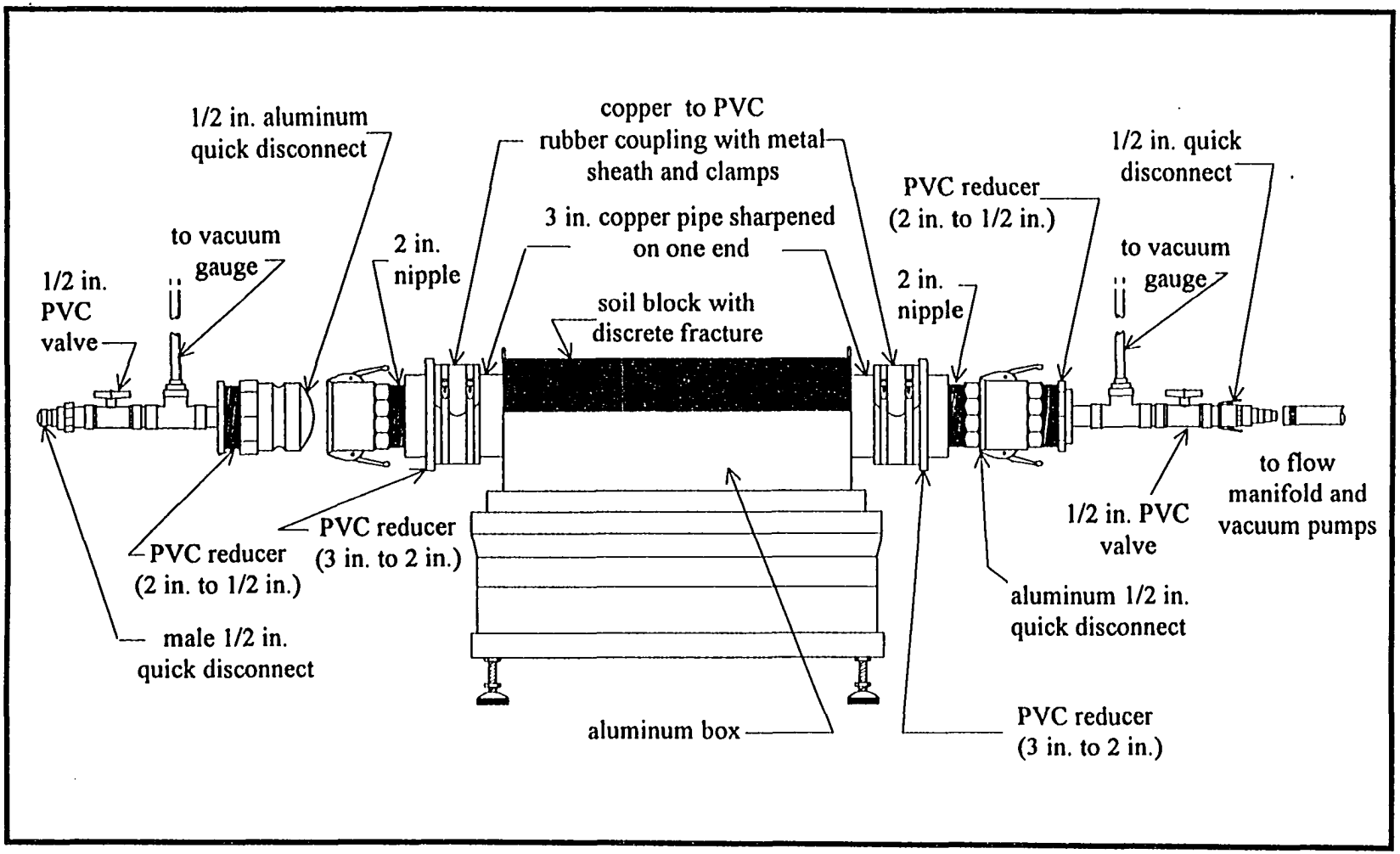

Figure 3.10 Setup Schematic of Semi-Confined Horizontal Infiltrometer Device.

A vacuum hose (3/8 in. diameter) connected the device to the flow manifold and vacuum pumps, which were previously described in the setup for the linear controls. The device was mounted on a scale to determine fluctuations in weight. Lateral confinement of the soil block was controlled with the removable plywood spacers and wedges.

3.2.4 Operation

Prior to an experimental run, the horizontal infiltrometers were tested for vacuum tightness. Flow was then induced through the simulated fracture by adjusting the pressure differential. All tests were run under a passive inlet condition, with the inlet end open to the atmosphere. Differential pressures were maintained as alternating sets of moist and dry air were pulled through the fracture. The flow rate and pressure at the extraction point were measured and recorded. A number of tests were run to refine the design and to improve the methods of inducing environmental changes. A more detailed discussion of the operational conditions and modifications performed are described in Chapter 4.

CHAPTER 4

EXPERIMENTAL RESULTS AND DISCUSSION

In accordance with the experimental approach outlined in Chapter 3, tests were performed with the control devices to investigate idealized fracture flow, and also with the horizontal infiltrometers filled with natural soil to investigate the mechanism of volume change. This chapter presents and discusses the results of these tests.

4.1 Linear and Radial Control Tests

The results of the linear and radial control tests are presented in this section and are organized into a discussion of flow conditions in the fracture (4.1.1), calculated effective apertures (4.1.2), effect of fluid compressibility (4.1.3), and effect of entrance geometry (4.1.4). Sample control data are provided in Appendix B and sample calculations are presented in Appendix C.

4.1.1 Flow Conditions

Flow of a fluid in a fracture may be of either laminar or turbulent type, depending on the fluid properties and the conditions prevailing in the fracture. Since the cubic law is valid only for laminar conditions, an analysis of the flow conditions during the control tests was essential for data analysis.

Flow conditions were evaluated by calculating Reynolds number, Re,

$$Re = \frac{2 \cdot b_e \cdot V}{\nu} \tag{4.1}$$

where b_e is the effective fracture aperture (as defined in the next section), V is the flow velocity, and ν is the kinematic viscosity (Lomize, 1951; Louis, 1969). Flow velocity is given by,

$$V = \frac{Q_s}{A} \tag{4.2}$$

where Q_s is the flow rate under standard conditions, and A is the area of the fracture. Sample calculations of flow velocity and Reynolds number for the linear and radial flow geometries are presented in Appendix C.

Flow in smooth planar fractures begins to deviate from laminar flow conditions at a Reynolds number of 1,800, but does not become completely turbulent until a Reynolds number of 4,000 is exceeded (Huitt, 1956). Data at low Re numbers were not included in the analysis because flow has not yet become laminar and because of inaccuracy of the lower ranges of the pressure and flow measurement systems.

For the linear controls, the flow velocities and Reynolds numbers were computed using experimental flow rates and calculated effective apertures at the extraction point. Results of the analysis on the linear control data are shown in Figure 4.1. Flow were generally laminar for all three plate lengths, and transitioned into the partially turbulent zone as aperture size increased and plate size decreased. It is also apparent that the effects of aperture size were more substantial than the effects of fracture length.

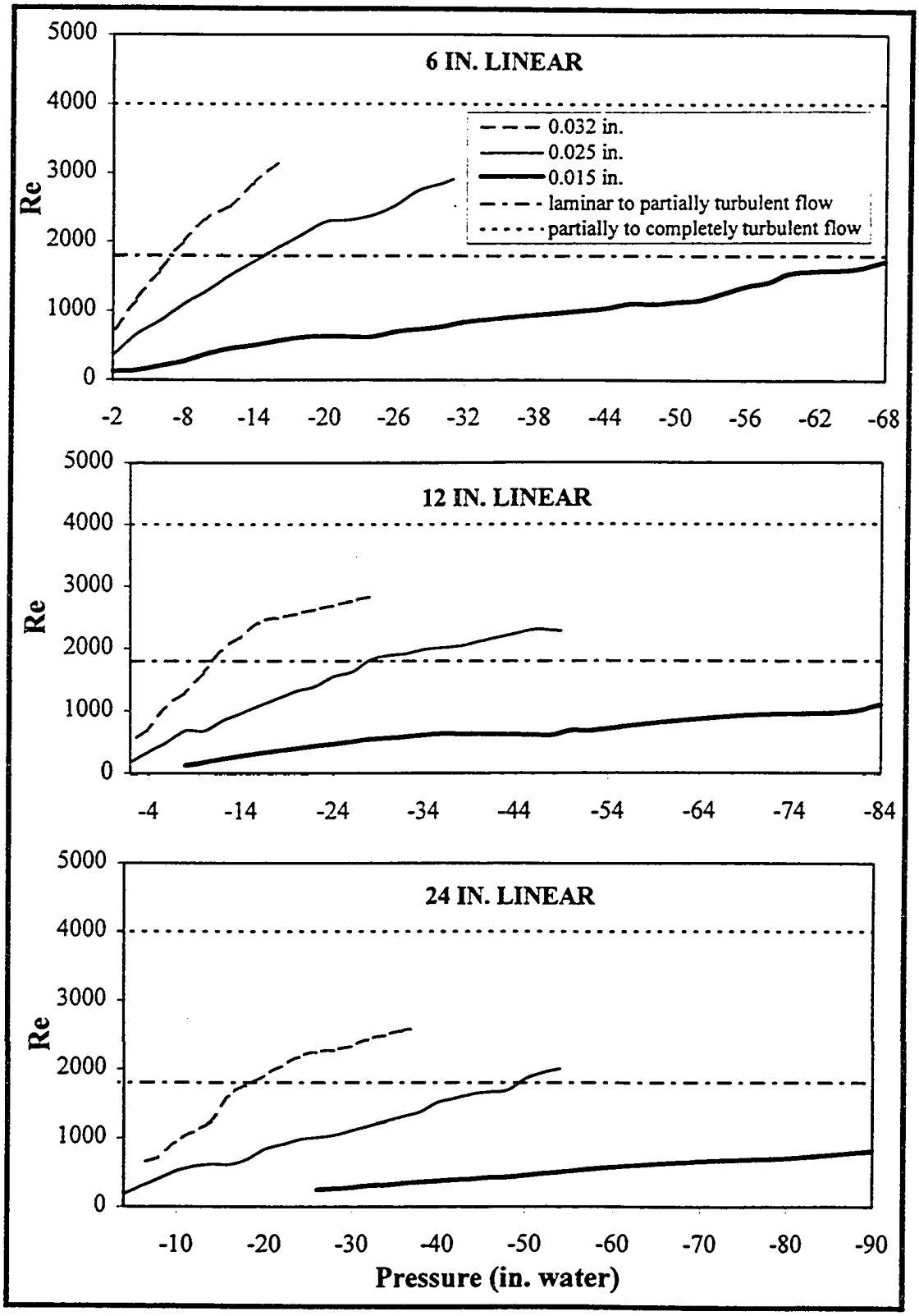

Figure 4.1 Flow Conditions for Linear Control Tests.

Complete turbulence (i.e., Re>4,000) did not occur in the linear control tests at the pressures achievable by the vacuum source. Although the flow began to transition from laminar to turbulent flow, aperture exponents for data with Re>1800 were consistently computed to be 3.0 using the average effective aperture, suggesting that flow was not measurably turbulent. For turbulent flow, exponent of the fracture aperture for parallel plates reduces from 3 (laminar conditions) to an exponent as low as 1.5 (Sharp and Maini, 1972). Further investigation of turbulence with the control devices would require an increase in vacuum pressure and/or an increase in fracture surface roughness.

Under radial flow configurations, the Reynolds number varies with the radius from the extraction point. Flow velocities and Reynolds numbers were computed for the radial control tests using experimental flow rates and calculated effective apertures at the extraction point with increasing radii. Results of the Reynolds number computations for the radial control tests are presented in Figure 4.2 for a negative pressure differential of 16 in. water. As seen in the figure, fluid flow conditions in the immediate vicinity of the extraction point extended far into the turbulent region, due to the high converging velocities. However, since laminar flow conditions prevail in the vast majority of the fracture, there was no observable effect on the aperture exponent. As expected, Reynolds number increased as the width of the aperture increased and the radial diameter decreased.

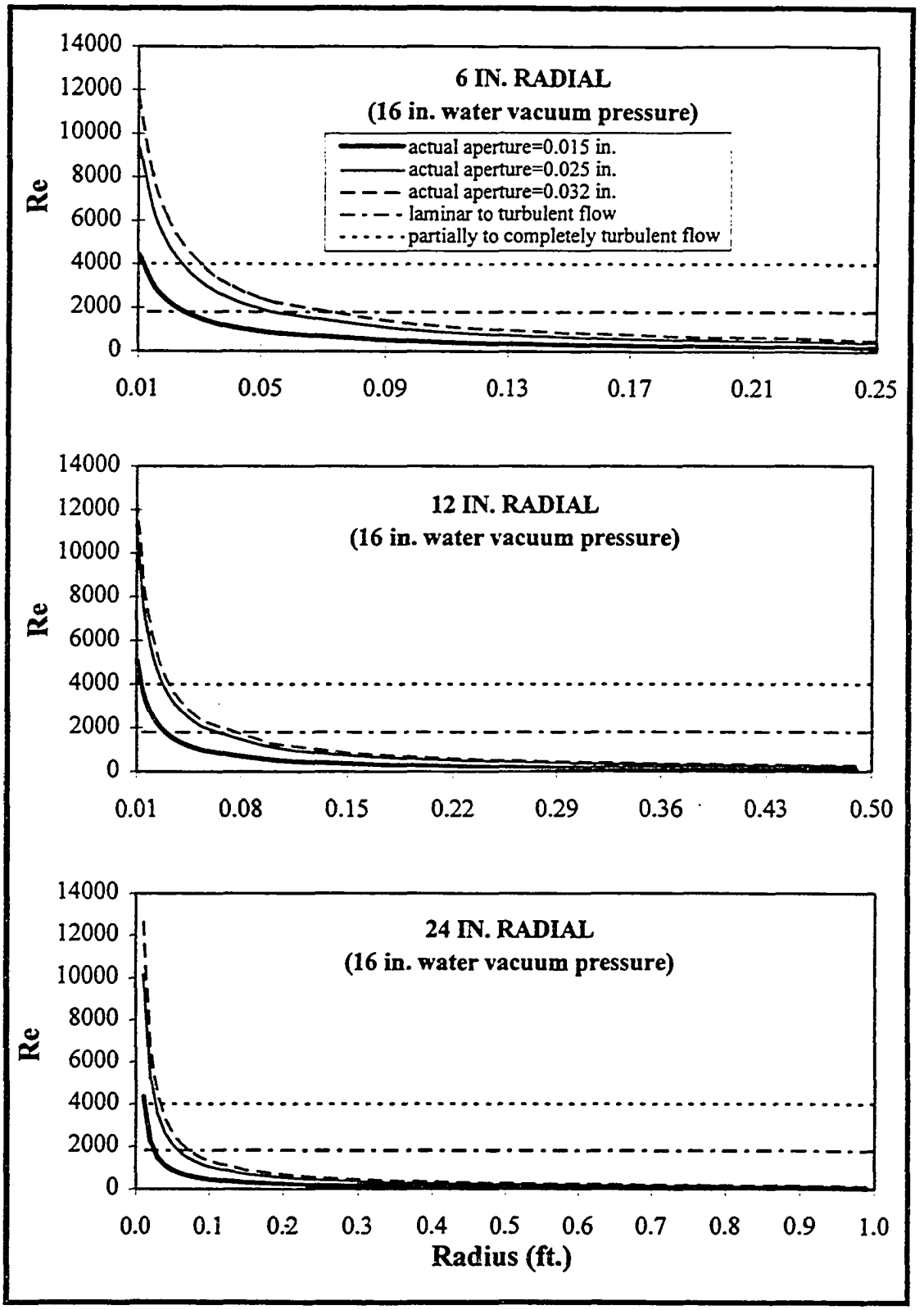

Figure 4.2 Flow Conditions for Radial Control Tests.

4.1.2 Calculated Effective Apertures

Using experimental flow rates and pressures under laminar flow conditions, experimental apertures were computed using the cubic law. The calculated experimental apertures are termed effective apertures because they represent the average aperture over the area of the fracture. The concept of an effective aperture, b_e, was originally developed by Wilson and Witherspoon (1970) who defined effective aperture as a series of "m" discrete segments, each with a different aperture, as follows:

$$b_e^3 = \frac{\sum_{i=1}^{m} l_i}{\sum_{i=1}^{m} (l_i / b_i^3)} \qquad (4.3)$$

where l_i is the length of the fracture segment which has an aperture of b_i. Thus, effective aperture reflects the variations and imperfections in the real fracture.

Calculated effective apertures (b_e) as compared with actual apertures (b_a), which were controlled by the sheet metal spacers, are presented in Figures 4.3 and 4.4, for the linear and radial control tests, respectively. Effective apertures were consistently seen to be less than actual apertures, particularly as length and diameter of the plates increased and aperture width decreased. Effective apertures averaged 84-87% lower than actual apertures for the linear control data, and 50-73% lower for the radial control data.

Localized deformation of the plastic plates was probably a significant factor in the deviations of effective aperture from actual aperture, particularly for the radial flow control devices. Apertures were further obstructed in the radial control devices by the sheet metal spacers, where the number of spacers increased as plate diameter increased.

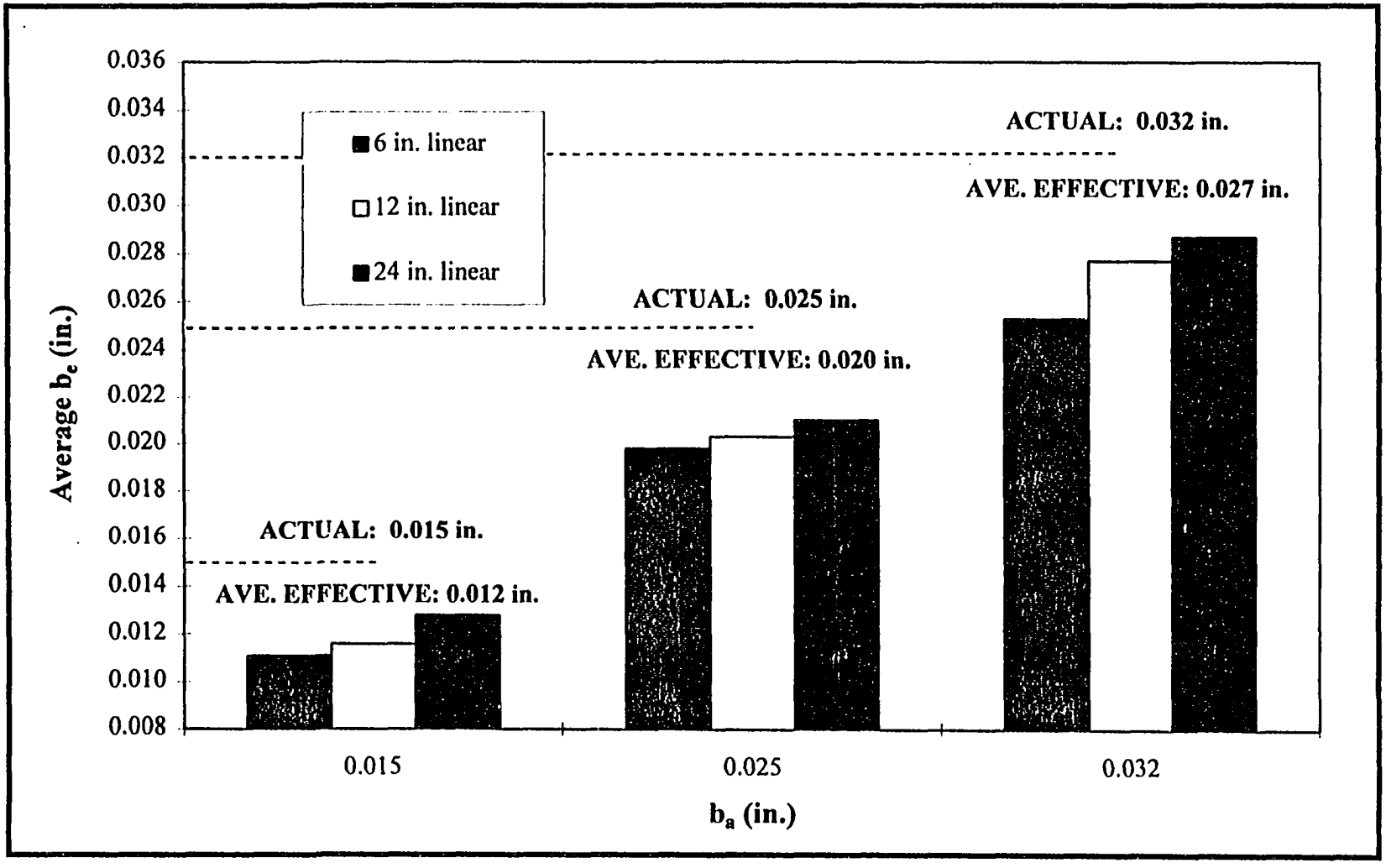

Figure 4.3 Comparison of Effective and Actual Apertures for Linear Control Tests.

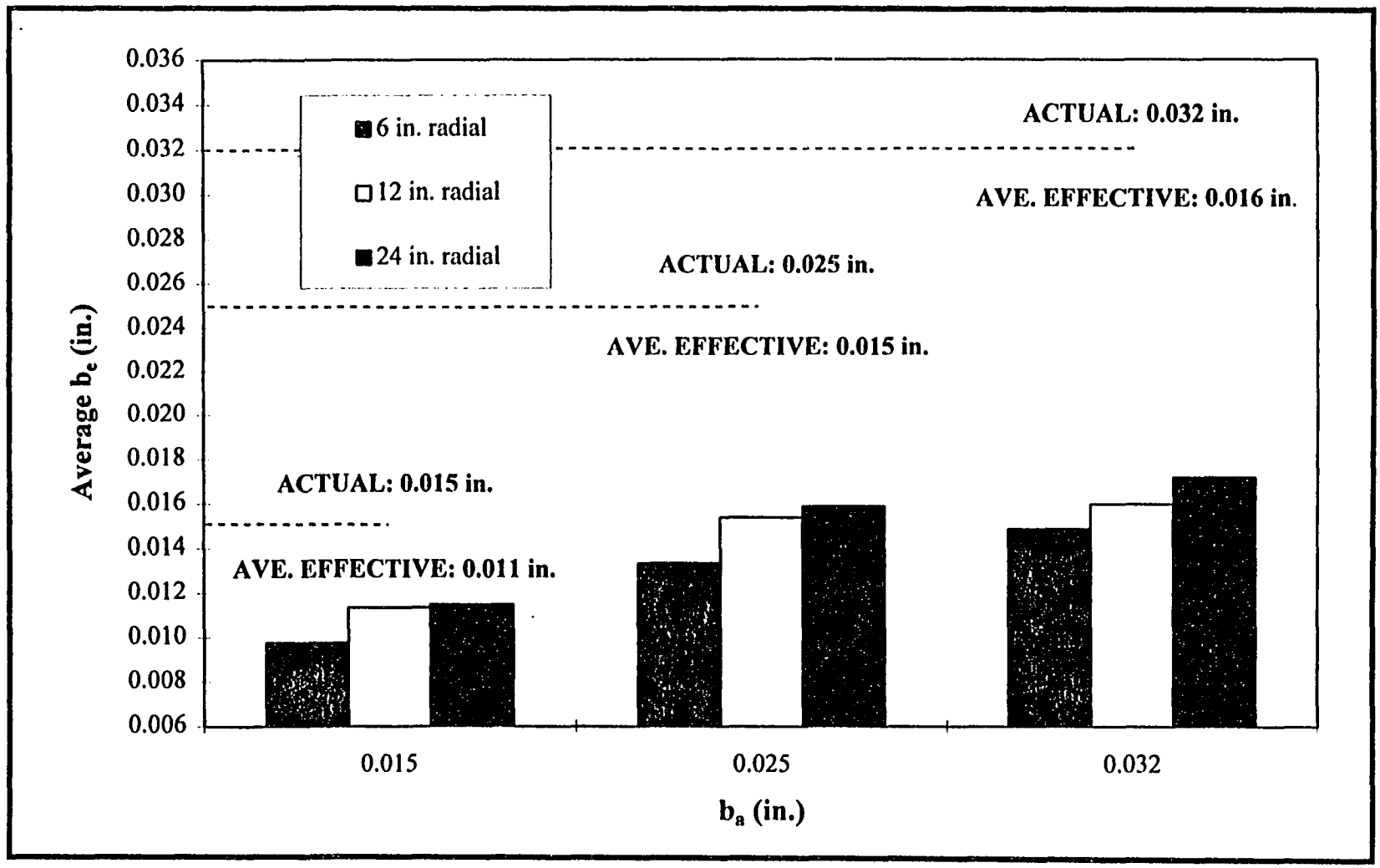

Figure 4.4 Comparison of Effective and Actual Apertures for Radial Control Tests.

Friction losses and minor losses also tended to decrease the apparent aperture. These included friction along the plate surfaces, entrance losses, exit losses, and losses associated with enlargements and constrictions. It is noted that the 0.25 in. extraction hole for radial control devices was probably undersized resulting in a significant constriction. This will be enlarged to 1 in. or more for future testing.

4.1.3 Effect of Fluid Compressibility

The data within the laminar flow region were used to determine the effect of gas compressibility on effective aperture. Figures 4.5 and 4.6 compares the normalized effective aperture, b_e/b_a, computed with and without the gas compressibility term. Although relatively minor deviations were seen at the low pressure differentials used for these experiments, the differences were consistently measurable. Effects of gas compressibility will increase as the pressure differential increases. Thus, when dealing with fluid flow of a compressible fluid in a discrete fracture, the gas compressibility term should be included when applying the cubic law. Calculations on all control data for this research accounted for the effects of gas compressibility unless otherwise stated.

4.1.3 Effect of Entrance Geometry

Results of radial control tests with square edges as compared with results of equivalent tests using round edges is shown in Figure 4.7. As expected, the calculated effective aperture for tests performed with round edges more closely approximated the actual aperture than results of equivalent tests using square edges. Data collected with rounded edges were used to present all radial control data for this research unless otherwise stated.

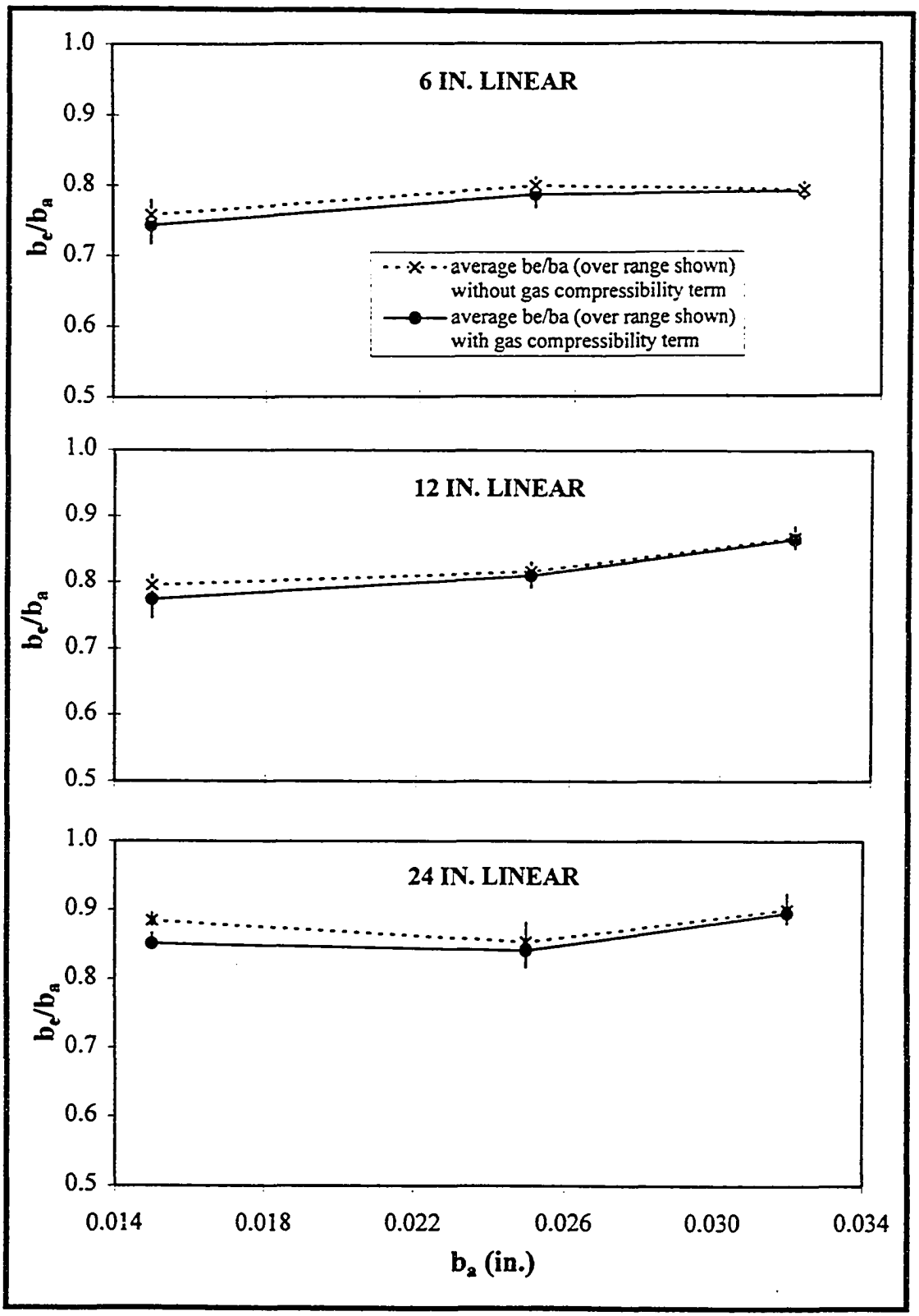

Figure 4.5 Effect of Gas Compressibility on Linear Control Data.

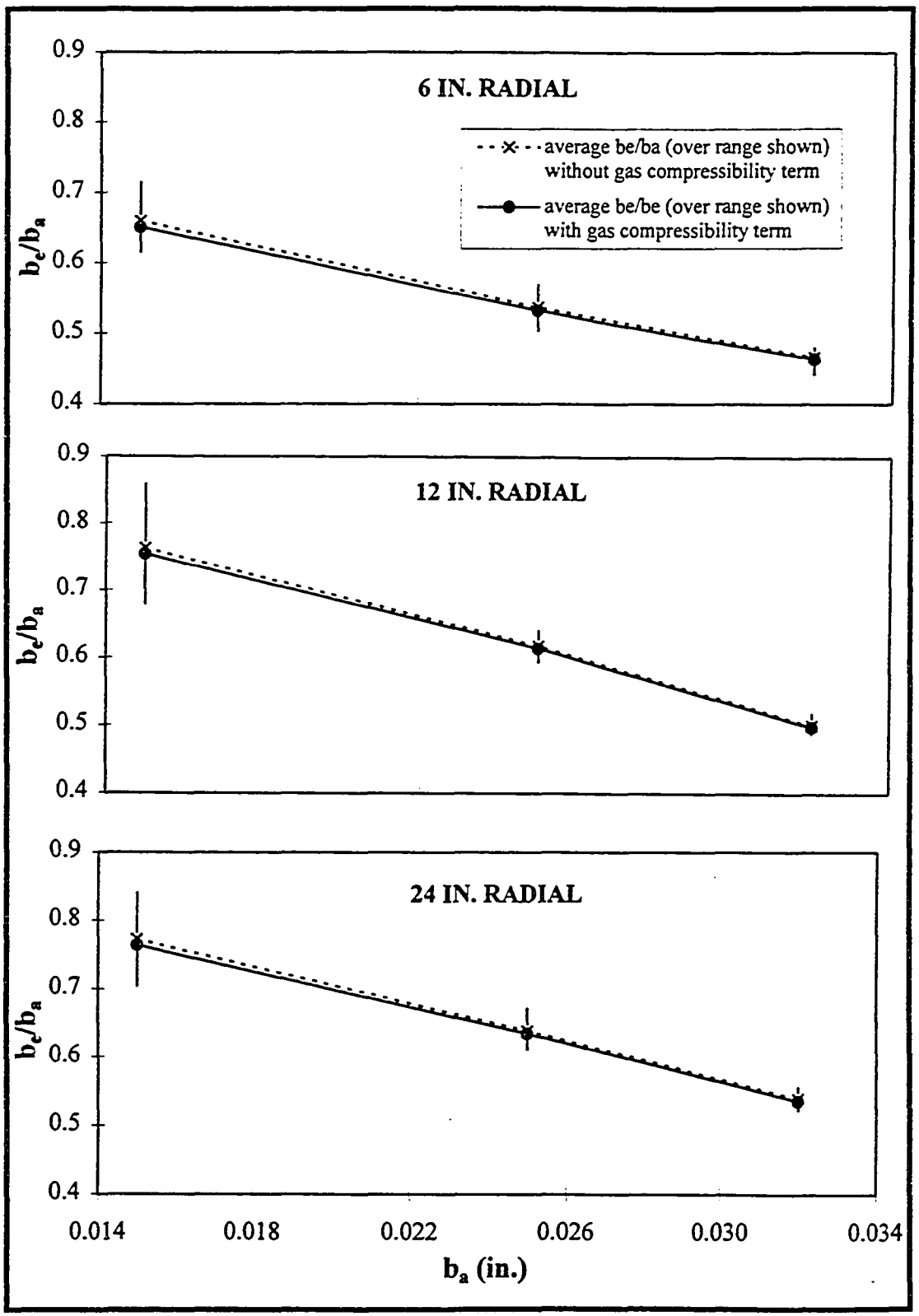

Figure 4.6 Effect of Gas Compressibility on Radial Control Data.

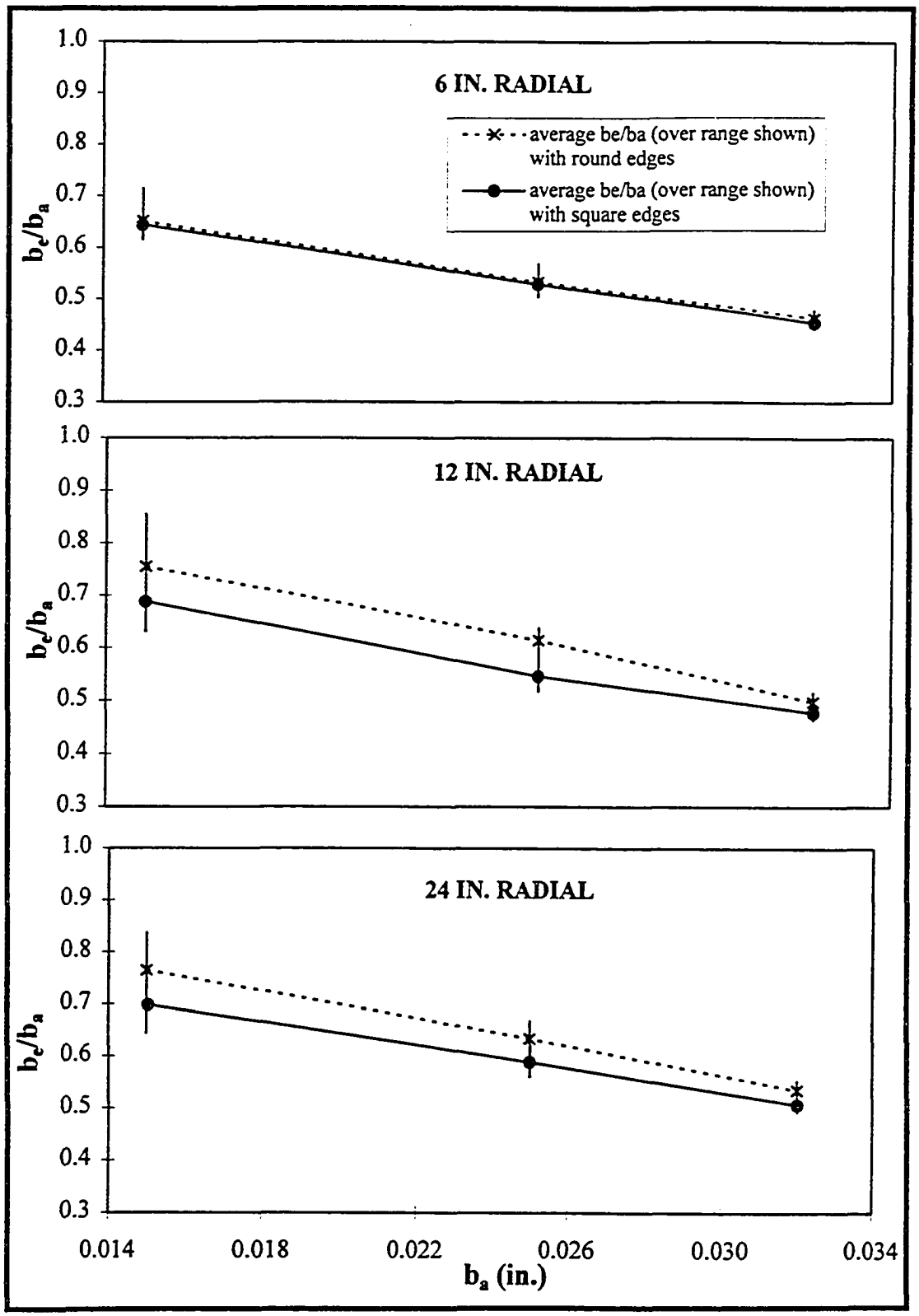

Figure 4.7 Effect of Square and Round Entrance Geometries on Radial Control Data.

4.2 Horizontal Infiltrometer Tests

Tests performed on the control devices, as described in the previous section, were used to investigate idealized flow through a discrete fracture. These results were essential for interpreting the results of the horizontal infiltrometer tests with natural soil, since aperture can only be determined indirectly by monitoring flow rate and pressure. An additional complication associated with natural soil is that the fractures are not parallel or smooth, and contain asperities. Flow patterns are also not restricted to fracture flow but include flow through the porous media, a situation typically modeled using a dual porosity approach. This section provides results and discussion of the horizontal infiltrometer tests using the rigid, confined device (4.2.1) and the semi-confined device (4.2.2).

4.2.1 Rigid, Confined Horizontal Infiltrometer

The rigid, confined device was a first attempt at inducing artificial fractures in natural soil and then monitoring volume changes. A total of three tests were performed, and modifications were made to the experimental methods and equipment after each test. A summary of the test runs, results, and modifications is presented in Table 4.1, and the experimental data are contained in Appendix D.

The major limitation of the device was the occurrence of significant radial soil shrinkage and transverse soil cracking, thus limiting its use to increasing moisture applications only. In addition, packing was difficult and time-consuming, and end filters often deformed the fracture resulting in abandonment and repacking. The humidifiers and water slugs were also found to be inadequate. One positive outcome was the establishment of a vacuum system which provided good pressure and flow control.

Table 4.1 Summary of Rigid, Confined Horizontal Infiltrometer Tests

Test No.	Initial Conditions	Run No.	Run Description	Results	Modifications
1	Dry Density: 93.9 lb/ft^3 Moisture Content: 30.0 wt% Initial Aperture: 0.0394 in.	A	Small vacuum pump with dry air for 143 hrs.	Flows increased from 5 l/min (18.5 in. Hg) to 12 l/min (12.0 in. Hg)	Small pump and building vacuum not dependable vacuum sources-try larger pumps that provide greater range and steady flow. Cool humidifier does not hold enough moisture-discontinue use. Reject direct water addition due to erosion problems. Best method for moistening soil is warm humidifier-maintain usage. Pressure differential was not held constant. Test No. 1 used to set up system-identify vacuum source and method of moistening soil. Data are preliminary.
		B	Small vacuum pump with cool humidifier for 51 hrs.	Flows leveled out at 12 l/min (12.5 in. Hg)-then suspected breakthrough-flows increased to 1 CFM (1.0 in. Hg)	
		C	Building vacuum with direct addition of water (2-8 oz. slugs) for 32 hrs.	Flows decreased from 1.5 CFM (2.5 in. Hg) to 1.1 CFM (7.0 in. Hg); soil erosion occurred on moisture inlet end	
		D	Building vacuum with warm humidifier for 142 hrs.	Flows increased from 1.25 CFM (3.5 in. Hg) to 1.75 CFM (3.25 in. Hg)	
2	Dry Density: 95.1 lb/ft^3 Moisture Content: 25.1 wt% Initial Aperture: 0.0394 in.	A	Two large vacuum pumps in parallel with warm humidifier, no electronic mass flow meter	Flows decreased from 36 CFH (47 in. H_2O) to 3.5 CFH (50 in. H_20); flows fluctuated up to 2.2 CFM due to inconsistent moisture from humidifier	Large vacuum pumps provide a steady vacuum source with a large range-maintain usage. Apparatus is limited to moistening; rigid cylinder does not conform to soil as it shrinks during drying. System not vacuum tight-try sealing device with silicone. Verify flow through fracture by terminating test in moist state and observe soil. Pressure differential not held constant-data are considered preliminary.
		B	Two large vacuum pumps in parallel with dry air, no electronic mass flow meter	Flows increased from 2.5 CFH (50 in. H_20) to 2.2 CFM (16 in. H_20); an annular space of 1mm was apparent between the cylinder and the soil due to shrinkage; measured flows do not represent flow through fracture	
3	Dry Density: 95.1 lb/ft^3 Moisture Content: 25.1 wt% Initial Aperture: 0.0394 in.	A	Two large vacuum pumps in parallel with warm humidifier, no electronic mass flow meter, silicone bead installed at contact between cylinder and end plates to provide seal; pressure differential held constant	Flows decreased from 20 CFH to 3-4 CFH at 48-49 in. H_2O; ended in moist state and found no annular space-fluid is believed to be traveling through fracture; filter collapsed a portion of the fracture; water was pooling at bottom of the cylinder	The pressure differential was not held constant-difficult to analyze data. Vacuum tightness still not obtained; all fittings should be caulked. A drain plug should be installed for removal of pooling water. Reinstall electronic mass flow meter when manufacturers calibration is complete for dual flow measurements.

Overall, the rigid, confined horizontal infiltrometer tests were valuable since they verified that volume changes could be induced and controlled in natural soils which contained an artificial fracture. In addition, it was determined that monitoring flow rate under a constant pressure differential is the best indicator of aperture change. Nevertheless, it was decided to develop an entirely new horizontal infiltrometer device to allow greater experimental versatility and control. The test results with this new device, called the semi-confined horizontal infiltrometer, are described in the next section.

4.2.2 Semi-Confined Horizontal Infiltrometer

A total of four tests were performed using the semi-confined horizontal infiltrometer device. These were limited to development and calibration testing only, and modifications were made to the experimental methods and equipment after each test. A summary of the test runs, results, and modifications is presented in Table 4.2, and the experimental data are contained in Appendix D.

The tests involved cycles of constricting aperture through moisture addition and reopening apertures by drying. Changes in aperture width over time were indicated by changes in flow rate under a constant pressure differential. The tests generally ran for one week with down times occurring each day during evening hours. Of the four tests, results of the three successful tests are shown graphically in Figures 4.8, 4.9, and 4.10. It should be noted that down times are represented only by day boundaries and were not included in the cumulative time scale.

Table 4.2 Summary of Semi-Confined Horizontal Infiltrometer Tests

Test No.	Initial Conditions	Packing Comments	Modifications from Previous Test	Run No.	Run Description	Results	Suggested Modifications
1	Moderate Dry Density Moisture: 25.1 wt% Initial Aperture: 0.0394 in.	Copper pipe broke away from soil when lifted without support	Two large vacuum pumps connected in parallel; added electronic mass flow meter.	A	Moistened with warm humidifier for 17 hours (bounded)	Net drying-flows increased from 2.3-2.4 (24 in. H_2O) to 3 CFM (10 in. H_2O); large crack developed in block (tension crack)	Too much surface cracking-increase soil above fracture; reduce infiltration into soil; improve leak tightness of fittings and add provision for vacuum testing soil block
2	Moderate Dry Density (estimated at 99.3 lb/ft^3) Moisture Content: 25.1 wt% Initial Aperture: 0.0394 in.	Not packed to a certain density-packed using moderate effort	Height of soil above fracture increased 1 in; plastic wrap used to cover soil block; resealed fittings. Provisions made in fittings to seal off soil block to measure rate of leak-in; first vacuum pressure tests on soil block	A	Moistened with warm humidifier for 1.9 hrs. (bounded)	Flows decreased from 33 to 10 CFH at 46-50 in. H_2O in 35 min. and held constant for 80 min.	Discontinue use of humidifier (unsteady supply of moisture with an uncontrollable rate)
				B	Dried for 3.3 hrs. (bounded)	Flows increased from 10 to 50 CFH at 46-50 in. H_2O	Increase the vacuum potential to aid in drying out soil
				C	Moistened for 1.5 hrs. with periodic, mist from spray bottle (bounded)	Flows decreased from 50 to 9 CFH at 46-50 in. H_2O in 1st hr. and stabilized for 30 min.	Discontinue use of spray bottle mist (need more continuous supply at constant rate)
				D	Dried for 1.8 hrs. after 55 hrs. of moisture diffusion (bounded)	Flows increased from 9 CFH (53 in. H_2O) to 2.3-2.4 CFM (28 in. H_2O)	
				E	Dried for 66 hrs. after 41 hrs. saturation with 1 ft hydraulic head (bounded)	Flows decreased to 4-10 CFH at 49 in. H_2O. Soil eroded by water; wet soil (2 in.) was pulled into pipe by vacuum	Discontinue use of direct hydraulic head saturation (soil too wet); need easier method of block removal.

(continued on next page)

Table 4.2 Summary of Semi-Confined Horizontal Infiltrometer Tests (Continued)

Test No.	Initial Conditions	Packing Comments	Modifications from Previous Test	Run No.	Run Description	Results	Suggested Modifications
3	Low Dry Density w/crumb structure (estimated at 96.8 lb/ft^3) Moisture: 24.1 wt% Initial Aperture: 0.0394 in.	Attempted to match Test 2 density, but plates shifted during compaction resulting in under-packing	Vacuum pumps connected in series; fittings resealed and caulked and tightness tested; fabricated wedges and acrylic plastic; use of continuous, variable flow rate spray nozzle; used plumbers putty to seal areas of potential leak	A	Moistened with continuous spray nozzle for 12.3 hrs. (unbounded)	Flows decreased from 1.5 CFM to 43-44 CFH at 50 in. H_2O; flows then fluctuated up and down -significant infiltration into soil	Pack at higher density and continue covering with plastic to minimize leak-in; continue with use of plumbers putty to seal off areas of potential leaks
				B	Dried out for 2.3 hrs.-took moisture content samples (unbounded)	Flows increased from 3.4 to 4.0 CFM at 50 in. H_2O	
4	Moderate to High Dry Density (101.0 lb/ft^3) Moisture Content: 24.1 wt% Initial Aperture: 0.0394 in.	Compacted to minimize porosity, cut to square dimensions for better volume estimation	Monitored leak through soil block during drying; bounded and unbounded block to control amount of infiltration	A	Moistened with continuous spray nozzle for 3.9 hrs. at 6-30 ml water/min. (bound on one side)	Flows decreased from 2.9 CFM to 5 CFH at 40 in. H_2O	Replace 1/2 in. valve on moisture inlet end with a 2 in. valve; will allow for moistening through valve and monitoring leak through soil during moistening. In addition, remove quick disconnect; use causes the seal between the soil and the copper pipe to weaken. Quick disconnect was originally added to allow for addition of hydraulic head which is no longer needed. Increase height of aluminum box to allow for more accurate volume measurements for dry density calculation.
				B	Dried out for 24.5 hrs. (alternate bounding and unbounding)	Flows increased to 2.6 CFM with 0.4 CFM leak through soil at 40 in. H_2O	
				C	Moistened with continuous spray nozzle for 2.8 hrs. at 2-18 ml water/min. (unbounded)	Flows decreased to 10 CFH at 40 in. H_2O in 1.8 hrs. and remained at this flow for remaining hour	
				D	Dried out for 18 hrs. & test terminated (alternate bounding and unbounding)	Majority of the fluid flow occurring from leak-in through soil-flows rose to 0.4-0.7 CFM at 40 in. H_2O	

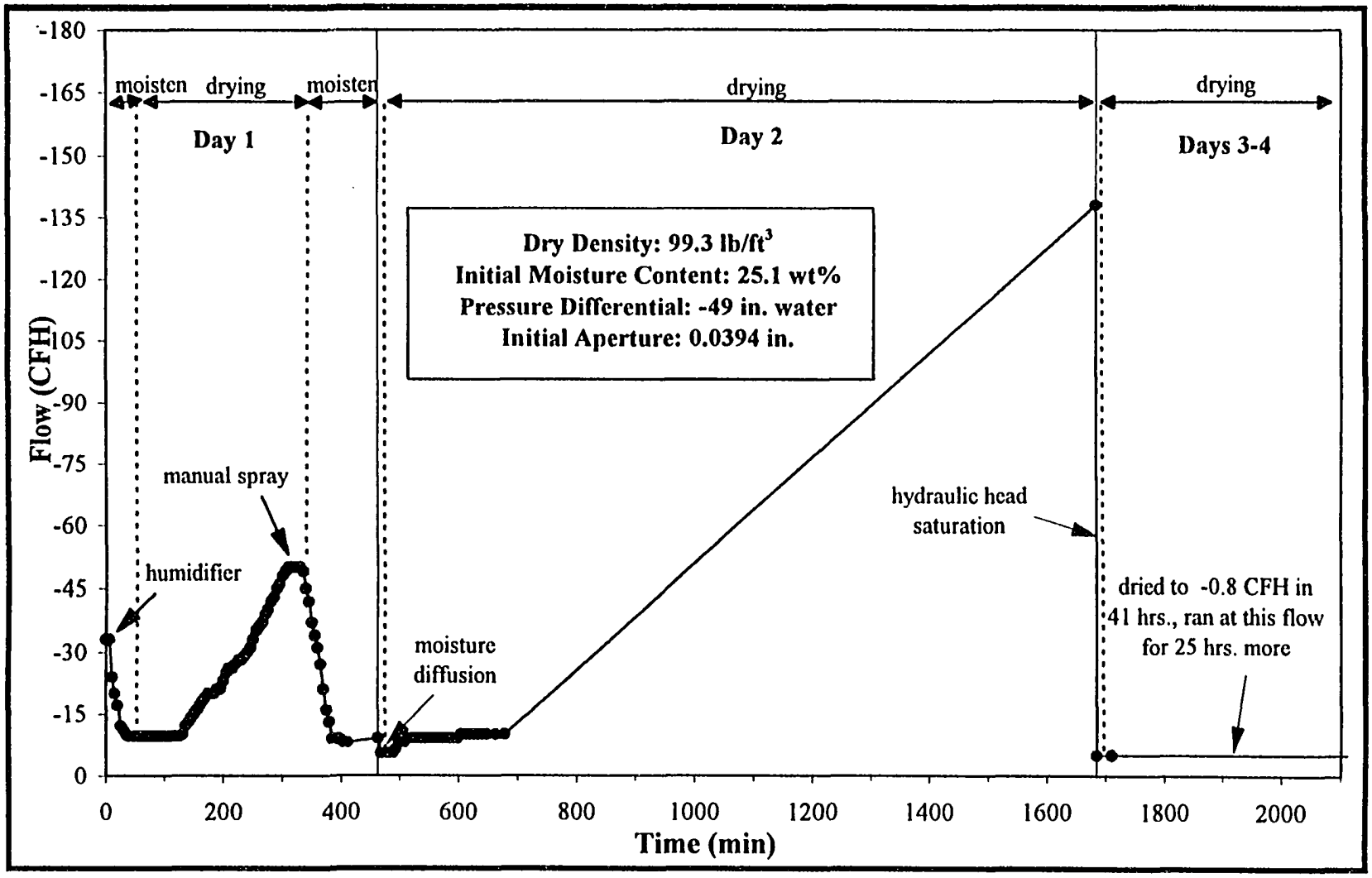

Figure 4.8 Results of Semi-Confined Horizontal Infiltrometer Test No. 2.

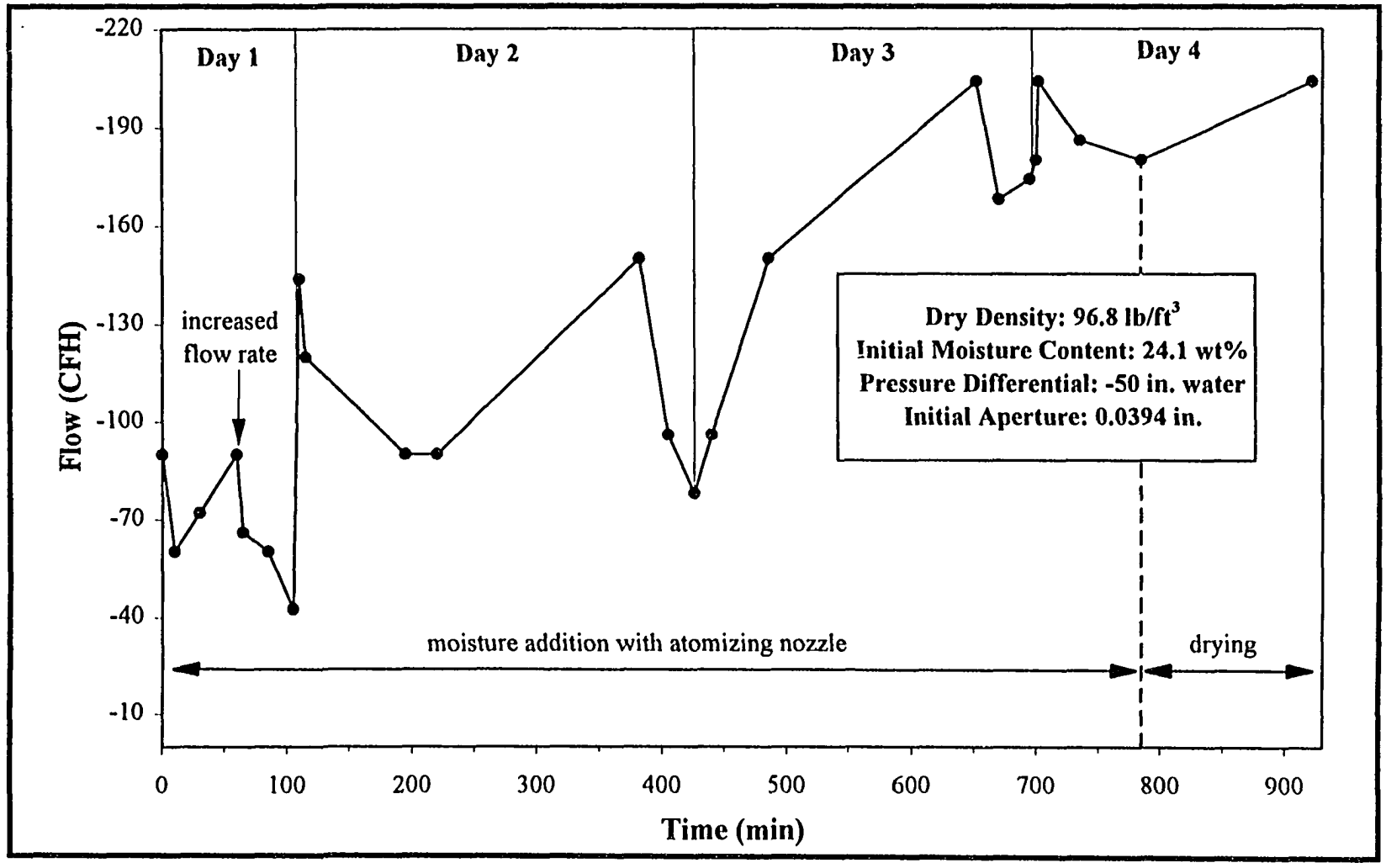

Figure 4.9 Results of Semi-Confined Horizontal Infiltrometer Test No. 3.

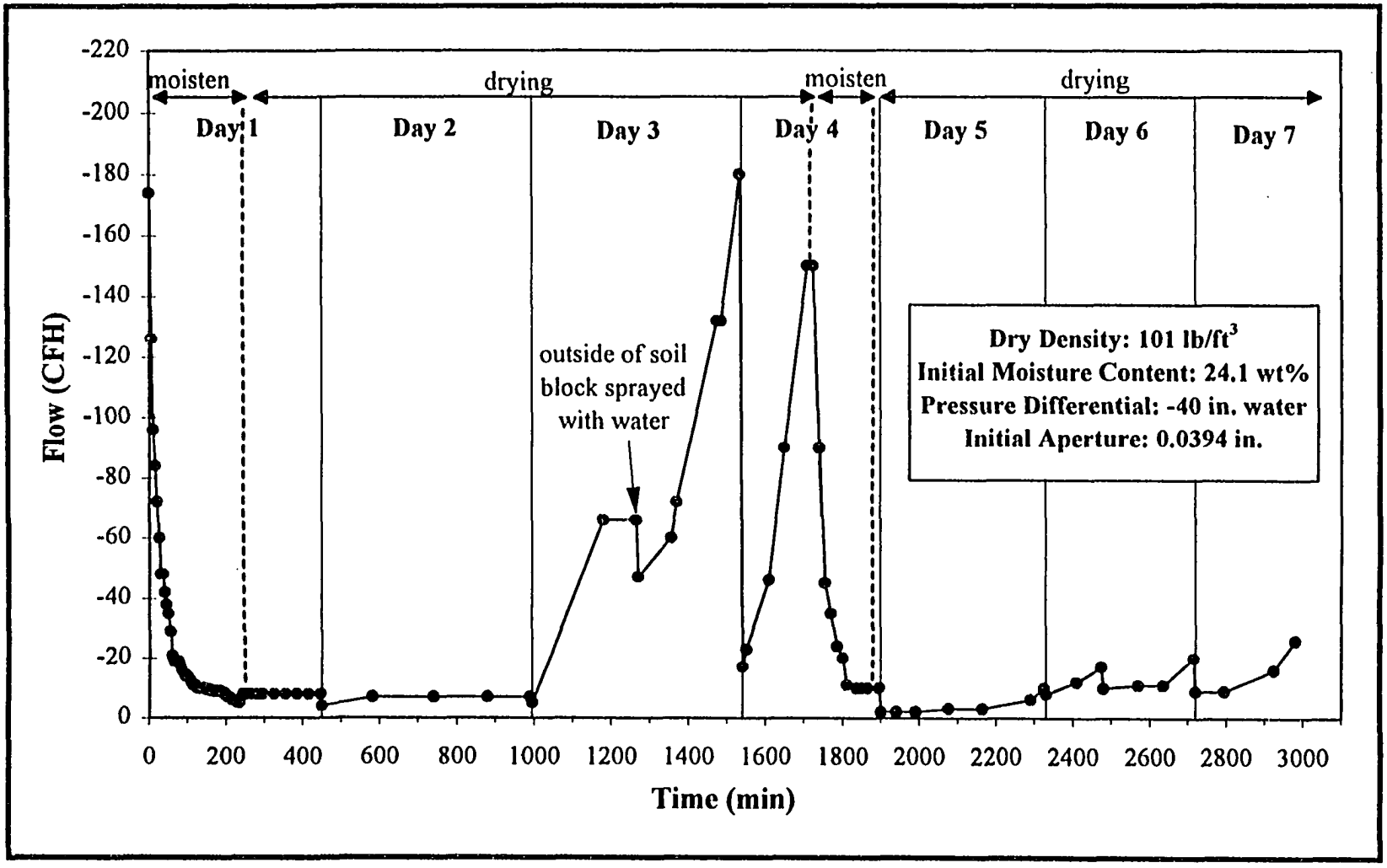

Figure 4.10 Results of Semi-Confined Horizontal Infiltrometer Test No. 4.

Based on these results, a discussion of the mechanism of volume change is provided in this section. In particular, the cyclic behavior of flow is addressed, followed by the effects of air infiltration through the soil, and finally the distribution of moisture in the test soil. Additional tests with the semi-confined horizontal infiltrometer are recommended for future studies, as described in Chapter 6, in view of the promising test results.

4.2.2.1 Cyclic Flow Behavior

Tests showed that fracture apertures can be affected by inducing volume changes in soils with low to moderate volume change potential such as the Woodbury Formation. The ability to expand and contract the fracture aperture is illustrated by the two cycles of increased and decreased flows in Test Nos. 2 and 4, which generally occurred over the interval of a week. Changes appeared to be fully reversible as shown in Test No. 4 by the cycle of moistening and drying from Days 1 to 3. This result suggests that although the fractures may constrict, they do not heal.

Cycles of moistening and drying generally exhibited hysteretic behavior, as the length of time for fracture constriction and reopening, respectively, varied greatly for a typical cycle. For example, in Test No. 4, aperture constriction occurred in 125 min. (i.e., flow rates decreased from -174 to -10 CFH) in the first cycle of moistening, and 110 min. (i.e., flow rates decreased from -150 to -10 CFH) in the second cycle of moistening. However, reopening the fracture by drying the soils generally took ten times longer than constricting the fracture by moistening. It was observed that the rate of drying was

definately dependent on the rate of flow through the porous media. The effects of air infiltration and the influence of moisture content and density of the soil are discussed in the next section.

4.2.2.2 Air Infiltration Through Soil

Since the soil block in the semi-confined horizontal infiltrometer tests was exposed to the atmosphere, the applied vacuum induced a dual porosity flow through both the discrete fracture and the porous media. The ability to measure the inflow through the porous media, i.e., air infiltration, therefore proved to be a key element in understanding the mechanisms of volume change for the semi-confined horizontal infiltrometer tests. These tests allowed separation of fracture flow from porous media flow, and also permitted investigation of the effects of moisture and density on infiltration rate. Results of the air infiltration tests, and the theoretical calculations used to support these results, are presented in this section.

Infiltration rates through the soil were monitored using two different methods. The first was a direct measurement of flow rate through the porous media accomplished by closing the inlet valve, and discontinuing flow through the fracture. Measured infiltration rates using this method ranged from 8 CFH for soils of relatively high moisture and density, to 0.5 CFM for soils with lower moisture and density.

The second method involved indirect measurement which was conducted by closing both the inlet and outlet valves, and monitoring the rate of pressure loss as air infiltrated through the soil. The test results of this indirect method, performed at various stages for Test No. 2, are presented in Figure 4.11. It is evident that pressure loss was

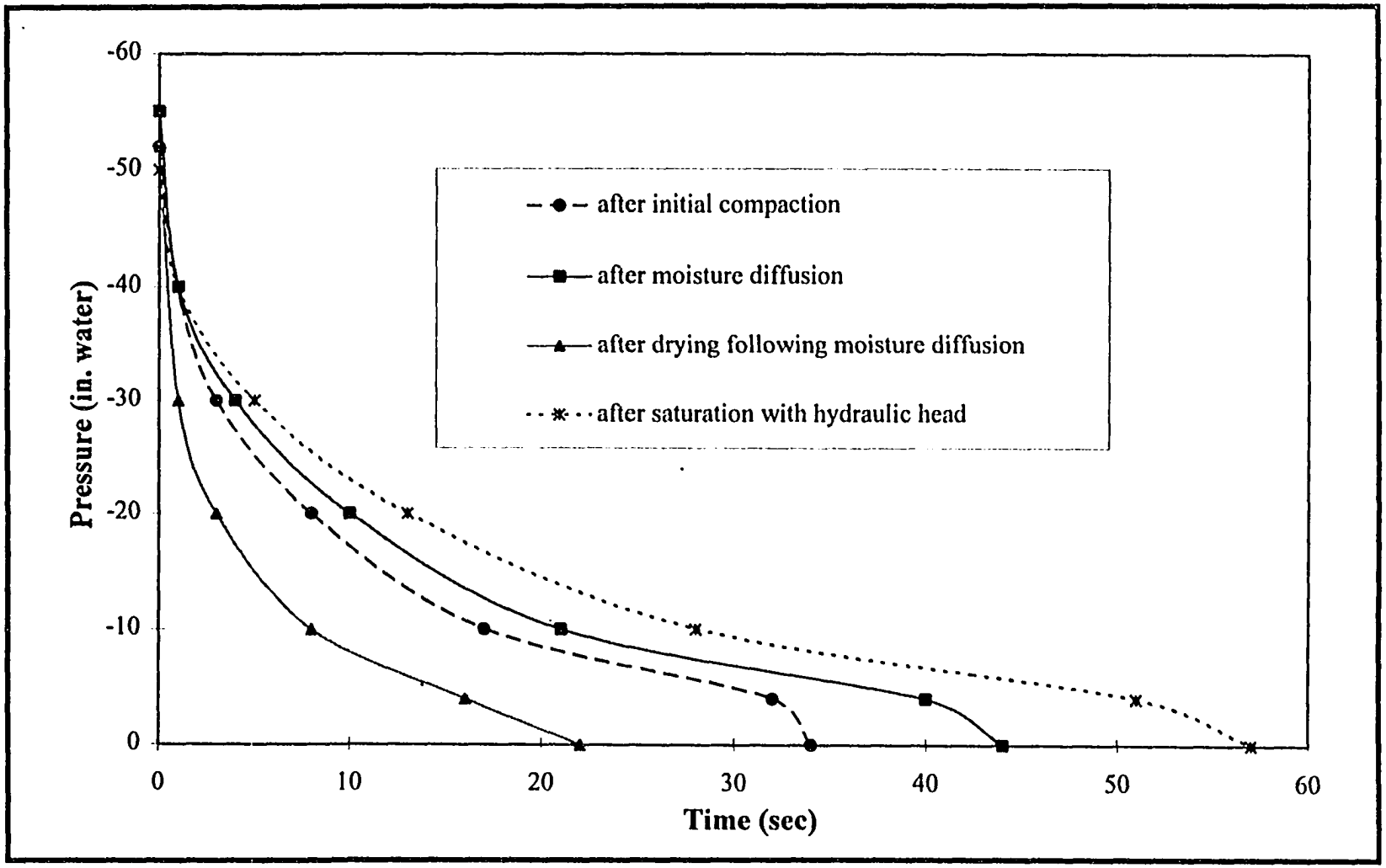

Figure 4.11 Results of Air Infiltration Testing for Semi-Confined Horizontal Infiltrometer Test No. 2.

slowest when the soil was in its wettest state, corresponding to a low infiltration rate. Conversely, pressure loss was greatest when soils were in their driest state, corresponding to a high infiltration rate. Infiltration rates calculated from these results ranged from -1 to -7 CFH, and sample calculations are presented in Appendix E.

The effect of density on infiltration rate was observed by the results of Test No. 3 (Figure 4.9) which was packed at a lower density and exhibited a crumb structure. In this experiment, drying through the soil matrix occurred so quickly that flows continuously increased from -90 to -205 CFH, even though moisture was being constantly added to the fracture. This behavior was attributed to an infiltration rate of 0.5 CFM, which was the highest measured of the four tests. This result shows that density is a significant factor in controlling rate of fracture recovery.

Using results of the air infiltration tests, equivalent hydraulic conductivities were calculated for the range of infiltration rates seen in the semi-confined horizontal infiltrometer tests. Based on a range of -0.5 to -0.01 CFM, hydraulic conductivities of the Woodbury Formation were calculated to range from 10^{-6} to 10^{-8} cm/sec, respectively. Sample calculations are provided in Appendix E. These results generally agree with the natural in situ hydraulic conductivities which are reported to be 10^{-7} cm/sec or greater (B&J Warren and Sons, 1994).

The results of the foregoing infiltration tests were then applied to Test No. 4, to maximize the rate of aperture recovery following moisture addition. To promote drying, the lateral confinement spacers were removed, thus encouraging flow through the porous media. As indicated in Figure 4.10, the fracture began to recover its aperture, apparently by drying associated with infiltration through the porous media. Once the fracture had

somewhat recovered, additional drying along the fracture boundary soils was encouraged by adding moisture to the outside of the soil block, covering it with plastic wrap, and replacing the lateral confinement spacers. This showed to be an effective method in controlling the rate of aperture recovery.

4.2.2.3 Moisture Distributions

Following termination of Tests No. 2 and 3, the soil blocks were removed from the horizontal infiltrometer device, opened to expose the surfaces of the fracture, and samples for moisture content analysis were collected. In both tests, the dissection occurred after a cycle of moistening, although the soils from Test No. 2 had been dried somewhat prior to dissection. The distribution of moisture within the Woodbury Formation soil determined from these dissections is illustrated in Figure 4.12.

As indicated in Figure 4.12, the greatest variations in soil moisture were observed in the fracture boundary soils. Localized increases in moisture contents averaged 3 to 4 wt% above initial moisture contents, and decreases averaged 4 to 5 wt% below initial moisture contents. As expected, moisture contents were higher at the moisture inlet end of the soil block and lower at the outlet end, with a maximum difference in moisture content of 8 wt% observed in Test No. 3. Variations in moisture along the fracture were almost certainly associated with an uneven pattern of volume change and effective aperture.

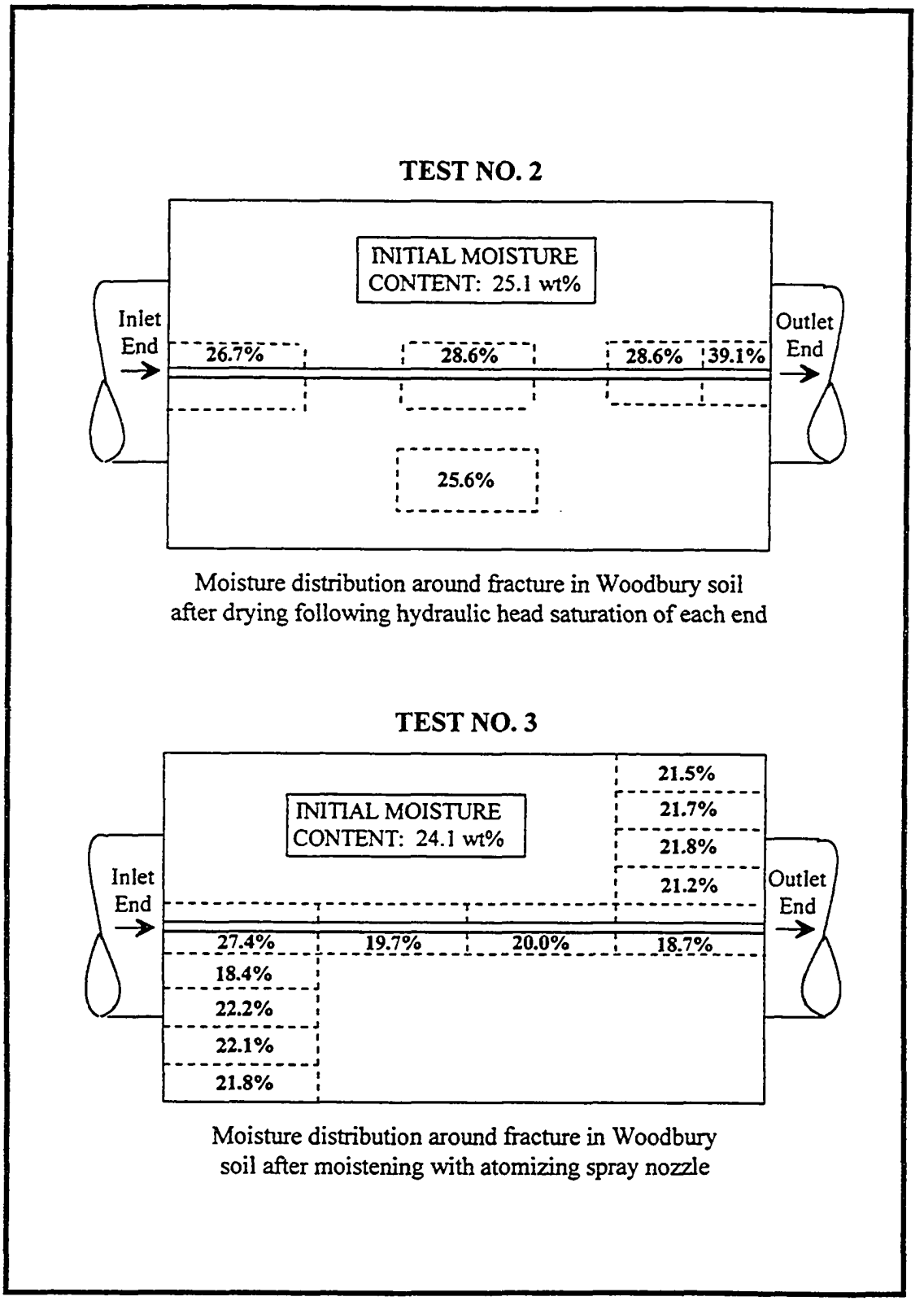

Figure 4.12 Moisture Distribution for Semi-Confined Horizontal Infiltrometer Tests.

Moisture content changes in the porous media away from the fracture were measurable, but were significantly less than changes in the fracture boundary soils. After drying, moisture contents were generally 1-2 wt% lower than original moisture contents, and after moistening were <1 wt% higher than original moisture contents. The fact that moisture contents were lower in surrounding soils following drying substantiates the fact that the porous media is an important mechanism for recovery of the fracture aperture.

The soils subjected to a standing hydraulic head in Test No. 2 exhibited moisture contents up to 39.1 wt%. It was further observed in this test that a 2 in. thick soil plug was pulled into the vacuum system. This result suggests that in addition to volume changes associated with fine-grained formations, saturation of soils along the fracture may result in loss of strength and may have implications of fracture collapse.

CHAPTER 5

SIGNIFICANCE TO PNEUMATIC FRACTURING

The potentially expansive nature of fine-grained formations has been judiciously established in the literature, and the swelling and shrinking of the upper few meters of the soil profile is well known. However, additional attention is warranted for volume changes in fine-grained soils which have been pneumatically fractured for remediation enhancement. This section introduces and develops the new concept of a secondary active zone (5.1), and presents a classification model for determining the volume change potential at pneumatically fractured sites (5.2). Suggested treatment alternatives to control these volume changes and optimize fracture longevity are also presented in the last section of this chapter (5.3).

5.1 New Concept of Secondary Active Zone

The portion of the soil profile which undergoes the greatest amount of shrinking and swelling is generally termed the active zone (Nelson and Miller, 1992). The active zone of an undisturbed formation is located in the upper few meters below ground surface. The major cause of the volume change is variations in environmental conditions, especially moisture fluctuations. Elevated activity levels result from changing hydrostatic conditions, low overburden stress, and lack of restrictions against movement. For purposes of this research, this zone is termed the "primary active zone."

The pneumatically induced fracture network is analogous to the primary active zone. The same mechanisms which establish pneumatic fracturing as an effective permeability enhancement tool also make the fracture network susceptible to volume changes. Attempts to use the fractures as conduits for primary remediation subject the fractures to multitudinous fluctuations of moisture, pressure, and pore fluid composition. In addition, the soil is unrestrained against movement, with the exception of non-continuous fracture surface asperities.

The term "secondary active zone" is introduced in this study to describe the active zone surrounding the pneumatically induced fracture network, and is illustrated in Figure 5.1. The secondary active zone is a discrete zone which can be influenced by conditions in the fracture, and may be located inside or outside the primary active zone as shown in the figure.

The extent of the discrete secondary active zone is dependent on the nature and geometry of the fracture network. Factors such as surface area, fracture connectivity, and aperture size will all affect volume change since they determine the rate at which fluids will be transported through the fracture, as well as the amount of soil which will be in contact with changing environmental conditions.

5.2 Proposed Classification Model

Based on the results of this research, a classification model has been developed for applying pneumatic fracturing to fine-grained formations, and is presented in Figure 5.2. The model incorporates the formation properties and environmental conditions affecting

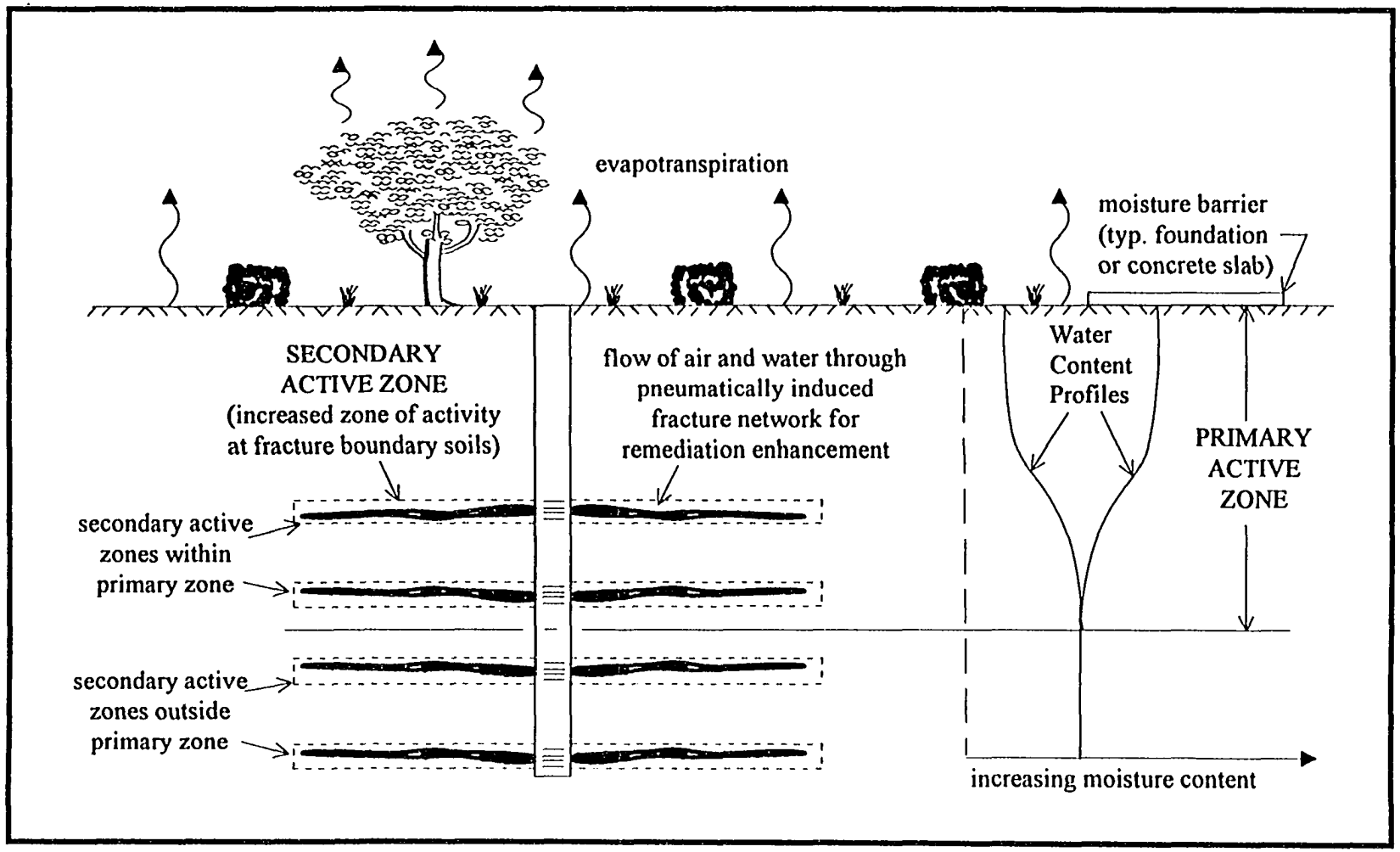

Figure 5.1 New Concept of Secondary Active Zone.

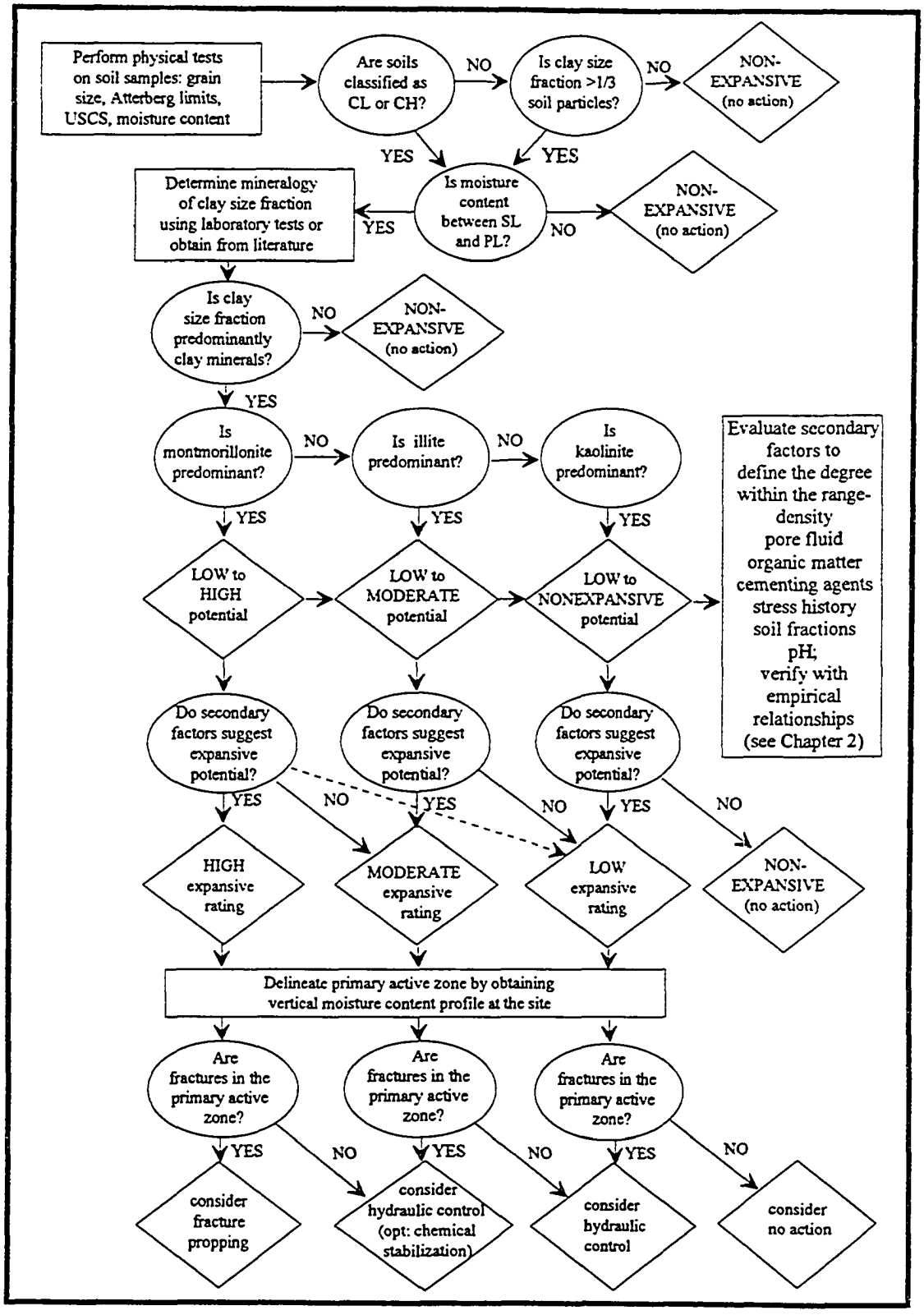

Figure 5.2 Proposed Classification Model.

volume change developed in Chapter 2, the results of horizontal infiltrometer calibration tests on natural soil described in Chapter 4, and the concepts of primary and secondary active zones described in the previous section.

5.2.1 Description

In order to apply the model, it is first necessary to perform some basic physical tests on soil samples from the formation of interest. Formations with USCS classifications of CL or CH, as well as those with more than one-third clay size particles (<2μm), are considered potentially expansive. Pneumatic fracturing conducted in all other soil types is not expected to be significantly influenced by volume changes associated with clay minerals.

The next decision point in the model is the soil moisture content and its relationship to the Atterberg limits. Water content changes below the shrinkage limit and above the plastic limit are generally expected to produce little or no changes in volume. Note that this step excludes all saturated zone conditions and limits the potentially expansive conditions to the unsaturated zone soils.

However, for soils which fall outside this range, it is essential to determine if the moisture content will at some time during pneumatic fracturing enhancement fall into the SL to PL range by loss or gain of moisture. Loss of moisture will occur by drying associated with a coupled extraction technology or lowering of the groundwater table. Increases in moisture could result from migration of water from nearby perched water

zones, surface infiltration of precipitation, or an increase in the height of the groundwater table. Artificial sources of moisture include watering of lawns or other irrigation, surface disposal of water, and leaking underground water or sewer lines and tanks.

Next, mineralogical testing is recommended for the clay size fraction of the test soils to further assess potential expansiveness. Mineralogical differentiation and quantification of the clay size fraction into three groups is recommended including primary rock forming minerals (e.g., feldspars, quartz), noncrystalline material (e.g., allophane), and clay minerals. Soils with a natural propensity for volume changes are those composed primarily of clay minerals. Soils high in allophane (typical of soils formed on a volcanic ash parent material) are associated with the clay mineral halloysite and may require special attention (Maeda et al., 1977).

Where the clay size fractions are composed predominantly of clay minerals, the identification and quantification of these is then recommended. Of the three most common clay minerals, montmorillonite is the most expansive, followed by illite, and then kaolinite. Other less common minerals which may be of concern include vermiculite (capable of hydrating and rehydrating) and halloysite (capable of dehydrating only). These minerals, however, were not addressed as part of this research.

At this point in the model it is possible to rate the formation's propensity to volume change. As observed in the horizontal infiltrometer tests, even formations of low to moderate volume change potential, such as the Woodbury, can influence fracture aperture. Thus, unless the soils are nonexpansive, any degree of potential expansivity should be addressed at pneumatic fracturing sites.

The volume change ratings are defined as a range, and the degree within that range is dependent on secondary factors such as density, pore fluid composition, organic matter, cementing agents, geologic stress history, soil fractions, and pH. Field data can be collected, literature consulted, and chemical tests can be performed to obtain this information as described in the next section. The degree of volume change within the specified range should be determined using the secondary factors described in Chapter 2. The empirical relationships in Table 2.8 and the geographically based ratings in Figure 2.3 can be used to support the rating established using the secondary factors. It is noted that where secondary factors are not investigated, the model is set up to deal conservatively with soils whose chemical properties are not well known.

Next, a vertical moisture profile should be obtained for delineation of the primary active zone. The depth at which the water content becomes nearly constant defines the base of this zone. In cases where the soil is not uniform with depth, or if several strata exist, the differences in soil type can be compensated for by plotting either water content divided by plasticity index or liquidity index (Nelson and Miller, 1992). The primary active zone typically extends a minimum of 10 ft below ground surface.

When fracturing occurs within the primary active zone, there is significant concern. Under these circumstances, volume changes occurring from both the primary and secondary active zones may influence the fracture aperture. Where fractures are propagated in deeper soils below the primary active zone, volume changes will be dominated by secondary active zone conditions and little influence is expected from the primary active zone.

Thus, the classification model distinguishes between the relative primary and secondary active zone locations, and uses the expansivity rating of the soil in recommending potential treatment alternatives. Generally, fracture propping is recommended for the most expansive conditions, hydraulic control is suggested when fracturing in the primary zone, and chemical stabilization is suggested for secondary active zone treatment. It should be noted that chemical stabilization to treat pneumatically induced fractures is not an established treatment alternative, but is recommended for additional study (Chapter 6). Additional discussion of these treatment alternatives is provided in Section 5.3.

The model is intended to be used both during the design stage of a pneumatic fracturing project, as well as for pre-existing pneumatically fractured sites. It is important to note that the classification model is only an approximate guide. A thorough examination of volume change mechanisms and suggested treatment technologies should be performed as part of a final design analysis.

5.2.2 Data Collection

Application of the classification model is dependent on collection of both field and laboratory data. Field data may be collected by performing a reconnaissance of the site, by drilling test borings, and from the literature. State agencies (e.g., Geological Survey), federal agencies (e.g., U.S. Department of Agriculture Soil Conservation Service, U.S. Geological Survey) and local agencies can be contacted to obtain expansive soil maps and available data on formations under study.

Laboratory tests for applying the classification model are generally of three types: mineralogical, physical, and chemical. The mineralogical tests are generally limited to university systems, the physical tests are performed by commercial geotechnical laboratories, and the chemical tests by commercial agricultural laboratories. A summary of the common tests methods used to obtain these data is presented in Table 5.1. It is noted that the methods presented in this table are only suggestions. Analytical methodologies should be chosen on a case-by-case basis because of interferences caused by the complexities of clay minerals and their interactions.

5.2.3 Woodbury Formation Case Study

This section presents a discussion of the volume change potential of the Woodbury Formation using the proposed classification model. The analysis is based on properties of the Woodbury Formation described in Section 3.2.1.2, and conditions under which the horizontal infiltrometer tests were run. A schematic of the decision analysis for applying the classification model to the Woodbury is presented in Figure 5.3.

The general physical properties of the Woodbury Formation (i.e., USCS-CL, 38% clay size fraction (<2μm), water content (24-25 wt%) between the SL and PL) were first used to determine that it is potentially expansive. An expansivity rating of low to high was generated based on the predominance of montmorillonite, obtained from reconnaissance information. The degree of expansivity within this range was then established by evaluating secondary factors based on properties of the Woodbury Formation summarized in Table 3.2. A discussion of the secondary factors follows.

Table 5.1 Summary of Laboratory Test Methods

Property	Method Number	Method Description	Reference
Physical Tests			
Atterberg Liquid and Plastic Limits	D 2217-85 D 4318-84	--	ASTM (1994)
Atterberg Shrinkage Limit	D 427	Mercury method	ASTM (1994)
Grain Size Analysis	D 2217-85 D 1140-92 D 422-63	Mechanical method Hydrometer method	ASTM (1994)
Specific Gravity	D 854-92	Psychrometer method	ASTM (1994)
USCS Classification	D 2487-93	--	ASTM (1994)
Moisture Content	D 2216-90	Drying at 105°C	ASTM (1994)
Chemical Tests			
Soil pH	9045a	Glass and calomel electrode-pH meter	EPA (1992)
Organic Matter	--	HCl and HF treatment with medium temperature dry combustion (900-1000°C)	Page et al. (1986)
CEC	9081	Sodium acetate method	EPA (1992)
Specific Surface	--	Ethylene glycol, glycerol, and ethylene glycol monoethyl	ASTM (1970); Carter et al. (1982)
Electrical Conductivity	--	Conductivity meter	Page et al. (1986)
Exchangeable Cations	--	Ammonium acetate	Page et al. (1986); Carter et al. (1982)
Soluble Salts	--	Atomic adsorption spectrometry	Rhoades (1982); Carter et al. (1982)
Mineralogical Tests			
Mineralogy/ Fabric	--	X-Ray Diffraction	Grim (1968); Carroll (1970); Brindley and Brown (1980); Whittig and Allardice (1986)
	--	Differential Thermal Analysis	Tan et al. (1986)
	--	Electron Microscopy	McCrone and Delly (1973); Sudo et al. (1981)
	--	Potash Content	Knudsen et al. (1960)

-- not applicable

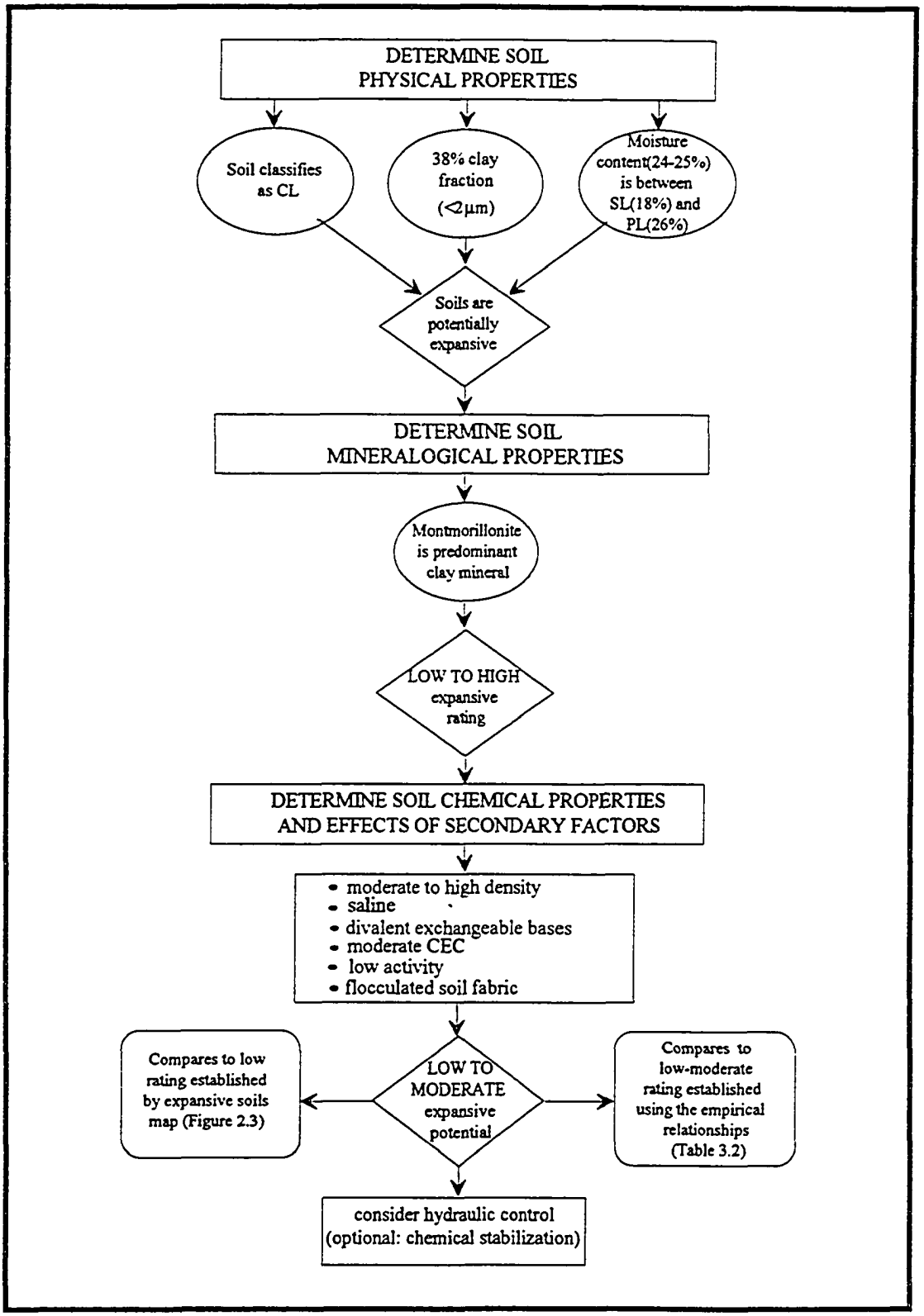

Figure 5.3 Woodbury Formation Case Study.

The prepared Woodbury soil is saline, as denoted by the high concentration of soluble salts and high electrical conductivity. The influence of salts is expected to be considerable because the moisture content is near the plastic limit. The predominance of divalent exchangeable bases (i.e., Ca and Mg) and the high base saturation of calcium serves to restrict interlayer expansion. In addition, the low pH of the soil suggests the potential for Fe and Al-hydroxy interlayering which would limit swelling potential.

The cation exchange capacity (CEC) and the activity of the Woodbury Formation soil also indicate a low-moderate expansivity. Although CECs and activities of expansive soils are less than those of pure clay minerals, referencing these properties is nonetheless useful. The CECs of 29.04 and 71.4 meq/100 L for the Woodbury suggest a surface reactivity intermediate between that of illite and montmorillonite, and the activity intermediate between kaolinite and illite.

The density and soil fabric indicate expansive potentials at the upper end of the range. Dry density for the horizontal infiltrometer tests were fairly high, and averaged 90% of maximum dry unit density. The remolded condition of the soil is also associated with increased swelling, from rupture of interparticle bonds which inhibit swelling in the undisturbed state. The saline nature of the Woodbury Formation would also suggest the presence of a natural flocculated structure.

Based on the foregoing discussion of secondary factors, a low to moderate expansivity rating was assigned to the Woodbury soil. This compares well with the low to moderate rating generated from the empirical relationships. The recommended treatment alternatives are thus hydraulic control for primary active zone stabilization, and optional use of chemical stabilization for secondary active zone stabilization.

5.2.4 Other Factors for Consideration

This section discusses factors which are not included in the classification model, but are equally important in evaluating fracture behavior and longevity. These include the following effects: addition and removal of structures, drying effects near buildings, coupled extraction technologies, pulsed versus continuous pumping, bioremediation, changes in contaminant plume, and time of scheduled remediation.

Effect of Addition or Removal of Structures: Removal of surcharge will decrease effective stresses and allow for swelling to occur in the primary active zone. Alternately, aperture constriction may occur from weight of the new structures, heavy equipment, and compaction associated with construction. The greatest effect, however, is probably not the superimposed load, but the removal of vegetation and associated "wetting up" of the formation which inevitably occurs.

Drying Effects Near Buildings: In cooler climates, foundations extend below the frost line and usually contain heated areas such as boiler rooms which may cause localized desiccation. Effects may be similar for industrial structures which use hot technological processes. These drying effects will tend to enhance fracture longevity, as long as there is no available source of moisture in the vicinity of the desiccated soils.

Effects of Coupled Extraction Technologies: Extraction technologies will also have significant effects on the fracture aperture. Utilizing the flow of air through fractures to remove contamination, such as soil vacuum extraction, will generally have a drying effect causing soil shrinkage. This condition is favorable as long as there is no available source of moisture adjacent to the desiccated soils. Alternately, pumping of water through a fracture may cause soil swelling, especially where water may have access to unsaturated soils.

Effect of Pulsed vs. Continuous Pumping: The use of pulsed pumping techniques for removal of contaminants from expansive fine-grained soils to reach termination criteria is probably not appropriate for pneumatically fractured formations. Apertures may not recover from changes to their apertures caused by changing fluid pressures. Continuous fluid pumping is preferable since pressures and flow rates remain constant. In addition, continuous pumping will maximize drying, which is generally beneficial.

Effects of Bioremediation: Microorganisms may have an important effect on pH and the chemical composition of the pore fluid from their metabolic processes and decomposition products. Dissociation of carbonic acid (H_2CO_3), which forms when the carbon dioxide produced by microbial respiration dissolves in water, will reduce the soil pH and potentially affect hydroxy interlayering. In addition, laboratory studies have shown that microbial action may decrease the percentage of expandable clays (Wall et al., 1974).

Changes in Contaminant Plume: Since pneumatic fractures are used primarily as conduits for removal of organic chemicals, local increases in concentration are expected as pockets of contaminants are accessed, followed by eventual decreases in concentration as remediation continues. Swelling will occur if the organic molecules are replaced by water, because of water's high dielectric constant and dipole moment.

Effect of Time: The objective of the remediation, including cleanup criteria (standards) and termination criteria (e.g., asymptotic level for fine-grained soils), defines the range over which remediation is expected to occur. The longer the scheduled remediation, the greater the risk of that volume changes may occur.

5.3 Suggested Treatment Alternatives

Suggested treatment alternatives are directed towards reducing volume changes by altering formation properties and/or inhibiting fluctuations in environmental conditions. These include reducing and stabilizing the moisture regime (hydraulic control), reducing activity of the clay minerals through use of chemical additives (chemical stabilization), and physical support for the fracture (fracture propping).

5.3.1 Hydraulic Control

Hydraulic control is most effective in controlling the moisture distribution in the primary active zone. Hydraulic control may be accomplished by decreasing and maintaining moisture content within the formation and reducing surface infiltration.

Soil moisture content can be reduced by coupling pneumatic fracturing with extraction technologies to induce flow through the porous media, which is expected to be significant factor in drying soils. In addition, vegetation can be maintained or established to aid in soil desiccation. Trees can extract up to 500 l/day water and grasses extract 1 l/m^2/day (Williams and Pidgeon, 1983). Thus, hydraulic control serves not only to inhibit swelling, but also to maximize shrinkage leading to larger fracture apertures and increased contaminant removal rates.

Maintaining soils in a desiccated state involves reducing infiltration into the soil. This can be accomplished by regrading and surface improvements or use of a surface cover cap. Either pre-existing caps such as pavement, or new caps such as synthetic covers may be used. It is noted that addition of a new cover will, over the long term (1 to 10 years), increase the water content of the soils. However, short term benefits of reduced infiltration are expected to outweigh this disadvantage, especially when daylighting caused by shallow fracturing produces conduits for water migration.

5.3.2 Chemical Stabilization

A proposed treatment alternative to control secondary active zone volume changes is the addition of stabilizing agents to chemically modify the relationship between the soil water and the surfaces of the clay minerals. This technique is commonly used to control expansive soils in the pavement and foundation engineering industry, where the injection of lime has been shown to be effective in reducing volume changes along planes of weakness or fissures (Higgins, 1956; Lundy and Greenfield, 1968; Wright, 1973).

However, chemical stabilization has not been integrated with pneumatic fracturing for this purpose. Additional investigation is required before this is considered a viable treatment technology.

5.3.3 Fracture Propping. Dry media may be injected into the fracture network to physically prop the soils in cases of highly expansive soils. This is especially true where fracturing occurs in the primary active zone. It is noted that propping agents may be chosen to enhance contaminant degradation. This might include nutrient pellets to enhance bioremediation, or iron pellets to enhance degradation of chlorinated solvents. In any case, medium to coarse-grained rounded particles would provide the highest permeability and the strength required to resist the swelling pressures associated with volume changes of fine-grained soil.

CHAPTER 6

CONCLUSIONS AND RECOMMENDATIONS

6.1 Conclusions

This investigation has determined that volume changes in fine-grained formations may affect pneumatically induced fracture apertures, causing both increases and decreases in aperture width. Based on the literature search and bench scale laboratory experiments, the specific conclusions of this research are as follows:

1) Two factors are necessary for expansive behavior of clay soils: the formation must be susceptible to volume changes, and there must be a shift in environmental conditions to initiate the change. Thus, properties of the formation generally define the range over which volume changes will occur, and environmental conditions dictate the degree of occurrence.

2) Clay mineralogy is the primary formation property affecting volume change. Of the three most common clay minerals, montmorillonite has the greatest potential for expansion followed by illite and kaolinite. Secondary factors requiring consideration include soil fractions, dry density, organic matter, irreversible cementing agents, geologic history, and soil pH.

3) Moisture is the primary environmental condition affecting volume change. Soils with a propensity for volume change are most expansive at moisture contents between the shrinkage limit and the plastic limit. Secondary environmental factors for consideration include pore fluid composition, temperature, surcharge pressure, and fluid pressure in the fracture.

4) Tests on control devices investigated idealized flow for both linear and radial flow geometries under laminar flow conditions. Effective apertures were less than actual apertures due to deformation of the plates, reduction in fracture area by the sheet metal spacers, friction losses, and minor losses. The ratio of effective to actual aperture with gas compressibility effects averaged 0.82 for the linear tests and 0.61 for the radial tests.

5) A device termed a horizontal infiltrometer was successfully developed to induce and control volume changes in natural soils which contained an artificial discrete fracture. Tests showed that fracture aperture can be affected, even in soils with low volume change potential. However, changes were fully reversible suggesting that although the fractures may constrict, they do not heal.

6) Measurements of the moisture distributions in the fracture of the Woodbury clay verified that soils located on the fracture boundary were highly susceptible to fluctuations in environmental conditions, while outlying soils were not. The results also suggested that the mechanism by which fractures recover their aperture after being constricted is by air flow through the porous media.

7) The artificial fractures created by the pneumatic fracturing process serve as conduits which subject the formation to fluctuating environmental conditions, thereby creating a zone of increased activity. This investigation introduces the concept of a "secondary active zone" to describe this effect.

8) A classification model was developed to assess fracture behavior of fine-grained formations. The model allows for the establishment of volume change ratings based primarily on clay mineralogy, grain size, Atterberg limits, and moisture content data. Primary and secondary active zone locations in relation to depth of fracturing were then used to define potential treatment alternatives.

9) Several treatment alternatives are recommended for optimizing longevity by reducing fluctuations in environmental conditions and/or by altering formation properties. These include removing moisture and maintaining a stable moisture regime (hydraulic control), reducing the activity of the clay minerals (chemical stabilization), and physically supporting the fracture (fracture propping).

6.2 Recommendations For Future Study

This research has provided insight into the volume change potential of fine-grained formations, and the effect of these changes on aperture and fluid flow properties of pneumatically fractured formations. The results of this study have provided a template for additional investigation to address the longevity of fractures used for remediation enhancement. This section gives recommendations for future investigations.

Control Tests: Additional control tests are recommended to determine the effects of turbulence under controlled conditions by increasing the pressure differential and adding fracture roughness.

Horizontal Infiltrometer Tests: Additional horizontal infiltrometer tests are recommended to determine the mechanisms of volume change using the calibrated semi-confined horizontal infiltrometer device. Soils of low, medium, and high expansive potentials should be tested with varying experimental parameters such as moisture, density, and surcharge pressure.

Validation of Classification Model with Field Data: Validation of the classification model should be performed using field data. This includes pre-existing pneumatically fractured sites, as well as new sites under consideration for pneumatic fracturing enhancement.

Numerical Model: A numerical model to theoretically determine volume change potential is recommended. The predicted volume changes should be correlated with field and experimental results, and an updated classification model developed.

Chemical Stabilization Potential: Bench scale tests are recommended to determine the effectiveness of addition of chemical stabilizers, such as lime, as a potential treatment alternative to limit formation volume changes. An apparatus to deliver these stabilizers by the pneumatic fracturing system should also be considered.

APPENDIX A

DERIVATION OF LINEAR FLUID FLOW EQUATIONS

This appendix presents the derivation of fluid flow equations for the linear flow geometry, idealized as flow between a set of parallel rectangular plates bounded on two sides. A flow equation for incompressible fluids is first derived followed by an equation which takes into account fluid compressibility.

Volumetric flow rate, Q, between the plates is equal to the mean velocity of the fluid in the direction of flow, $\overline{V}_x$, multiplied by the cross sectional area of the fracture,

$$Q = \overline{V}_x \cdot (area) \tag{A.1}$$

Substituting into Equation A.1 the area for a cross section of the fracture, where w is the width of the fracture (L) and b is the fracture aperture (L),

$$Q = \overline{V}_x \cdot (w \cdot b) \tag{A.2}$$

As derived by Nautiyal (1994), the equation describing mean velocity in the direction of flow (L/θ) is as follows, where γ is the specific weight of the fluid (F/L^3), μ is the dynamic viscosity of the fluid ($F\text{-}\theta/L^2$), and ϕ is a potential function,

$$\overline{V}_x = \frac{-\gamma}{12 \cdot \mu} \cdot b^2 \cdot \frac{\partial \phi}{\partial x} \tag{A.3}$$

Substituting Equation A.3 into Equation A.2,

$$Q = \left(\frac{-\gamma}{12 \cdot \mu} \cdot b^2 \cdot \frac{\partial \phi}{\partial x} \right) \cdot (w \cdot b) \tag{A.4}$$

or, $$Q = \frac{-\gamma}{12 \cdot \mu} \cdot b^3 \cdot \frac{\partial \phi}{\partial x} \cdot w \qquad (A.5)$$

Equation A.5 can be rewritten as,

$$\partial \phi = \frac{-12 \cdot \mu \cdot Q}{\gamma \cdot b^3 \cdot w} \cdot \partial x \qquad (A.6)$$

Boundary conditions for x and ϕ are defined, respectively, as (1) L_1 and L_2, the linear distances from the extraction point where $L_2 > L_1$ (L); and (2) P_1 and P_2, the pressures at L_1 and L_2, where $P_2 > P_1$ (L). Integrating Equation A.6 for these conditions, the following equation is obtained,

$$\int_{P_1}^{P_2} \partial \phi = -\frac{12 \cdot \mu \cdot Q}{\gamma \cdot b^3 \cdot w} \int_{L_1}^{L_2} \partial x \qquad (A.7)$$

or, $$(P_2 - P_1) = -\frac{12 \cdot \mu \cdot Q}{\gamma \cdot b^3 \cdot w} \cdot (L_2 - L_1) \qquad (A.8)$$

Equation A.8 can be written as,

$$Q = -\frac{\gamma \cdot b^3 \cdot w}{12 \cdot \mu} \cdot \frac{(P_2 - P_1)}{(L_2 - L_1)} \qquad (A.9)$$

Substituting into Equation A.9 the following relationship,

$$\frac{\gamma}{\mu} = \frac{g}{\nu} \qquad (A.10)$$

where g is acceleration due to gravity (L/θ^2) and ν is kinematic viscosity (L^2/θ), the equation for the volumetric flow rate (L^3/θ) of an incompressible fluid for a linear flow geometry becomes,

$$Q = -\frac{g \cdot b^3 \cdot w \cdot (P_2 - P_1)}{12 \cdot \nu \cdot (L_2 - L_1)} \qquad (A.11)$$

As described by Sullivan and Hertel (1940), Muskat (1946), Langfelder et al. (1968), and Ziegler (1976), the gradient term, P_2-P_1, for the flow of gases in a steady-state fluid system can be replaced by,

$$\frac{\left(P_2^{(1+m)} - P_1^{(1+m)}\right)}{(1+m)\cdot P_1^m} \tag{A.12}$$

where m is a constant which varies according to the thermodynamic nature of the gas as it moves from regions of higher to lower pressures. For isothermal expansion of an ideal gas, m=1.0, and for adiabatic expansion, m<1.0. Substituting Equation A.12 into Equation A.11,

$$Q = -\frac{g\cdot b^3\cdot w}{12\cdot\nu\cdot(L_2 - L_1)}\cdot\frac{\left(P_2^{1+m} - P_1^{1+m}\right)}{(1+m)\cdot P_1^m} \tag{A.13}$$

Assuming isothermal conditions, the volumetric flow rate of a compressible fluid for a linear flow geometry is,

$$Q = -\frac{g\cdot b^3\cdot w}{12\cdot\nu\cdot(L_2 - L_1)}\cdot\frac{\left(P_2^2 - P_1^2\right)}{2\cdot P_1} \tag{A.14}$$

APPENDIX B

LINEAR AND RADIAL CONTROL TEST DATA

This appendix presents data collected from tests performed on linear control devices (Table B.1) and radial control devices (Table B.2). Rotameter flow rate data for both linear and radial flow geometries, and flow rates using round edges for the radial flow geometries were used in calculations for this research unless otherwise specified.

Table B.1 Linear Control Data

Experimental Constants	P_1 (in. H_20)	$Q_{rotameter}$ (CFM)	$Q_{electronic}$ (CFM)	P_1 (cont.) (in. H_20)	$Q_{rotameter}$ (CFM)	$Q_{electronic}$ (CFM)
6 in. linear	-68	-2.5	-2.2	-32	-1.1	-1.4
b_a=0.015 in.	-65	-2.3	-2.15	-30	-1.0	-1.3
L_2-L_1=0.46 ft.	-60	-2.2	-2.1	-28	-0.95	-1.2
w=0.24 ft.	-58	-2.0	-2.1	-26	-0.9	-1.1
Temp.: 80°F	-56	-1.9	-2.1	-24	-0.8	-1.0
P_2: 30.00 in. Hg	-54	-1.75	-2.0	-22	-0.8	-1.0
	-52	-1.6	-1.9	-20	-0.8	-0.9
	-50	-1.55	-1.9	-18	-0.78	-0.9
	-48	-1.5	-1.8	-16	-0.71	-0.8
	-46	-1.5	-1.8	-14	-0.63	-0.7
	-44	-1.4	-1.7	-12	-0.57	-0.6
	-42	-1.35	-1.7	-10	-0.47	-0.6
	-40	-1.3	-1.6	-8	-0.33	-0.4
	-38	-1.25	-1.6	-6	-0.25	-0.3
	-36	-1.2	-1.5	-4	-0.17	-0.2
	-34	-1.15	-1.5	-2	-0.15	-0.1
6 in. linear	-31	-3.8	-3.9	-16	-2.4	-2.7
b_a=0.025 in.	-30	-3.7	-3.7	-14	-2.15	-2.5
L_2-L_1=0.46 ft.	-28	-3.55	-3.6	-12	-1.9	-2.3
w=0.24 ft.	-26	-3.25	-3.4	-10	-1.6	-2.1
Temp.: 80°F	-24	-3.05	-3.2	-8	-1.35	-1.8
P_2: 30.01 in. Hg	-22	-2.95	-3.1	-6	-1.05	-1.45
	-20	-2.9	-3.0	-4	-0.8	-1.0
	-18	-2.65	-2.9	-2	-0.43	-0.6

(continued on next page)

Table B.1 Linear Control Data (Continued)

Experimental Constants	P_1 (in. H_20)	$Q_{rotameter}$ (CFM)	$Q_{electronic}$ (CFM)	P_1 (cont.) (in. H_20)	$Q_{rotameter}$ (CFM)	$Q_{electronic}$ (CFM)
6 in. linear	-16	-4.1	-4.4	-4	-1.45	-1.95
b_a=0.032 in.	-14	-3.7	-4.1	-2	-0.8	-1.2
L_2-L_1=0.46 ft.	-12	-3.25	-3.75	--	--	--
w=0.24 ft.	-10	-3.0	-3.3	--	--	--
Temp.: 80°F	-8	-2.55	-2.9	--	--	--
P_2: 30.01 in. Hg	-6	-2.0	-2.45	--	--	--
12 in. linear	-84	-1.6	-1.9	-34	-0.77	-0.9
b_a=0.015 in.	-80	-1.4	-1.8	-32	-0.73	-0.9
L_2-L_1=0.99 ft.	-70	-1.3	-1.6	-30	-0.70	-0.9
w=0.23 ft.	-60	-1.1	-1.4	-28	-0.67	-0.8
Temp.: 80°F	-56	-1.0	-1.3	-26	-0.62	-0.8
P_2: 30.01 in. Hg	-52	-0.9	-1.3	-24	-0.57	-0.7
	-50	-0.9	-1.2	-22	-0.53	-0.7
	-48	-0.8	-1.1	-20	-0.48	-0.6
	-46	-0.8	-1.1	-18	-0.43	-0.6
	-44	-0.8	-1.1	-16	-0.38	-0.5
	-42	-0.8	-1.1	-14	-0.33	-0.5
	-40	-0.8	-1.0	-12	-0.27	-0.4
	-38	-0.8	-1.0	-10	-0.2	-0.3
	-36	-0.8	-1.0	-8	-0.15	-0.3
12 in. linear	-49	-3.0	-3.1	-24	-1.9	-2.4
b_a=0.025 in.	-48	-3.0	-3.1	-22	-1.7	-2.2
L_2-L_1=0.99 ft.	-46	-3.0	-3.1	-20	-1.6	-2.1
w=0.23 ft.	-44	-2.9	-3.0	-18	-1.45	-2.0
Temp.: 80°F	-42	-2.8	-3.0	-16	-1.3	-1.8
P_2: 30.01 in. Hg	-40	-2.7	-3.0	-14	-1.15	-1.6
	-38	-2.6	-2.9	-12	-1.0	-1.4
	-36	-2.55	-2.9	-10	-0.8	-1.1
	-34	-2.5	-2.8	-8	-0.8	-1.0
	-32	-2.4	-2.7	-6	-0.58	-0.8
	-30	-2.35	-2.7	-4	-0.4	-0.6
	-28	-2.25	-2.6	-2	-0.2	-0.3
	-26	-2.0	-2.5	--	--	--
12 in. linear	-28	-3.5	-4.0	-14	-2.6	-2.8
b_a=0.032 in.	-26	-3.4	-3.9	-12	-2.35	-2.6
L_2-L_1=0.99 ft.	-24	-3.3	-3.7	-10	-1.9	-2.4
w=0.23 ft.	-22	-3.2	-3.45	-8	-1.5	-2.0
Temp.: 80°F	-20	-3.1	-3.2	-6	-1.25	-1.7
P_2: 30.01 in. Hg	-18	-3.0	-3.05	-4	-0.8	-1.1
	-16	-2.9	-2.95	-2	-0.57	-0.8

(continued on next page)

Table B.1 Linear Control Data (Continued)

Experimental Constants	P_1 (in. H_2O)	$Q_{rotameter}$ (CFM)	$Q_{electronic}$ (CFM)	P_1 (cont.) (in. H_2O)	$Q_{rotameter}$ (CFM)	$Q_{electronic}$ (CFM)
24 in. linear	-90	-1.3	-1.1	-40	-0.52	-0.65
b_a=0.015 in.	-80	-1.1	-1.0	-38	-0.50	-0.6
L_2-L_1=1.99 ft.	-70	-1.0	-0.9	-36	-0.47	-0.6
w=0.25 ft.	-60	-0.85	-0.85	-34	-0.43	-0.6
Temp.: 80°F	-50	-0.65	-0.8	-32	-0.42	-0.5
P_2: 30.02 in. Hg	-48	-0.61	-0.7	-30	-0.38	-0.5
	-46	-0.60	-0.7	-28	-0.35	-0.5
	-44	-0.57	-0.7	-26	-0.33	-0.4
	-42	-0.55	-0.7	--	--	--
24 in. linear	-54	-2.9	-2.9	-28	-1.4	-1.9
b_a=0.025 in.	-52	-2.8	-2.9	-26	-1.35	-1.8
L_2-L_1=1.99 ft.	-50	-2.65	-2.8	-24	-1.3	-1.7
w=0.25 ft.	-48	-2.4	-2.7	-22	-1.2	-1.6
Temp.: 80°F	-46	-2.4	-2.7	-20	-1.1	-1.5
P_2: 30.03 in. Hg	-44	-2.3	-2.6	-18	-0.9	-1.3
	-42	-2.2	-2.5	-16	-0.8	-1.2
	-40	-2.1	-2.5	-14	-0.8	-1.0
	-38	-1.9	-2.4	-12	-0.76	-0.9
	-36	-1.8	-2.3	-10	-0.67	-0.8
	-34	-1.7	-2.2	-8	-0.52	-0.7
	-32	-1.6	-2.1	-6	-0.38	-0.5
	-30	-1.5	-2.0	-4	-0.23	-0.3
24 in. linear	-37	-3.55	-3.7	-20	-2.5	-2.7
b_a=0.032 in.	-36	-3.5	-3.55	-18	-2.3	-2.5
L_2-L_1=1.99 ft.	-34	-3.4	-3.45	-16	-2.1	-2.3
w=0.25 ft.	-32	-3.3	-3.3	-14	-1.6	-2.1
Temp.: 80°F	-30	-3.15	-3.2	-12	-1.4	-1.9
P_2: 30.03 in. Hg	-28	-3.05	-3.1	-10	-1.2	-1.7
	-26	-3.0	-3.0	-8	-0.9	-1.3
	-24	-2.9	-3.0	-6	-0.8	-1.0
	-22	-2.7	-2.85	--	--	--

Table B.2 Radial Control Data

Experimental Constants	P_1 (in. H_2O)	$Q_{rotameter}$ (CFM)	$Q_{electronic}$ (CFM)	P_1 (cont.) (in. H_2O)	$Q_{rotameter}$ (CFM)	$Q_{electronic}$ (CFM)
6 in. radial	-52	-3.2	-3.5	-24	-1.9	-2.4
b_a=0.015 in.	-48	-3.0	-3.2	-22	-1.8	-2.3
R_1=0.0104 ft.	-46	-2.9	-3.1	-20	-1.6	-2.2
R_2=0.25 ft.	-44	-2.8	-3.0	-18	-1.5	-2.1
Temp.: 80°F	-42	-2.8	-2.9	-16	-1.4	-1.9
P_2: 30.00 in. Hg	-40	-2.7	-2.9	-14	-1.3	-1.8
Square Edges	-38	-2.7	-2.8	-12	-1.2	-1.7
	-36	-2.6	-2.8	-10	-1.0	-1.5
	-34	-2.6	-2.7	-8	-0.9	-1.2
	-32	-2.5	-2.7	-6	-0.8	-1.0
	-30	-2.2	-2.6	-4	-0.7	-0.8
	-28	-2.1	-2.5	-2	-0.4	-0.5
	-26	-2.0	-2.4	--	--	--
6 in. radial	-47	-3.4	-3.6	-24	-2.1	-2.5
b_a=0.015 in.	-46	-3.3	-3.25	-22	-1.9	-2.4
R_1=0.0104 ft.	-44	-3.2	-3.15	-20	-1.8	-2.3
R_2=0.25 ft.	-42	-3.1	-3.1	-18	-1.6	-2.2
Temp.: 80°F	-40	-2.9	-3.0	-16	-1.5	-2.1
P_2: 30.00 in. Hg	-38	-2.8	-3.0	-14	-1.4	-1.95
Round Edges	-36	-2.6	-2.9	-12	-1.3	-1.8
	-34	-2.5	-2.9	-10	-1.2	-1.6
	-32	-2.4	-2.8	-8	-0.9	-1.3
	-30	-2.4	-2.7	-6	-0.9	-1.1
	-28	-2.3	-2.6	-4	-0.7	-0.9
	-26	-2.2	-2.6	-2	-0.4	-0.6
6 in. radial	-25	-4.2	-4.5	-12	-2.5	-2.8
b_a=0.025 in.	-24	-4.0	-4.1	-10	-2.3	-2.6
R_1=0.0104 ft.	-22	-3.8	-3.8	-8	-2.0	-2.3
R_2=0.25 ft.	-20	-3.5	-3.6	-6	-1.5	-2.0
Temp.: 80°F	-18	-3.3	-3.3	-4	-1.2	-1.65
P_2: 30.00 in. Hg	-16	-3.0	-3.1	-2	-1.0	-1.1
Square Edges	-14	-2.7	-2.9	--	--	--
6 in. radial	-23	-4.2	-4.4	-10	-2.4	-2.7
b_a=0.025 in.	-22	-3.7	-4.3	-8	-2.0	-2.5
R_1=0.0104 ft.	-20	-3.5	-4.0	-6	-1.6	-2.2
R_2=0.25 ft.	-18	-3.4	-3.7	-4	-1.3	-1.8
Temp.: 80°F	-16	-3.2	-3.3	-2	-0.8	-1.1
P_2: 30.00 in. Hg	-14	-3.0	-3.0	--	--	--
Round Edges	-12	-2.6	-2.9	--	--	--
6 in. radial	-19	-4.4	-4.8	-6	-2.0	-2.4
b_a=0.032 in.	-18	-4.2	-4.4	-4	-1.6	-2.1
R_1=0.0104 ft.	-16	-4.0	-4.1	-2	-1.2	-1.5
R_2=0.25 ft.	-14	-3.5	-3.6	--	--	--
Temp.: 80°F	-12	-3.1	-3.2	--	--	--
P_2: 30.00 in. Hg	-10	-2.8	-3.0	--	--	--
Square Edges	-8	-2.5	-2.7	--	--	--

(continued on next page)

Table B.2 Radial Control Data (Continued)

Experimental Constants	P_1 (in. H_2O)	$Q_{rotameter}$ (CFM)	$Q_{electronic}$ (CFM)	P_1 (cont.) (in. H_2O)	$Q_{rotameter}$ (CFM)	$Q_{electronic}$ (CFM)
6 in. radial	-17	-4.1	-4.4	-4	-1.6	-2.15
b_a=0.032 in.	-16	-4.0	-4.2	-2	-1.1	-1.6
R_1=0.0104 ft.	-14	-3.7	-3.85	--	--	--
R_2=0.25 ft.	-12	-3.3	-3.4	--	--	--
Temp.: 81°F	-10	-2.9	-3.0	--	--	--
P_2: 29.99 in. Hg	-8	-2.5	-2.8	--	--	--
Round Edges	-6	-2.0	-2.5	--	--	--
12 in. radial	-50	-3.2	-3.1	-24	-1.8	-2.3
b_a=0.015 in.	-48	-3.1	-3.0	-22	-1.7	-2.2
R_1=0.0104 ft.	-46	-3.0	-3.0	-20	-1.6	-2.1
R_2=0.49 ft.	-44	-2.8	-2.9	-18	-1.5	-2.0
Temp.: 76°F	-42	-2.7	-2.85	-16	-1.4	-1.9
P_2: 30.12 in. Hg	-40	-2.6	-2.8	-14	-1.3	-1.8
Square Edges	-38	-2.6	-2.8	-12	-1.2	-1.6
	-36	-2.5	-2.7	-10	-1.0	-1.4
	-34	-2.5	-2.7	-8	-0.9	-1.2
	-32	-2.4	-2.6	-6	-0.8	-1.0
	-30	-2.2	-2.5	-4	-0.6	-0.8
	-28	-2.1	-2.5	-2	-0.4	-0.5
	-26	-2.0	-2.4	--	--	--
12 in. radial	-44	-3.5	-3.3	-22	-2.2	-2.5
b_a=0.015 in.	-42	-3.3	-3.2	-20	-2.1	-2.4
R_1=0.0104 ft.	-40	-3.2	-3.1	-18	-1.9	-2.3
R_2=0.49 ft.	-38	-3.1	-3.0	-16	-1.7	-2.2
Temp.: 76°F	-36	-3.0	-3.0	-14	-1.5	-2.1
P_2: 30.12 in. Hg	-34	-2.9	-2.9	-12	-1.4	-2.0
Round Edges	-32	-2.8	-2.9	-10	-1.3	-1.8
	-30	-2.7	-2.8	-8	-1.1	-1.56
	-28	-2.6	-2.7	-6	-0.9	-1.2
	-26	-2.5	-2.7	-4	-0.8	-1.0
	-24	-2.4	-2.6	-2	-0.4	-0.6
12 in. radial	-27	-4.1	-4.3	-14	-2.6	-2.7
b_a=0.025 in.	-26	-4.0	-4.0	-12	-2.4	-2.5
R_1=0.0104 ft.	-24	-3.8	-3.7	-10	-2.2	-2.4
R_2=0.49 ft.	-22	-3.5	-3.4	-8	-2.0	-2.15
Temp.: 76°F	-20	-3.3	-3.2	-6	-1.4	-1.8
P_2: 30.12 in. Hg	-18	-3.1	-3.0	-4	-1.2	-1.5
Square Edges	-16	-2.9	-2.9	-2	-0.8	-1.0
12 in. radial	-18	-4.0	-4.6	-4	-1.4	-2.0
b_a=0.025 in.	-16	-3.6	-4.1	-2	-1.0	-1.4
R_1=0.0104 ft.	-14	-3.3	-3.7	--	--	--
R_2=0.49 ft.	-12	-3.2	-3.3	--	--	--
Temp.: 76°F	-10	-2.7	-3.0	--	--	--
P_2: 30.11 in. Hg	-8	-2.5	-2.7	--	--	--
Round Edges	-6	-1.9	-2.4	--	--	--

(continued on next page)

Table B.2 Radial Control Data (Continued)

Experimental Constants	P_1 (in. H_20)	$Q_{rotameter}$ (CFM)	$Q_{electronic}$ (CFM)	P_1 (cont.) (in. H_20)	$Q_{rotameter}$ (CFM)	$Q_{electronic}$ (CFM)
12 in. radial	-20	-4.5	-4.5	-6	-2.1	-2.3
b_a=0.032 in.	-18	-4.1	-4.1	-4	-1.6	-1.9
R_1=0.0104 ft.	-16	-3.7	-3.7	-2	-1.2	-1.4
R_2=0.49 ft.	-14	-3.3	-3.3	--	--	--
Temp.: 80°F	-12	-3.1	-3.0	--	--	--
P_2: 30.12 in. Hg	-10	-2.8	-2.8	--	--	--
Square Edges	-8	-2.5	-2.6	--	--	--
12 in. radial	-16	-4.1	-4.6	-2	-1.2	-1.6
b_a=0.032 in.	-14	-3.6	-4.2	--	--	--
R_1=0.0104 ft.	-12	-3.3	-3.8	--	--	--
R_2=0.49 ft.	-10	-3.0	-3.3	--	--	--
Temp.: 76°F	-8	-2.7	-2.9	--	--	--
P_2: 30.11 in. Hg	-6	-2.4	-2.6	--	--	--
Round Edges	-4	-1.7	-2.3	--	--	--
24 in. radial	-52	-3.1	-3.1	-26	-1.7	-2.2
b_a=0.015 in.	-50	-3.1	-3.0	-24	-1.6	-2.1
R_1=0.0104 ft.	-48	-3.0	-2.95	-22	-1.5	-2.0
R_2=0.9896 ft.	-46	-2.7	-2.9	-20	-1.4	-1.9
Temp.: 80°F	-44	-2.5	-2.8	-18	-1.3	-1.8
P_2: 30.07 in. Hg	-42	-2.5	-2.8	-16	-1.2	-1.7
Square Edges	-40	-2.4	-2.7	-14	-1.1	-1.6
	-38	-2.3	-2.65	-12	-1.0	-1.4
	-36	-2.3	-2.6	-10	-0.9	-1.2
	-34	-2.2	-2.5	-8	-0.9	-1.0
	-32	-2.0	-2.4	-6	-0.7	-0.9
	-30	-1.9	-2.3	-4	-0.5	-0.7
	-28	-1.8	-2.3	-2	-0.3	-0.5
24 in. radial	-44	-3.4	-3.4	-22	-2.1	-2.4
b_a=0.015 in.	-42	-3.1	-3.2	-20	-2.0	-2.3
R_1=0.0104 ft.	-40	-3.0	-3.1	-18	-1.9	-2.2
R_2=0.9896 ft.	-38	-2.9	-3.1	-16	-1.5	-2.1
Temp.: 82°F	-36	-2.8	-3.0	-14	-1.4	-1.9
P_2: 30.02 in. Hg	-34	-2.7	-2.9	-12	-1.3	-1.8
Round Edges	-32	-2.5	-2.8	-10	-1.1	-1.6
	-30	-2.4	-2.8	-8	-0.9	-1.3
	-28	-2.3	-2.7	-6	-0.9	-1.0
	-26	-2.3	-2.6	-4	-0.6	-0.8
	-24	-2.2	-2.5	-2	-0.3	-0.4
24 in. radial	-26	-4.2	-4.1	-12	-2.4	-2.6
b_a=0.025 in.	-24	-3.9	-3.75	-10	-2.2	-2.4
R_1=0.0104 ft.	-22	-3.7	-3.5	-8	-2.0	-2.2
R_2=0.9896 ft.	-20	-3.5	-3.2	-6	-1.6	-1.9
Temp.: 80°F	-18	-3.3	-3.0	-4	-1.2	-1.5
P_2: 30.07 in. Hg	-16	-3.0	-2.9	-2	-0.8	-0.9
Square Edges	-14	-2.7	-2.7	--	--	--

(continued on next page)

Table B.2 Radial Control Data (Continued)

Experimental Constants	P_1 (in. H_20)	$Q_{rotameter}$ (CFM)	$Q_{electronic}$ (CFM)	P_1 (cont.) (in. H_20)	$Q_{rotameter}$ (CFM)	$Q_{electronic}$ (CFM)
24 in. radial	-21	-4.3	-4.4	-8	-2.3	-2.5
b_a=0.025 in.	-20	-4.2	-4.3	-6	-1.9	-2.2
R_1=0.0104 ft.	-18	-4.0	-4.0	-4	-1.4	-1.8
R_2=0.9896 ft.	-16	-3.5	-3.6	-2	-0.9	-1.1
Temp.: 82°F	-14	-3.1	-3.1	--	--	--
P_2: 30.02 in. Hg	-12	-3.0	-3.0	--	--	--
Round Edges	-10	-2.6	-2.8	--	--	--
24 in. radial	-20	-4.5	-4.3	-6	-1.9	-2.2
b_a=0.032 in.	-18	-4.1	-3.9	-4	-1.4	-1.7
R_1=0.0104 ft.	-16	-3.7	-3.6	-2	-1.0	-1.1
R_2=0.9896 ft.	-14	-3.4	-3.2	--	--	--
Temp.: 80°F	-12	-3.0	-2.9	--	--	--
P_2: 30.07 in. Hg	-10	-2.8	-2.75	--	--	--
Square Edges	-8	-2.5	-2.5	--	--	--
24 in. radial	-17	-4.5	-4.5	-4	-1.8	-2.1
b_a=0.032 in.	-16	-4.4	-4.4	-2	-1.2	-1.5
R_1=0.0104 ft.	-14	-3.9	-3.9	--	--	--
R_2=0.9896 ft.	-12	-3.5	-3.5	--	--	--
Temp.: 82°F	-10	-3.1	-3.05	--	--	--
P_2: 30.02 in. Hg	-8	-2.7	-2.8	--	--	--
Round Edges	-6	-2.3	-2.5	--	--	--

APPENDIX C

SAMPLE CALCULATIONS ON CONTROL DATA

This appendix provides sample calculations for (1) general conversions; (2) linear control data; and (3) radial control data. The appropriate equation and symbols are presented followed by a calculation using sample data.

C.1 General Conversions

C.1.1 Conversion of Gauge Vacuum Pressure Measured in Inches of Water to Absolute Pressure Measured in Inches of Air

$$P_{abs} = \left(P_{atm} + P_g\right) \cdot \left(\frac{\gamma_w}{\gamma_a}\right) \qquad \text{(C.1)}$$

where: P_{abs} = absolute pressure (L)

P_{atm} = atmospheric pressure (L)

P_g = gauge pressure (L)

γ_w = specific weight of water (F/L^3) at operating temperature (T)

γ_a = specific weight of air (F/L^3) at operating temperature (T)

Kinematic viscosity (ν), specific weight of water (γ_w), and specific weight of air (γ_a) were interpolated from graphical representations for a range of temperatures. Values of ν, γ_w, and γ_a used for this research are presented in Table C.1.

Table C.1 Properties of Air and Water over Temperature Variation

Temperature (°F)	Kinematic Viscosity of Air (ft^2/sec)	Specific Weight of Water (lb/ft^3)	Specific Weight of Air (lb/ft^3)
63	0.000159	62.35	0.076
64	0.000159	62.33	0.076
65	0.000159	62.34	0.076
66	0.000160	62.33	0.075
67	0.000160	62.32	0.075
68	0.000160	62.31	0.075
69	0.000161	62.31	0.075
*70	0.000162	62.30	0.075
71	0.000163	62.29	0.075
72	0.000164	62.28	0.075
73	0.000164	62.27	0.074
74	0.000165	62.27	0.074
75	0.000165	62.26	0.074
76	0.000166	62.25	0.074
77	0.000166	62.24	0.074
78	0.000167	62.23	0.074
79	0.000168	62.23	0.074
80	0.000169	62.22	0.073
81	0.000169	62.21	0.073
82	0.000170	62.20	0.073
83	0.000170	62.19	0.073
84	0.000171	62.18	0.073
85	0.000171	62.17	0.073

* Standard temperature and pressure for this research were set at 70°F and 1 atmosphere because the variable area flow meters are calibrated to these parameters.

$$P_s = \frac{29.92 \text{ in.Hg} \cdot \frac{13.596 \text{ in. } H_2O}{\text{in. Hg}} \cdot 62.30 \frac{\text{lb}}{\text{ft}^3}}{12 \cdot 0.075 \frac{\text{lb}}{\text{ft}^3}}$$

Thus standard pressure at standard temperature of 70°F is equal to 28,159 ft of air absolute.

Sample Calculation:

P_{atm} = 30.00 in. Hg

P_g = -52 in. H_2O

γ_w = 62.22 lb/ft^3 at 80 °F

γ_a = 0.073 lb/ft^3 at 80 °F

$$P_{abs} = \left(\left(30.00 \text{ in Hg} \cdot 13.596 \frac{\text{in } H_2O}{\text{in Hg}}\right) - 52 \text{ in } H_2O\right) \cdot \left(\frac{62.22 \frac{\text{lb}}{\text{ft}^3}}{0.073 \frac{\text{lb}}{\text{ft}^3}}\right)$$

$$P_{abs} = 303{,}326 \text{ in air absolute} \cdot \frac{\text{ft}}{12 \text{ in}} = 25{,}277 \text{ ft air absolute}$$

C.1.2 Conversion of Flows at Operating Conditions to Standard Conditions

$$Q_S = Q_O \cdot \left(\frac{P_O}{P_S}\right) \cdot \left(\frac{T_S}{T_O}\right) \qquad \text{(C.2)}$$

where: Q_s = volumetric flow at standard temperature and pressure (L^3/θ)

Q_o = volumetric flow at operating temperature and pressure (L^3/θ)

P_s = absolute standard pressure (L)

P_o = absolute gauge operating pressure (L)

T_s = standard temperature (T)

T_o = operating temperature (T)

The rotameters used to measure flow rate are calibrated at 70°F and 1 atmosphere. Thus, these values were used as standard temperature and pressure (STP) for this research.

Sample Calculation:

Q_o = -3.2 ACFM

P_s = 28,159 ft of air absolute (70°F and 1 atm.)

P_o = 25, 277 ft of air absolute

T_s = 70°F + 460 = 530R

T_o = 80°F + 460 = 540R

$$Q_S = -3.2\frac{ft^3}{min}\cdot\left(\frac{25{,}277 \text{ ft air absolute}}{28{,}159 \text{ ft air absolute}}\right)\cdot\left(\frac{530R}{540R}\right)$$

$$Q_S = \text{-2.82 SCFM}\cdot\frac{min}{60 \text{ sec}} = -0.047 \text{ SCFS}$$

C.2 Linear Control Calculations

This section presents sample calculations for the linear controls which were run under a passive inlet condition. The following symbols will be used to present the sample calculations for this section:

b_a = thickness of sheet metal spacers; "actual aperture" (L)

b_e = calculated effective fracture aperture (L)

g = acceleration due to gravity (L/θ^2)

L_1, L_2 = linear distance from extraction point, $L_2 > L_1$ (L)

P_1, P_2 = absolute air pressure at L_1 and L_2, $L_2 > L_1$ (L)

Q_s = volumetric flow at STP (L^3/θ)

R_e = Reynolds number (dimensionless)

ν = kinematic viscosity of air at operating temperature (L^2/θ)

V = average flow velocity (L/θ)

w = fracture width (L)

The following data were obtained from the 24 in. length linear control tests and will be used to present the sample calculations for this section:

b_a = 0.00125 ft

g = 32.2 ft/sec^2

L_1, L_2 = 0 ft, 1.99 ft

P_1, P_2 = 25.439 ft air absolute, 28.990 ft air absolute

Q_s = -0.0096 SCFS

ν = 0.000169 ft^2/sec at 80°F

w = 0.25 ft

C.2.1 Calculation of Effective Aperture from Experimental Pressures and Flows Under Laminar Flow Conditions with Gas Compressibility Effects

$$b_e = \left(-\frac{(2 \cdot P_1) \cdot 12 \cdot Q_s \cdot \nu \cdot (L_2 - L_1)}{(P_2^2 - P_1^2) \cdot g \cdot w} \right)^{\frac{1}{3}} \qquad \text{(C.3)}$$

Sample Calculation:

$$b_e = \left(-\frac{(2 \cdot 25{,}439 \text{ ft air absolute}) \cdot 12 \cdot \left(-0.0096 \frac{\text{ft}^3}{\text{sec}} \right) \cdot 0.000169 \frac{\text{ft}^2}{\text{sec}} \cdot 1.99 \text{ ft}}{\left((28{,}990 \text{ ft air absolute})^2 - (25{,}439 \text{ ft air absolute})^2 \right) \cdot 32.2 \frac{\text{ft}}{\text{sec}^2} \cdot 0.25 \text{ ft}} \right)^{\frac{1}{3}}$$

$$b_e = 0.00108 \text{ ft} \cdot \frac{12 \text{ in.}}{\text{ft}} = 0.013 \text{ in.}$$

C.2.2 Calculation of Effective Aperture from Experimental Pressures and Flows Under Laminar Flow Conditions without Gas Compressibility Effects

$$b_e = \left(-\frac{12 \cdot Q_s \cdot \nu \cdot (L_2 - L_1)}{(P_2 - P_1) \cdot g \cdot w} \right)^{\frac{1}{3}} \tag{C.4}$$

Sample Calculation:

$$b_e = \left(-\frac{12 \cdot \left(-0.0096 \frac{ft^3}{sec} \right) \cdot 0.000169 \frac{ft^2}{sec} \cdot 1.99 \text{ ft}}{(28.990 \text{ ft air absolute} - 25.439 \text{ ft air absolute}) \cdot 32.2 \frac{ft}{sec^2} \cdot 0.25 \text{ ft}} \right)^{\frac{1}{3}}$$

$$b_e = 0.00111 \text{ ft} \cdot \frac{12 \text{ in.}}{\text{ft}} = 0.033 \text{ in.}$$

C.2.3 Calculation of Average Flow Velocity from Standard Flow Rate and Effective Aperture with Gas Compressibility Effects

$$V = \frac{Q_s}{w \cdot b_e} \tag{C.5}$$

Sample Calculation:

$$V = \frac{-0.0096 \frac{ft^3}{sec}}{0.25 \text{ ft} \cdot 0.00108 \text{ ft}} = -35.56 \frac{ft}{sec}$$

C.2.4 Calculation of Reynolds Number from Flow Velocity and Effective Aperture with Gas Compressibility Effects

$$Re = \frac{2 \cdot b_e \cdot |V|}{\nu} \tag{C.6}$$

Sample Calculation:

$$Re = \frac{2 \cdot 0.00108 \text{ ft} \cdot \left| -35.56 \frac{\text{ft}}{\text{sec}} \right|}{0.000169 \frac{\text{ft}^2}{\text{sec}}} = 454$$

C.2.5 Calculation of Exponent Under Turbulent Flow Conditions with Gas Compressibility Effects

$$n = \frac{\ln\left(-\frac{(2 \cdot P_1) \cdot 12 \cdot Q_s \cdot \nu \cdot (L_2 - L_1)}{(P_2^2 - P_1^2) \cdot g \cdot w} \right)}{\ln(\text{average } b_e \text{ (laminar flow)})} \qquad \text{(C.7)}$$

Sample Calculation: Note that these data were not collected under turbulent flow conditions, and are used only to express the calculation.

$$n = \frac{\ln\left(-\frac{(2 \cdot 25{,}439 \text{ ft air absolute}) \cdot 12 \cdot \left(-0.0096 \frac{\text{ft}}{\text{sec}^2} \right) \cdot 0.000169 \frac{\text{ft}^2}{\text{sec}} \cdot 1.99 \text{ ft}}{\left((28{,}990 \text{ ft air absolute})^2 - (25{,}439 \text{ ft air absolute})^2 \right) \cdot 32.2 \frac{\text{ft}}{\text{sec}^2} \cdot 0.25 \text{ ft}} \right)}{\ln(0.00108 \text{ ft})}$$

$n = 3.00$

C.3 Radial Control Calculations

This section presents sample calculations for the radial controls which were run under a passive inlet condition. The following symbols will be used to present the sample calculations for this section:

b_a = thickness of sheet metal spacers; "actual aperture" (L)

b_e = calculated effective fracture aperture (L)

g = acceleration due to gravity (L/θ^2)

P_1, P_2 = absolute air pressure at R_1 and R_2, $P_2 > P_1$ (L)

Q_s = flow rate at standard conditions of 70°F and 1 atm. (L^3/θ)

Re = Reynolds number (dimensionless)

R_1, R_2 = radial distance from extraction point, $R_2 > R_1$ (L)

ν = kinematic viscosity of air at operating temperature (L^2/θ)

V = flow velocity (L/θ)

The following data were obtained from the 12 in. diameter radial control setup and will be used to present the sample calculations for this section:

b_a = 0.00125 ft

g = 32.2 ft/sec^2

P_1, P_2 = 25,623 ft air absolute, 28,707 ft air absolute

Q_s = -0.0420 SCFS

R_1, R_2 = 0.0104 ft, 0.49 ft

ν = 0.000166 ft^2/sec at 76°F

C.3.1 Calculation of Effective Aperture from Experimental Pressures and Flows Under Laminar Conditions with Gas Compressibility Effects

$$b_e = \left(-\frac{(2 \cdot P_1) \cdot Q_s \cdot 6 \cdot \nu \cdot \ln\left(\frac{R_2}{R_1}\right)}{(P_2^2 - P_1^2) \cdot g \cdot \pi} \right)^{\frac{1}{3}} \qquad \text{(C.8)}$$

Sample Calculation:

$$b_e = \left(-\frac{(2 \cdot 25{,}623 \text{ ft air absolute}) \cdot \left(-0.042 \frac{\text{ft}^3}{\text{sec}}\right) \cdot 6 \cdot 0.000166 \frac{\text{ft}^2}{\text{sec}} \cdot \ln\left(\frac{0.49 \text{ ft}}{0.0104 \text{ ft}}\right)}{\left((28{,}707 \text{ ft air absolute})^2 - (25{,}623 \text{ ft air absolute})^2\right) \cdot 32.2 \frac{\text{ft}}{\text{sec}^2} \cdot \pi} \right)^{\frac{1}{3}}$$

$$b_e = 0.00079 \text{ ft} \cdot 12 \frac{\text{in.}}{\text{ft}} = 0.0094 \text{ in}$$

C.3.2 Calculation of Effective Aperture from Experimental Pressures and Flows Under Laminar Flow Conditions without Gas Compressibility Effects

$$b_e = \left(-\frac{Q_s \cdot 6 \cdot \nu \cdot \ln\left(\frac{R_2}{R_1}\right)}{(P_2 - P_1) \cdot g \cdot \pi} \right)^{\frac{1}{3}} \qquad \text{(C.9)}$$

Sample Calculation:

$$b_e = \left(-\frac{\left(-0.0420 \frac{\text{ft}^3}{\text{sec}}\right) \cdot 6 \cdot 0.000166 \frac{\text{ft}^2}{\text{sec}} \cdot \ln\left(\frac{0.49 \text{ ft}}{0.0104 \text{ ft}}\right)}{(28{,}707 \text{ ft air absolute} - 25{,}623 \text{ ft air absolute}) \cdot 32.2 \frac{\text{ft}}{\text{sec}^2} \cdot \pi} \right)^{\frac{1}{3}}$$

$$b_e = 0.00080 \text{ ft} \cdot \frac{12 \text{ in.}}{\text{ft}} = 0.0096 \text{ in.}$$

C.3.3 Calculation of Flow Velocity from Standard Flow Rate and Effective Aperture with Gas Compressibility Effects

$$V = \frac{Q_s}{2 \cdot \pi \cdot R_{(\text{of interest})} \cdot b_e} \tag{C.10}$$

Sample Calculation-Velocity at a Radius of 0.5 in.:

$$V = \frac{-0.0420 \frac{\text{ft}^3}{\text{sec}}}{2 \cdot \pi \cdot 0.05 \text{ ft} \cdot 0.00079 \text{ ft}} = -169.23 \frac{\text{ft}}{\text{sec}}$$

C.3.4 Calculation of Reynolds Number from Flow Velocity and Effective Aperture with Gas Compressibility Effects

$$Re = \frac{2 \cdot b_e \cdot |V|}{\nu} \tag{C.11}$$

Sample Calculation-Reynolds Number at a Radius of 0.5 in.:

$$Re = \frac{2 \cdot 0.00079 \text{ ft} \cdot \left| -169.23 \frac{\text{ft}}{\text{sec}} \right|}{0.000166 \frac{\text{ft}^2}{\text{sec}}} \qquad Re=1,611$$

C.3.5 Calculation of Exponent Under Turbulent Flow Conditions with Gas Compressibility Effects

$$n = \frac{\ln\left(-\dfrac{(2\cdot P_1)\cdot Q_s\cdot 6\cdot \nu\cdot \ln\left(\dfrac{R_2}{R_1}\right)}{\left(P_2^2 - P_1^2\right)\cdot g\cdot \pi}\right)}{\ln(\text{average } b_e \text{ (laminar flow)})} \qquad \text{(C.12)}$$

Sample Calculation: Note that these data were not collected under turbulent flow conditions, and are used only to express the calculation.

$$n = \frac{\ln\left(-\dfrac{(2\cdot 25{,}623 \text{ ft air absolute})\cdot\left(-0.042\dfrac{\text{ft}^3}{\text{sec}}\right)\cdot 6\cdot 0.000166\dfrac{\text{ft}^2}{\text{sec}}\cdot\ln\left(\dfrac{0.49 \text{ ft}}{0.0104 \text{ ft}}\right)}{\left((28{,}707 \text{ ft air absolute})^2 - (25{,}623 \text{ ft air absolute})^2\right)\cdot 32.2\dfrac{\text{ft}}{\text{sec}^2}\cdot\pi}\right)}{\ln(0.00079\text{ft})}$$

$$n = 3.00$$

APPENDIX D

HORIZONTAL INFILTROMETER TEST DATA

This appendix presents data collected using the horizontal infiltrometer devices. Results are presented for three tests performed with the rigid, horizontal infiltrometer, and for four tests performed with the semi-confined horizontal infiltrometer. The test consisted of creating an artificial discrete fracture in samples of the Woodbury Formation which were compacted into the horizontal infiltrometers. Experiments were performed by increasing or decreasing the moisture content of the soil through the fracture, and then monitoring the changes in fracture flow rate as an indicator of aperture change. It is noted that the results presented in this appendix are limited to calibration and development testing only. Additional experiments will be conducted as part of future studies.

Table D.1 Results of Rigid, Confined Horizontal Infiltrometer Test No. 1

Date	Elapsed Time(min)	Time	Density (lb/ft^3)	Temperature (°C)	Weight of System (lb)	Weight of Soil (lb)	Water (lb)	Average Moisture (%)	Pressure (in Hg)	Flow (l/min)
Vacuum Pump with Dry Air										
11.22.94	0	2100	93.9	24	23.48	3.07	0.92	30.0	-18.5	-5 l/min
11.22.94	30	2130	93.9	24	23.48	3.07	0.92	30.0	-16.4	-7 l/min
11.22.94	70	2210	93.9	24	23.47	3.07	0.91	29.6	-15.5	-8 l/min
11.23.94	712	0852	93.9	21	23.25	3.07	0.69	22.5	-11.0	-13 l/min
11.23.94	1190	1650	93.9	22	23.13	3.07	0.57	18.6	-11.5	-13 l/min
11.28.94	8055	1115	93.9	25	22.61	3.07	0.05	1.63	-12.0	-12 l/min
11.28.94	8590	2010	93.9	27	22.58	3.07	0.02	0.65	-12.0	-12 l/min
Vacuum Pump with Cool Moist Air (third gauge added to system)										
12.06.94	0	1535	93.9	25	24.07	3.07	0.02	0.65	-12.5	-11.5 l/min
12.07.94	1052	0907	93.9	25	24.06	3.07	0.01	0.33	-12.5	-11.5 l/min
12.09.94	2740	1315	93.9	24	24.02	3.07	<0.01	<0.33	-12.5	-11.5 l/min
12.09.94	3079	1854	93.9	22	24.02	3.07	<0.01	<0.33	-12.5	-11.5 l/min
Comparison of Vacuum Pump to Building Vacuum										
Pump	--	--	--	--	--	--	--	--	-1.0	-0.5 CFM
Bldg.	--	--	--	--	--	--	--	--	-1.0	-1.0 CFM
Distilled Water Added Through Flow Meter-Building Vacuum										
12.12.94	initial	--	93.9	--	24.74	3.07	<0.01-0.69?	<0.33-22.5?	-2.5	-1.5 CFM
12.12.94	8 oz.	1935	93.9	--	24.85	3.07	0.08-0.80?	2.6-26.0?	-6.0	-1.25 CFM
12.12.94	8 oz.	1940	93.9	--	24.87	3.07	0.09-0.82?	2.9-26.7?	-7.0	-1.1 CFM
Building Vacuum (fluctuates from 15 to 21" Hg) with Warm Moist Air										
12.14.94	initial	1515	93.9	--	24.25	3.07	0.20?	6.5?	-3.5	-1.25 CFM
12.15.94	1440	1515	93.9	--	24.17	3.07	0.12?	3.9?	-3.75	-1.25 CFM
12.15.94	1740	2015	93.9	--	24.25	3.07	0.20?	6.5?	-3.75	-1.25 CFM
12.19.94	filled	1805	93.9	--	24.26	3.07	0.21?	6.8?	-3.0	-1.25 CFM
12.19.94	7435	1910	93.9	--	24.30	3.07	0.25?	8.1?	-3.0	-2 CFM
12.20.94	8295	0930	93.9	--	24.68	3.07	0.63?	20.52?	-3.25	-1.75 CFM
12.20.94	8500	1255	93.9	--	24.70	3.07	0.65?	21.17?	-3.25	-1.75 CFM

Table D.2 Results of Rigid, Confined Horizontal Infiltrometer Test No. 2

Date	Time	Atm. P ("Hg)	Hum. (%)	Temp (°C)	Weight (lb)	Extr. P1 ("H_2O)	Extr. P2 ("H_2O)	System P ("H_2O)	Filter P ("H_2O)	Flow
Cool Humidifier										
2.19.95	5:10 PM	30.27	32	78	-25.57	-50	-47	-47	0	-36 CFH
2.20.95	8:05 AM	30.25	36	78	-25.36	-33	-18	-20	-2	-1.75 CFM
Warm Humidifier										
2.20.95	9:52 AM	30.21	36	78	-25.36	-31	-18	-20	-2	-2.1 CFM
	11:32 AM	30.12	34	78	-25.25	-31	-19	-20	-2	-2.25 CFM
	4:05 PM	29.98	34	82	-25.18	-32	-20	-20	-2	-1.9 CFM
	6:13 PM	29.95	34	81	-25.27	-31	-18	-19	-2	-1.9 CFM
	7:17 PM	29.93	35	81	-25.28	-30	-17	-18	-2	-1.9 CFM
	8:14 PM	29.94	36	81	-25.28	-30	-17	-18	-2	-1.9 CFM
2.21.95	10:25 AM	29.58	44	76	-25.56	-30	-16	-18	-2	-1.9 CFM
	11:40 AM	29.60	45	80	-25.31	-30	-17	-18	2	-1.9 CFM
	2:04 PM	29.52	41	79	-25.31	-31	-19	-20	-2	-1.8 CFM
	6:20 PM	29.59	40	79	-25.35	-34	-24	-25	-1.5	-1.4 CFM
2.22.95	9:27 AM	29.59	34	78	-25.59	-45	-45	-44	0	-17 CFH
	11:35 AM	29.58	33	78	-25.58	-45	-44	-42	0	-14 CFH
	2:20 PM	29.52	31	80	-25.51	-37	-30	-30	-0.5	-1.3 CFM
2.23.95	9:20 PM	29.68	32	77	-25.31	-31	-19	-20	-2	-1.9 CFM
	12:51 PM	29.66	31	75	-25.49	-37	-28	-28	-1.5	-1.6 CFM
	2:50 PM	29.68	32	74	-25.58	-40	-33	-34	-1	-1.3 CFM
	6:30 PM	29.72	34	70	-25.55	-42	-37	-38	0	-1 CFM
2.24.95	9:35 AM	29.89	35	66	-25.59	-45	-44	-46	0	-15 CFH
	2:45 PM	29.90	30	68	-25.62	-47	-48	-50	0	-6.5 CFH
	9:22 PM	30.03	29	66	-25.62	-48	-48	-50	0	-3.5 CFH
Humidifier Off-Begin Drying										
2.25.95	10:45 AM	30.10	23	67	-25.58	-47	-48	-50	0	-2.5 CFH
	3:45 PM	29.98	18	63	-25.58	-47	-48	-49	0	-4 CFH
2.26.95	12:30 PM	30.19	23	70	-25.56	-47	-49	-50	0	-4 CFH

(continued on next page)

Table D.2 Results of Rigid, Confined Horizontal Infiltrometer Test No. 2 (Continued)

Date	Time	Atm. P ("Hg)	Hum. (%)	Temp (°C)	Weight (lb)	Extr. P1 ("H_2O)	Extr. P2 ("H_2O)	System P ("H_2O)	Filter P ("H_2O)	Flow
2.27.95	9:43 AM	30.23	27	67	25.54	-47	-49	-50	0	-4 CFH
	4:05 PM	30.15	23	74	25.54	-47	-49	-50	0	-4 CFH
	9:10 PM	30.16	22	71	25.53	-47	-48	-49	0	-5 CFH
2.28.95	9:27 AM	30.14	24	74	25.33	-36	-26	-27	-1	-1.4 CFM
	2:45 PM	30.00	19	81	25.26	-36	-26	-27	-1.5	-1.4 CFM
	6:50 PM	30.05	19	74	25.21	-32	-20	-18	-2	-1.7 CFM
2.29.95	9:10 AM	30.22	23	72	25.14	-32	-19	-17	-2	-1.8 CFM
2.30.95	11:10 AM	30.18	39	72	25.20	-31	-18	-16	-2	-2.2 CFM

Table D.3 Results of Rigid, Confined Horizontal Infiltrometer Test No. 3

Date	Time	System P ("H_2O)	Extr. P1 ("H_2O)	Extr. P2 ("H_2O)	Filter P ("H_2O)	Weight (lbs)	Flow	Atm. P ("Hg)	Humidity (%)	Temperature (°F)
Warm Humidifier										
04.01.95	2:05 PM	-50	-48	-48	0	24.97	-20 CFH	30.07	26	70
	2:45 PM	-49	-48	-48	0	25.08	-6 CFH	30.04	24	71
	3:25 PM	-49	-48	-48	0	25.09	-6 CFH	30.03	24	72
	4:45 PM	-48	-47	-47	0	25.12	-5 CFH	30.03	23	71
	5:35 PM	-48	-47	-47	0	25.14	-6 CFH	30.03	22	70
	7:55 PM	-49	-48	-48	0	25.14	-7 CFH	30.03	22	74
04.02.95	12:30 PM	-49	-49	-49	0	25.18	-3 CFH	30.12	22	70
(Daylight	1:30 PM	-49	-49	-49	0	25.18	-3 CFH	30.13	22	70
Savings	2:45 PM	-49	-49	-49	0	25.18	-3 CFH	30.13	22	70
Time)	4:45 PM	-49	-49	-49	0	25.18	-3 CFH	30.13	24	69
	5:25 PM	-49	-49	-49	0	25.18	-3 CFH	30.14	24	69
04.03.95	9:05 AM	-49	-49	-49	0	25.18	-3 CFH	30.36	24	72

Table D.4 Results of Semi-Confined Horizontal Infiltrometer Test No. 1

Experimental Constants	Minutes	P_1 ("H_2O)	P_2 ("H_2O)	$Q_{rotameter}$ (CFH)	$Q_{electronic}$ (CFM)	Temp. (°F)	Weight (lb)
L_2-L_1=1.33 ft.	0	-24	29.85	-144	-138	71	54.01
w=0.21 ft.	15	-24	29.85	-138	-138	71	51.15
initial aperture:	55	-24	29.84	-84	-102	72	--
0.0394 in.	135	-24	29.84	-43	-54	74	51.48
	1755	-10	29.92	-180	-180	75	50.38

Table D.5 Results of Semi-Confined Horizontal Infiltrometer Test No. 2

Experimental Constants	Minutes	P_1 ("H_2O)	P_2 ("H_2O)	$Q_{rotameter}$ (CFH)	$Q_{electronic}$ (CFM)	Temp. (°F)	Weight (lb)
L_2-L_1=1.33 ft.	0	-50	30.27	-33	-0.45	77	90.18
w=0.21 ft.	5	-50	30.27	-33	-0.5	77	--
initial aperture:	10	-49	30.27	-24	-0.3	77	--
0.0394 in.	15	-49	30.27	-20	-0.3	77	89.93
moistening-	20	-49	30.27	-17	-0.2	77	--
warm	25	-49	30.27	-12	-0.2	78	--
humidifier	30	-48	30.27	-11	-0.2	78	89.88
	35	-48	30.27	-10	-0.2	78	--
	40	-48	30.27	-9.5	-0.2	78	--
	45	-48	30.27	-9.5	-0.2	78	89.89
	50	-49	30.27	-9.5	-0.2	79	--
	55	-49	30.27	-9.5	-0.2	79	--
	60	-49	30.27	-9.5	-0.2	79	89.89
	65	-49	30.26	-9.5	-0.2	80	--
	70	-49	30.26	-9.5	-0.2	80	--
	75	-49	30.25	-9.5	-0.2	80	89.91
	80	-49	30.25	-9.5	-0.2	80	--
	85	-49	30.24	-9.5	-0.2	80	--
	90	-49	30.24	-9.5	-0.2	80	89.91
	95	-49	30.24	-9.5	-0.2	80	--
	100	-49	30.24	-9.5	-0.2	80	--
	105	-49	30.24	-9.5	-0.2	80	89.93
	110	-49	30.24	-9.5	-0.2	80	--
no moisture-	115	-48	30.24	-9.5	-0.2	80	89.94
drying	120	-47	30.24	-9.5	-0.2	80	--
	125	-47	30.24	-9.5	-0.2	80	--
	130	-47	30.24	-10	-0.2	80	89.94
	135	-47	30.24	-12	-0.3	80	--
	140	-47	30.24	-13	-0.3	80	--
	145	-47	30.24	-14	-0.3	80	89.93
	150	-47	30.24	-15	-0.3	80	--
	155	-47	30.24	-16	-0.3	80	--
	160	-47	30.24	-17	-0.3	80	89.93
	165	-47	30.24	-18	-0.3	80	

(continued on next page)

Table D.5 Results of Semi-Confined Horizontal Infiltrometer Test No. 2 (Continued)

Experimental Constants	Minutes	P_1 ("H_2O)	P_2 ("H_2O)	$Q_{rotameter}$ (CFH)	$Q_{electronic}$ (CFM)	Temp. (°F)	Weight (lb)
no moisture-drying	170	-47	30.24	-19	-0.35	80	--
	175	-47	30.24	-20	-0.4	80	89.92
	180	-47	30.24	-20	-0.4	80	--
	185	-47	30.24	-20	-0.4	80	--
	190	-47	30.24	-21	-0.4	80	89.92
	195	-47	30.23	-21	-0.4	80	--
	200	-47	30.23	-23	-0.45	80	--
	205	-47	30.23	-25	-0.5	80	89.92
	210	-47	30.23	-26	-0.5	80	--
	215	-47	30.23	-26	-0.5	80	--
	220	-47	30.23	-27	-0.5	80	89.91
	225	-47	30.23	-28	-0.5	80	--
	230	-47	30.23	-28	-0.5	80	--
	235	-47	30.23	-29	-0.55	80	89.91
	240	-47	30.23	-30	-0.55	80	--
	245	-47	30.24	-31	-0.6	80	--
	250	-47	30.24	-33	-0.6	80	89.91
	255	-47	30.24	-35	-0.6	80	--
	260	-47	30.24	-36	-0.7	80	--
	265	-47	30.24	-37	-0.7	80	89.91
	270	-47	30.24	-39	-0.7	80	--
	275	-46	30.24	-40	-0.8	80	--
	280	-46	30.24	-42	-0.8	80	90.00
	285	-46	30.24	-43	-0.8	80	--
	290	-46	30.24	-45	-0.8	80	--
	295	-46	30.23	-46	-0.9	80	89.99
	300	-46	30.23	-48	-0.9	80	--
	305	-46	30.23	-49	-0.9	80	--
	310	-46	30.23	-50	-0.9	80	89.97
	315	-45	30.23	-50	-1.0	80	--
moisture-manual spray mist	320	-45	30.23	-50	-0.9	80	--
	325	-45	30.23	-50	-0.9	80	89.96
	330	-45	30.23	-50	-0.9	80	--
	335	-45	30.23	-49	-0.9	80	--
	340	-45	30.23	-45	-0.8	80	--
	345	-46	30.23	-42	-0.8	80	90.01
	350	-46	30.23	-37	-0.7	80	--
	355	-46	30.23	-34	-0.6	80	--
	360	-46	30.23	-31	-0.6	80	90.03
	365	-47	30.23	-27	-0.5	80	--
	370	-47	30.23	-21	-0.4	80	--
	375	-47	30.23	-16	-0.3	80	90.05
	380	-47	30.23	-13	-0.3	80	--
	385	-48	30.23	-9	-0.2	80	--
	390	-48	30.23	-9	-0.2	80	90.10

(continued on next page)

Table D.5 Results of Semi-Confined Horizontal Infiltrometer Test No. 2 (Continued)

Experimental Constants	Minutes	P_1 ("H_20)	P_2 ("H_20)	$Q_{rotameter}$ (CFH)	$Q_{electronic}$ (CFM)	Temp. (°F)	Weight (lb)
moisture-	395	-49	30.23	-9	-0.2	80	--
manual spray	400	-49	30.23	-8.5	-0.2	80	--
moisture	405	-49	30.23	-8	-0.2	80	90.15
diffusion (55 hrs.)	410	-49	30.23	-8	-0.2	80	--
no moisture-	463	-53	30.53	-9	-0.1	71	89.39
drying	468	-48	30.53	-5.5	-0.1	71	--
	473	-48	30.53	-5.5	-0.1	71	--
	478	-48	30.53	-5.5	-0.1	71	89.39
	483	-47	30.53	-5.5	-0.1	71	--
	488	-46	30.53	5.5	-0.1	71	--
	493	-49	30.53	-6.5	-0.1	71	89.38
	498	-49	30.52	-8	-0.1	72	--
	503	-49	30.52	-8	-0.1	72	--
	508	-49	30.52	-8	-0.1	72	89.37
	513	-49	30.52	-9	-0.1	72	--
	518	-49	30.52	-9	-0.1	72	--
	523	-49	30.52	-9	-0.1	72	--
	528	-49	30.52	-9	-0.1	72	89.36
	533	-49	30.52	-9	-0.1	72	--
	538	-49	30.52	-9	-0.1	72	89.36
	543	-48	30.52	-9	-0.1	72	--
	548	-48	30.51	-9	-0.1	72	--
	553	-48	30.51	-9	-0.1	72	89.35
	558	-48	30.51	-9	-0.1	72	--
	563	-48	30.51	-9	-0.1	72	--
	568	-48	30.51	-9	-0.1	72	89.34
	573	-48	30.51	-9	-0.1	72	--
	578	-48	30.50	-9	-0.1	73	--
	583	-48	30.50	-9	-0.1	73	89.34
	588	-48	30.50	-9	-0.1	73	--
	593	-48	30.50	-9	-0.1	73	--
	598	-48	30.50	-9	-0.1	73	89.32
	603	-48	30.50	-10	-0.15	73	--
	608	-48	30.49	-10	-0.2	73	--
	613	-48	30.49	-10	-0.2	73	--
	618	-48	30.49	-10	-0.2	73	89.32
	623	-48	30.49	-10	-0.2	73	--
	628	-48	30.49	-10	-0.2	73	--
	633	-48	30.49	-10	-0.2	73	89.31
	638	-48	30.49	-10	-0.2	73	--
	643	-48	30.49	-10	-0.2	74	--
	648	-48	30.49	-10	-0.2	74	--
	663	-48	30.49	-10	-0.2	74	--
	678	-47	30.48	-10	-0.2	74	--
saturation(1'head)	1683	-28	30.28	-138	-2.4	72	89.00

(continued on next page)

Table D.5 Results of Semi-Confined Horizontal Infiltrometer Test No. 2 (Continued)

Experimental Constants	Minutes	P_1 ("H_2O)	P_2 ("H_2O)	$Q_{rotameter}$ (CFH)	$Q_{electronic}$ (CFM)	Temp. (°F)	Weight (lb)
no moisture-drying	1684	-49	30.20	-5	-0.1	79	--
	1709	-49	30.20	-5	-0.1	79	--
	2734	-49	30.27	-5	-0.1	78	--
	2958	-49	30.23	-5	-0.1	81	--
	4139	-49	30.26	-5	-0.1	79	--
	4499	-49	30.20	-5	-0.1	82	--
	4851	-49	30.17	-5	-0.1	80	--
	5619	-49	30.14	-5	-0.1	80	91.50

Table D.6 Results of Semi-Confined Horizontal Infiltrometer Test No. 3

Experimental Constants	Minutes	P_1 ("H_2O)	P_2 ("H_2O)	$Q_{rotameter}$ (CFH)	$Q_{electronic}$ (CFM)	Temp. (°F)	Weight (lb)
L_2-L_1=1.33 ft.	0	-50	30.04	-90	-1.5	80	--
w=0.21 ft.	10	-50	30.04	-60	-1.0	80	--
initial aperture:	30	-50	30.03	-72	-1.1	82	--
0.0394 in.	60	-50	30.02	-90	-1.7	82	--
moistening	65	-50	30.02	-66	-1.2	82	--
with spray	85	-50	30.01	-60	-1.0	82	--
nozzle	105	-51	30.00	-42.5	-0.9	82	--
	110	-50	30.20	-144	-2.1	75	--
	115	-49	30.20	-120	-2.0	75	--
	195	-50	30.21	-90	-2.0	78	--
	220	-50	30.21	-90	-2.0	78	--
	382	-50	30.21	-150	-2.7	77	--
	405	-50	30.21	-96	-1.6	76	--
	426	-50	30.21	-78	-1.6	76	--
	440	-50	30.48	-96	-2.0	72	--
	486	-49	30.48	-150	-2.6	73	--
	652	-42	30.48	-204	-3.5	73	--
	670	-50	30.48	-168	-3.0	73	--
	695	-48	30.48	-174	-3.1	73	--
	700	-50	30.50	-180	-2.3	71	--
	702	-50	30.50	-204	-2.5	71	--
	735	-42	30.50	-186	-3.4	71	--
no moisture-drying	785	-38	30.48	-180	-3.6	74	--
	922	-37	30.45	-204	-4.0	74	--

Table D.7 Results of Semi-Confined Horizontal Infiltrometer Test No. 4

Experimental Constants	Minutes	P_1 ("H_20)	P_2 ("H_20)	$Q_{rotameter}$ (CFH)	$Q_{electronic}$ (CFM)	Temp. (°F)	Weight (lb)
L_2-L_1=1.33 ft.	0	-40	30.10	-174	-2.9	75	68.28
w=0.21 ft.	5	-41	30.10	-126	-2.2	76	--
initial aperture:	10	-40	30.10	-96	-1.8	76	--
0.0394 in.	15	-40	30.10	-84	-1.6	76	--
moistening	20	-40	30.10	-72	-1.4	76	--
with spray	25	-40	30.10	-60	-1.2	76	--
nozzle	30	-40	30.10	-48	-1.0	76	--
	35	-40	30.10	-48	-0.9	76	--
	40	-40	30.10	-42	-0.8	76	--
	45	-40	30.10	-38	-0.7	76	--
	50	-40	30.10	-35	-0.7	77	--
	55	-40	30.10	-29	-0.6	77	--
	60	-40	30.10	-21	-0.5	77	69.66
	65	-40	30.10	-19	-0.5	77	--
	70	-40	30.10	-19	-0.5	78	--
	75	-40	30.10	-19	-0.5	78	--
	80	-40	30.10	-18	-0.4	78	--
	85	-40	30.10	-16	-0.4	78	--
	90	-40	30.10	-15	-0.4	78	--
	95	-40	30.10	-14	-0.4	78	--
	100	-40	30.10	-14	-0.3	78	--
	105	-40	30.10	-13	-0.3	78	--
	110	-40	30.10	-12	-0.3	78	--
	115	-40	30.09	-11	-0.3	78	--
	120	-40	30.09	-11	-0.3	78	69.66
	125	-40	30.09	-10	-0.3	78	--
	130	-40	30.09	-10	-0.3	78	--
	135	-40	30.09	-10	-0.3	78	--
	140	-40	30.09	-10	-0.3	78	--
	145	-40	30.09	-10	-0.2	78	--
	150	-40	30.08	-9.5	-0.2	78	--
	155	-40	30.08	-9.5	-0.2	78	--
	160	-40	30.08	-9.5	-0.2	78	--
	165	-40	30.08	-9.0	-0.2	78	--
	170	-40	30.08	-9.0	-0.2	78	--
	175	-40	30.08	-9.0	-0.2	78	--
	180	-40	30.08	-9.0	-0.2	78	69.72
	185	-40	30.08	-9.0	-0.2	78	--
	190	-40	30.08	-8.5	-0.2	78	--
	195	-40	30.08	-8.5	-0.2	78	--
	200	-40	30.08	-7.5	-0.2	79	--
	205	-40	30.08	-7.0	-0.2	79	--
	210	-40	30.08	-6.5	-0.2	79	--
	215	-40	30.07	-6.0	-0.2	79	--

(continued on next page)

Table D.7 Results of Semi-Confined Horizontal Infiltrometer Test No. 4 (Continued)

Experimental Constants	Minutes	P_1 ("H_2O)	P_2 ("H_2O)	$Q_{rotameter}$ (CFH)	$Q_{electronic}$ (CFM)	Temp. (°F)	Weight (lb)
moistening with spray nozzle	220	-40	30.07	-6	-0.2	79	--
	225	-40	30.07	-5.5	-0.2	79	--
	230	-40	30.06	-5	-0.2	79	--
	235	-40	30.06	-5	-0.2	79	69.80
no moisture-drying	240	-40	30.06	-7	-0.2	79	--
	245	-40	30.06	-8	-0.2	79	--
	250	-40	30.06	-8	-0.2	79	--
	255	-40	30.06	-8	-0.2	80	--
	265	-40	30.06	-8	-0.2	80	--
	280	-40	30.06	-8	-0.2	80	--
	295	-40	30.06	-8	-0.2	80	--
	325	-40	30.06	-8	-0.2	80	--
	355	-40	30.06	-8	-0.2	80	--
	385	-40	30.05	-8	-0.2	80	--
	415	-40	30.03	-8	-0.2	80	--
	445	-40	30.03	-8	-0.2	80	--
	450	-40	30.20	-4	-0.0	71	69.74
	580	-40	30.19	-7	-0.0	74	--
	740	-40	30.16	-7	-0.1	76	--
	880	-40	30.12	-7	-0.1	76	--
	990	-40	30.04	-7	-0.15	81	--
	995	-40	30.08	-5	0.0	74	--
	1180	-40	30.08	-66	-1.0	76	--
	1265	-40	30.07	-66	-1.0	75	--
	1270	-40	30.07	-47	-0.9	75	--
	1355	-40	30.07	-60	-1.2	76	--
	1370	-40	30.07	-72	-1.1	76	--
	1475	-40	30.06	-132	-2.4	76	--
	1485	-40	30.06	-132	-2.5	76	--
	1535	-40	30.13	-180	-3.0	76	--
	1540	-40	30.27	-17	-0.3	72	--
	1550	-40	30.27	-23	-0.5	72	--
	1610	-40	30.27	-46	-0.9	72	--
	1650	-40	30.26	-90	-1.5	74	--
	1710	-40	30.26	-150	-2.7	74	--
moistening with spray nozzle	1725	-40	30.27	-150	-2.7	74	--
	1740	-40	30.27	-90	-2.0	74	--
	1755	-40	30.27	-45	-0.9	74	--
	1770	-40	30.27	-35	-0.7	74	--
	1785	-40	30.27	-24	-0.5	75	--
	1800	-40	30.27	-20	-0.4	74	--
	1810	-40	30.27	-11	-0.2	74	--
	1835	-40	30.27	-10	-0.2	74	--
	1850	-40	30.27	-10	-0.2	75	--

(continued on next page)

Table D.7 Results of Semi-Confined Horizontal Infiltrometer Test No. 4 (Continued)

Experimental Constants	Minutes	P_1 ("H_20)	P_2 ("H_20)	$Q_{rotameter}$ (CFH)	$Q_{electronic}$ (CFM)	Temp. (°F)	Weight (lb)
moistening-spray nozzle	1865	-40	30.26	-10	-0.2	76	--
	1895	-40	30.25	-10	-0.2	78	--
no moisture-drying	1900	-40	30.28	-2	0.0	72	--
	1940	-40	30.30	-2	0.0	72	--
	1990	-40	30.37	-2	0.0	72	--
	2075	-40	30.37	-3	0.0	74	--
	2165	-40	30.33	-3	0.0	74	--
	2290	-40	30.31	-6	-0.1	74	--
	2325	-40	30.30	-10	-0.2	74	--
	2330	-40	30.23	-8	0.0	71	--
	2410	-40	30.23	-12	-0.2	74	--
	2475	-40	30.22	-17	-0.5	74	--
	2480	-40	30.22	-10	-0.2	74	--
	2570	-40	30.22	-11	-0.3	76	--
	2635	-40	30.19	-11	-0.4	76	--
	2715	-40	30.10	-20	-0.6	78	--
	2720	-40	30.12	-9	-0.2	76	--
	2795	-40	30.12	-9	-0.2	77	--
	2925	-40	30.10	-16	-0.5	78	--
	2980	-40	30.10	-26	-0.7	78	--

APPENDIX E

AIR INFILTRATION CALCULATIONS

This appendix presents sample calculations which were performed on data from the semi-confined horizontal infiltrometer tests, including calculations of infiltration rate and equivalent pneumatic and hydraulic conductivities.

E.1 Infiltration Rates

Using results of the air tightness test for driest condition of semi-confined horizontal infiltrometer Test No. 2, the infiltration rate was calculated as follows:

E.1.1 Calculating Total Volume of Pipes and Fittings

$$V_t = (2 \cdot V_{3"\phi}) + (2 \cdot V_{0.5"\phi})$$

$$V_{3"\phi} = \pi \cdot (1.5 \text{ in.})^2 \cdot (7 \text{ in.}) = 49.48 \text{ in.}^3 / 12 \text{ in.}^3 = 0.0286 \text{ ft}^3$$

$$V_{0.5"\phi} = \pi \cdot (0.25 \text{ in.})^2 \cdot (5.5 \text{ in.}) = 1.08 \text{ in.}^3 / 12 \text{ in.}^3 = 0.0006 \text{ ft}^3$$

$$V_t = 0.0346 \text{ ft}^3 = 0.9799 \text{ L}$$

E.1.2 Calculating the Change in Density with Change in Pressure

$$\rho_{std.} = \frac{(1 \text{ atm}) \cdot (29 \text{g / mole})}{\left(0.0821 \frac{\text{l} \cdot \text{atm}}{\text{K / mole}}\right) \cdot (298 K)} = 1.1853 \text{ g / L} = 0.074 \text{ lb / ft}^3$$

$$\rho_{vac(52"water).} = \frac{(0.8729 \text{ atm}) \cdot (29 \text{g / mole})}{\left(0.0821 \frac{\text{l} \cdot \text{atm}}{\text{K / mole}}\right) \cdot (298 K)} = 1.034 \text{ g / L}$$

E.1.3 Calculating the Weight of Air for Each Density

$$\rho = \frac{\text{specific weight of air (g)}}{\text{total volume (L)}}$$

$$\gamma_{std.} = (1.1853\ g/L)\cdot(0.9799\ L) = 1.1615\ g = 0.00256\ lb$$
$$\gamma_{vac.(52"water)} = (1.034\ g/L)\cdot(0.9799\ L) = 1.0132\ g = 0.00223\ lb$$

E.1.4 Calculating the Mass Flow Rate (Infiltration) for Loss of Pressure

Note: This assumes a linear drop in pressure (52 in. water) over time (20 sec.).

$$Q_{inf.(mass)} = \frac{\gamma_{std.} - \gamma_{vac.}}{\text{time}}$$

$$Q_{inf.(mass)} = \frac{0.00256\ lb - 0.00223\ lb}{20\ sec} = 1.65\ X\ 10^{-5}\ lb/sec$$

E.1.5 Converting Volumetric Flow Rate to Mass Flow Rate

$$Q_{inf(vol)} = \frac{Q_{inf(mass)}}{\rho_{std.}}$$

$$Q_{inf(vol)} = \frac{1.65X10^{-5}\ lb/sec}{0.074\ lb/sec} = 0.0002\ ft^3/sec = 0.013\ ft^3/min = 0.8\ ft^3/hr$$

E.1.6 Calculating Infiltration Rate for Loss of 22 in. Water Vacuum Pressure

Note: This represents the early portion of the pressure-time curve, and assumes a linear drop in pressure (22 in. water) over time (1 sec.).

$$\rho_{vac.} = \frac{(0.9459\ atm)\cdot(29\ g/mole)}{\left(0.0821\frac{l\cdot atm}{K/mole}\right)\cdot(298K)} = 1.1212\ g/L$$

$$\gamma_{vac(22"water)} = (1.1212\ g/L)\cdot(0.9799\ L) = 1.0987\ g = 0.002423\ lb$$

$$Q_{inf(mass)} = \frac{0.00256\ lb - 0.002423\ lb}{1\ sec} = 1.37\ X\ 10^{-4}\ lb/sec$$

$$Q_{inf(vol)} = \frac{1.37X10^{-4}\ lb/sec}{0.074\ lb/ft^3} = 0.00185\ ft^3/sec = 0.111\ ft^3/sec = 6.66\ ft^3/hr$$

E.2 Equivalent Pneumatic and Hydraulic Conductivities

One-dimensional Darcy's law was applied to results of the semi-confined horizontal infiltrometer test no. 3 by assuming infiltration from top and bottom of block and compensating for other areas by increasing the control volume beyond the width of the aperture. Pneumatic and hydraulic conductivities were calculated as follows:

E.2.1 Gradient Determination

$\Delta h = 33.99$ ft water - 38.16 ft water = -4.17 in. water = -3.253 ft air

$$i = \frac{\Delta h}{\Delta l} = \frac{-3.253\ ft\ air}{0.237\ ft} = -13,724$$

E.2.2 Calculation of Pneumatic and Hydraulic Conductivities

$$K = \frac{Q}{i \cdot A};\ \text{where } Q = -0.5\ CFM$$

$$Area = (\pi)\cdot(4.86\ in.)\cdot(16\ in.) = 235\ in^2/12\ ft^2 = 1.6\ ft^2$$

$$K_{pneumatic} = \frac{-0.5\ ft^3/min}{(-13,724)\cdot(1.6\ ft^2)} = 2.3\ X\ 10^{-5}\ ft/min = 1.2\ X\ 10^{-5}\ cm/sec$$

$$K_{hydraulic} = \frac{K_{pneumatic}}{12} = \frac{1.2\ X\ 10^{-5}\ cm/sec}{12} = 1.0\ X\ 10^{-6}\ cm/sec$$

E.2.3 Computing Hydraulic Conductivities for Other Infiltration Rates

where Q = 0.3 CFM $K_{hydraulic} = 6 \text{ X } 10^{-7}$ cm / sec

where Q = 0.1 CFM (see results of Test No. 2 above) $K_{hydraulic} = 2 \text{ X } 10^{-7}$ cm / sec

where Q = 0.01 CFM (see results of Test No. 2 above) $K_{hydraulic} = 4 \text{ X } 10^{-8}$ cm / sec

REFERENCES

Altmeyer, W.T. 1955. "Discussion of the Engineering Properties of Expansive Clays," *Proceedings of the American Society Civil Engineers 81* (Separate No. 658): 17-19.

American Society for Testing and Materials. 1970. Special Procedures for Testing Soil and Rock for Engineering Purposes, Special Technical Publication 479, 5th edition.

American Society for Testing and Materials. 1994. Annual Book of Standards, Vol. 4.08, Philadelphia, PA.

Atterberg, A.. 1911. "Uber die Physikalische Bodenuntersuchung und uber die Plastizitat der Tone," *Inter. Mitt. Bodenkunde*, 1: 10-43.

B&J Warren and Sons. 1994. Personal Communication, October 1994, State Highway No. 33, Hightstown, NJ.

Barone, F.S., Rowe, R.K., and R.M. Quigley. 1992. "Laboratory Estimation of Diffusion and Adsorption Coefficients for Several Volatile Organics in a Natural Clayey Soil," *Journal of Contaminant Hydrology*, 10(3):225-250.

Blaser, H.D. and K. Arulanandan. 1973. "Expansion of Soils Containing Sodium Sulfate," *Proceedings of the Third International Conference on Expansive Soils*, Haifa, Israel, July 30-August 1, Israel Society of Soil Mechanics and Foundation Engineering.

Bohn, H.L., McNeal, B.L., and G.A. O'Connor. 1985. Soil Chemistry, 2nd edition, John Wiley and Sons, New York, NY.

Brasher, B.R., Franzmeier, D.P., Valassis, V., and S.E. Davidson. 1966. "Use of Saran Resin to Coat Natural Soil Clods for Bulk Density and Water Retention Measurements," *Soil Science*, 101:108.

Brindley, G.W. and G. Brown (eds.). 1980. "Crystal Structure of Clay Minerals and Their X-Ray Identification," Mineralogical Society Monograph No. 5, London.

Carroll, D. 1970. "Clay Minerals: A Guide to Their X-Ray Identification," Geological Society of America, Special Paper 126.

Carter, D.L., Mortland, M.M., and Kemper, W.D. 1982. Methods of Soil Analysis, Chapter 16, Agronomy No. 9, Part 1, 2nd ed., American Society of Agronomy, Madison, WI.

REFERENCES
(Continued)

Chen, F.H. 1965. "The Use of Piers to Prevent the Uplifting of Lightly Loaded Structures Founded on Expansive Soil," Supplementing the Symposium in Print, Texas A&M Press, pp.152-171.

Chen, F.H. 1973. "The Basic Physical Property of Expansive Soils," *Proceedings of the Third International Conference on Expansive Soils*, Haifa, Israel, July 30-August 1, Israel Society of Soil Mechanics and Foundation Engineering.

Chen, F.H. 1988. Foundations on Expansive Soils. American Elsevier Science Publishers, New York, NY.

Coleman, N.T., and G.W. Thomas. 1963. "Buffer Curves of Acid Clays as Affected by the Presence of Ferric Iron and Aluminum," *Soil Science Society of America Proceedings*, 28:187-190.

Compton, P.V. 1970. "A Study of the Swelling Behavior of an Expansive Clay as Influenced by the Clay Microstructure, Soil Suction, and External Loading," Ph.D. Dissertation, Graduate School of Texas A&M University, Austin, TX.

Czurda, K.A. and J. Wagner. 1991. "Cation Transport and Retardation Processes in View of the Toxic Waste Deposition Problem in Clay Rocks and Clay Liner Encapsulation," *Engineering Geology*, 30(1):103-113.

Demetracopoulos, A.C., Korfiatis, G.P., and J.R. Schuring. 1985. "Experimental and Mathematical Investigations on the Effects of Flow and Mass Transport of Hazardous Liquids Through Soils," for NSF Industry/University Cooperative Center for Research in Hazardous and Toxic Substances.

DiCola, R. 1986. "The Effect of Toxic Substances on the Index Properties of Soils," M.S. Thesis, Graduate School of New Jersey Institute of Technology, Newark, NJ.

Ding, Y. 1995. "A Theoretical Analysis of Volatile Contaminant Removal by the Pneumatic Fracturing Process," Ph.D. Dissertation, Department of Civil and Environmental Engineering, New Jersey Institute of Technology, Newark, NJ.

Donaldson, G.W. 1969. "The Occurrence of Problems of Heave and the Factors Affecting its Nature," *Proceedings of the Second International Conference on Expansive Soils*, Texas A & M University, Austin, TX.

REFERENCES
(Continued)

Edil, T.B., Berthouex, P.M., Park, J.K., P.C. Hargett, Sandstrom, L., and S. Zelmanowitz. 1991. "Effects of Volatile Organic Compounds on Clay Landfill Liner Performance," *Waste Management and Research*, 9(3):171-187.

EPA (Environmental Protection Agency). 1992. "Test Methods for Evaluating Solid Waste, Physical/Chemical Methods, SW-846," Office of Solid Waste and Emergency Response, Washington, DC.

EPA (Environmental Protection Agency). 1993. "Accutech Pneumatic Fracturing Extraction and Hot Gas Injection, Phase I, Applications Analysis Report," EPA/540/AR-93/509, Superfund Innovative Technology Evaluation, Risk Reduction Engineering Laboratory, Office of Research and Development, Cincinnati, OH.

Fitzgerald, C.D. 1993. "Integration of Pneumatic Fracturing to Enhance in Situ Bioremediation," M.S. Thesis, Department of Civil and Environmental Engineering, New Jersey Institute of Technology, Newark, NJ.

Gale, J.E. 1975. "A Numerical, Field and Laboratory Study of Flow in Rocks with Deformable Fractures," Ph.D. Dissertation, University of California, Berkeley, CA.

Gillott, J.E. 1987. Clay in Engineering Geology. Developments in Geotechnical Engineering 41. Elsevier Science Publishers, New York, NY.

Grim, R.E. 1962. Applied Clay Mineralogy. McGraw Hill, New York, NY.

Grim, R.E. 1968. Clay Mineralogy, 2nd edition, McGraw Hill, New York, NY.

Hamburg, D.J. 1985. "A Simplified Method for Predicting Heave in Expansive Soils," M.S. Thesis, Colorado State University, Fort Collins, CO.

Higgins, C.M. 1965. "High Pressure Lime Injection," Louisiana Department of Highways, Research Report 17, Interim Report 2.

Holt, J.H. 1969. "A Study of the Physico-Chemical, Mineralogical and Engineering Index Properties of Fine-Grained Soil in Relation to Their Expansive Characteristics," Ph.D. Dissertation, Texas A&M University, College Station, TX.

Holtz, W.G. and H.J. Gibbs. 1956. "Engineering Properties of Expansive Clays," *Transactions of American Society of Civil Engineers*, 21(2814): 641-663.

REFERENCES
(Continued)

Huitt, J.L. 1956. "Fluid Flow in Simulated Fractures," *Journal of the American Institute of Chemical Engineering*, 2:259.

Kassiff, G., Livneh, M., and G. Wiseman. 1969. Pavements on Expansive Clays. Jerusalem Academic Press, Jerusalam, Israel.

King, T.C. 1993. "Mechanism of Pneumatic Fracturing," M.S. Thesis, Department of Civil and Environmental Engineering, New Jersey Institute of Technology, Newark, NJ.

Kinney, D.M. (compiler). 1966. Geology--National Atlas Sheet 74-75: U.S. Geological Survey, Scale 1:7,500,000.

Knudsen, D., Peterson, G.A., and P.F. Pratt. 1986. "Lithium, Sodium, and Potassium," in Methods of Soil Analysis, Chapter 12, Agronomy No. 9, Part 2, 2nd ed., American Society of Agronomy, Madison, WI.

Komornik, A. and M. Livneh. 1969. "Influence of Granular Constituents on the Swelling Characteristics of Expansive Clays," *Proceedings of the Second International Conference on Expansive Soils*, Texas A & M University, Austin, TX.

Krohn, J.P., and J.E. Slosson. 1980. "Assessment of Expansive Clay Soils in the United States," *Proceedings of the Fourth International Conference on Expansive Soils*, June 16-18, Denver, CO. American Society of Civil Engineers, New York, NY.

Lambe, T.W. 1960. "Compacted Clay: Engineering Behavior," *Transactions, The American Society of Civil Engineers*, 125:719-741.

Lambe, T.W. and R.V. Whitman. 1969. Soil Mechanics. John Wiley and Sons, New York, NY.

Langfelder, L.J., Chen, C.F., and J.A. Justice. 1968. "Air permeability of Compacted Cohesive Soils," *Journal of the Soil Mechanics and Foundations Division*, American Society of Civil Engineers, No. SM4, 981-1001.

Liljestrand, H.W., Lo, I.M-C., and Y. Shimizu. 1992. "Sorption of Humic Materials onto Inorganic Surfaces for the Mitigation of Facilitated Pollutant Transport Processes," *Water Science and Technology*, 26(5-6):1221-1228.

Lomize, G.M. 1951. "Fluid Flow in Fractured Rocks,". in Russian, *Gosenergoizdat*, Moscow, Russia.

REFERENCES
(Continued)

Louis, C. 1969. "A Study of Groundwater Flow in Jointed Rock and its Influence on the Stability of Rock Masses," *Rock Mechanics Research*, Report No. 10, Imperial College, University of London.

Lambe, T.W. 1953. "The Structure of Inorganic Soil," *Proc. Am. Soc. Civil Engrs., J. Soil Mech. Found. Div.*, 79, Separate No. 315:1-49.

Lundy, H.L., Jr. and B.J. Greenfield. 1968. Evaluation of Deep in Situ Soil Stabilization by High Pressure Lime Slurry Injection," Highway Res. Rec. 235:27-35.

Maeda, T., Takenaka, H., and B.P. Warkentin. 1977. "Physical Properties of Allophane Soils," In Advances in Agronomy, N.C. Brady (Ed.), Vol. 29, pp. 229-264, Academic Press, New York, NY.

McCrone, W.C. and J.G. Delly. 1973. The Particle Atlas, 2nd edition, Ann Arbor Science, Ann Arbor, MI.

McGonigal, S.T. 1995. "Integration of Pneumatic Fracturing and In Situ Vitrification," M.S. Thesis, Department of Civil and Environmental Engineering, New Jersey Institute of Technology, Newark, NJ.

McKeen, R.G. and D.J Hamburg. 1981. "Characterization of Expansive Soils," Trans. Res. Rec. 790, Trans. Res. Board 73-78.

Mitchell, J.D. 1993. Fundamentals of Soil Behavior. John Wiley and Sons, New York, NY.

Mitchell, J.K. 1973a. "Recent Advances in the Understanding of the Influences of Mineralogy and Pore Solution Chemistry on the Swelling and Stability of Clays," *Proceedings of the Third International Conference on Expansive Soils*, Haifa, Israel, July 30-August 1, Israel Society of Soil Mechanics and Foundation Engineering.

Mitchell, J.K. (Chairman). 1973b. "Swelling Potential," General Report and Discussion, *Proceedings of the Third International Conference on Expansive Soils*, Haifa, Israel, July 30-August 1, Israel Society of Soil Mechanics and Foundation Engineering.

Morgenstern, N.R. and B.I. Balasubramonian. 1980. "Effects of Pore Fluid on the Swelling of Clay-Shale," *Proceedings of the Fourth International Conference on Expansive Soils*, June 16-18, Denver, CO. American Society of Civil Engineers, New York, NY.

REFERENCES
(Continued)

Muskat, M. 1946. The Flow of Homogenous Fluids Through Porous Media. J.W. Edwards, Inc., Ann Arbor, MI.

Nautiyal, D. 1994. "Fluid Flow Modeling for Pneumatically Fractured Formations," M.S. Thesis, Department of Civil and Environmental Engineering, New Jersey Institute of Technology, Newark, NJ.

Nelson, J.D. and D.J. Miller. 1992. Expansive Soils: Problems and Practice in Foundation and Pavement Engineering. John Wiley and Sons, New York, NY.

Newman, A.C.D., ed. 1987. Chemistry of Clays and Clay Minerals. Mineralogical Society Monograph No. 6, John Wiley and Sons, New York, NY.

Ng, N. 1991. "Enhancement of Air Flow and Contaminant Removal in Fractured Soil," M.S. Project, Department of Civil and Environmental Engineering, New Jersey Institute of Technology, Newark, NJ.

NJIT (New Jersey Institute of Technology) and ARS (Accutech Remedial Systems). 1994. "Integration of Pneumatic Fracturing with In Situ Vitrification-DOE Hanford Facility," for Battelle Pacific Northwest Laboratories, Richland, WA.

Odell, R.T., Thronburn, T.H., and L. McKenzie. 1960. "Relationships of Atterberg Limits to Some Other Properties of Illinois Soils," *Proceedings of the Soil Science Society of America*, 24(5): 297-300.

Page, A.L, Miller, R.H., and D.R. Keeney (eds.). 1986. Methods of Soil Analysis, 2nd edition, Parts 1 and 2, Agronomy 9, American Society of Agronomy, Soil Science Society of America, Madison, WI.

Papanicolaou, P. 1989. "Laboratory Model Studies of Pneumatic Fracturing of Soils to Remove Volatile Organic Compounds," M.S. Thesis, Department of Civil and Environmental Engineering, New Jersey Institute of Technology, Newark, NJ.

Park, J., Edil, T.B., and P.M. Berthouex. 1991. "Transport of Volatile Organic Compounds through a Clay Liner," *Proceedings of the 1991 Specialty Conference on Environmental Engineering*, Reno, NV, ASCE, New York, NY.

Pearring, J.R. 1963. "A Study of Basic Mineralogical, Physical-Chemical, and Engineering Index Properties of Laterite Soils," Ph.D. Dissertation, Texas A&M University, College Station, TX.

REFERENCES
(Continued)

Rahman, A.M. 1994. "Integration of Surfactants and Time Release Nutrients with Pneumatic Fracturing Process," M.S. Thesis, Department of Civil and Environmental Engineering, New Jersey Institute of Technology, Newark, NJ.

Raman, V. 1967. "Identification of Expansive Soils from the Plasticity Index and the Shrinkage Index Data," *Indian Engineering*, Calcutta 11(1):17-22.

Ranganatham, B.V. and B. Satyanarayana. 1965. "A Rational Method of Predicting Swelling Potential for Compacted Expansive Clays," *Proceedings of the 6th International Conference of Soil Mechanics Foundation Engineering*, 1:92-96.

Rebhun, M., Kalabo, R., Grossman, L., Manka, J. and Ch. Rav-Acha. 1992. "Sorption of Organics on Clay and Synthetic Humic-Clay Complexes Simulating Aquifer Processes," *Water Research*, 26(1):79-84.

Rhoades, J.D. 1982. "Soluble salts," in Methods of Soil Analysis, Agronomy No. 9, Chapter 10, Part 2, 2nd edition, American Society of Agronomy, Madison, WI, pp. 167-179.

Rubin, D.K. and M.B. Powers. 1994. "Congress and Regulators Prepare to Chew on a Plateful of New Rules," *Engineering News Record*, Feb. 21:32-33.

Schuring, J. and P. Chan. 1992. "Removal of Contaminants from the Vadose Zone by Pneumatic Fracturing," U.S. Geological Survey, Department of the Interior, U.S.G.S. Award 14-08-0001-G1739.

Schuring, J., Jurka, V., and P. Chan. 1991. "Pneumatic Fracturing of a Clay Formation to Enhance Removal of VOCs," *Proceedings of the Fourteenth Annual Madison Waste Conference*, University of Wisconsin, Madison, WI.

Seed, H.B., Woodward, R.J., and R. Lungren. 1962. "Prediction of Swelling Potential for Compacted Clays," *Journal of Soil Mechanics Foundation Division*, American Society of Civil Engineering, 88(SM3):53-87.

Shah, N.P. 1991. "Study of Pneumatic Fracturing to Enhance Vapor Extraction of the Vadose Zone," M.S. Thesis, Department of Civil and Environmental Engineering, New Jersey Institute of Technology, Newark, NJ.

REFERENCES
(Continued)

Sharp, J.S. and Y.N.T. Miani. 1972. "Fundamental Consideration of the Hydraulic Characteristics of Joints in Rock," *Proceedings of the Symposium on Percolation Through Fissured Rock*, International Society for Rock Mechanics and International Association of Engineering Geology, T1-F.

Skempton, A.W. 1953. "The Colloidal Activity of Clay," Proceedings of the Third International Conference on Soil Mechanics. *Foundation Engineering*, 1: 57-61.

Snethen, D.R., Johnson, L.D., and D.M. Patrick. 1977. "An Evaluation of Expedient Methodology for Identification of Potentially Expansive Soils," Soils and Pavement Lab, U.S. Army Corps of Engineers, Waterways Experimental States, Vicksburg, MS, and Report No. FHWA-RE-77-94.

Snow, D.T. 1965. "A Parallel Plate Model of Permeable Fractured Media," Ph.D. Dissertation, University of California, Berkeley, CA.

Soil Science Society of America. 1977. "Minerals in Soil Environments," Surface and Colloid Chemistry, Soil Science Society of America, p.44.

Sposito, G. 1989. The Chemistry of Soils. Oxford University Press, New York, NY.

Stockmeyer, M.R. 1991. "Adsorption of Organic Compounds on Organophilic Bentonites," *Applied Clay Science*, 6(1):39-57.

Storey, J.M.E. and J.J. Peirce. 1989. "Influence of Changes in Methanol Concentration on Clay Particle Interactions," *Canadian Geotechnical Journal*, 26(1):57-63.

Sudo, T., Shimoda, S., Yotsumoto, H., S. Aita. 1981. Electron Micrographs of Clay Minerals, Developments of Sedimentology, 31, Elsevier Scientific Publication, New York, NY.

Sullivan, R.R. and K.L. Hertel. 1940. "The Flow of Air Through Porous Media," *Journal of Applied Physics*, 11:761-765.

Tan, K.H., Hajek, B.F., and I. Barshad. 1986. "Thermal Analysis Techniques," in Methods of Soil Analysis, Chapter 7, Agronomy No. 9, Part 1, 2nd edition, American Society of Agronomy, Madison, WI.

Thomas, G.W. 1967. "Problems Encountered in Soil Testing Methods," in Soil Testing and Plant Analysis, Part I. Soil Science Society of America Special Publication No. 2, Madison, WI.

REFERENCES
(Continued)

Thomson, S. and P. Ali. 1969. "A Laboratory Study of the Swelling Properties of Sodium and Calcium Modifications of Lake Edmonton Clay," *Proceedings of the Second International Conference on Expansive Soils*, Texas A & M University, Austin, TX.

Tourtelot, H.A. 1973. "Geologic Origin and Distribution of Swelling Clays," *in Proceedings of Workshop on Expansive Clays and Shales in Highway Design and Construction*, D.R. Lamb and S.J. Hanna (eds.), Federal Highway Administration, Washington, D.C.

Wall, G.J., Wilding, L.P. and R.H. Miller. 1974. "Biological Transformations of Clay-sized Sediments in Simulated Aquatic Environments," *Proceedings of the 7th Conference of Great Lakes Res.*, pp. 207-211.

Whittig, L.D. and W.R. Allardice. 1986. "X-Ray Diffraction Techniques," in Methods of Soil Analysis, Chapter 12, Agronomy No. 9, Part 1, 2nd ed., American Society of Agronomy, Madison, WI.

Wiegner, G. 1935. "Ionenumtausch und Struktur," *Transactions of the 3rd Internatl. Congr. Soil Sci.*, Oxford, 3:5-28.

Williams, A.A.B. and J.T. Pidgeon. 1983. "Evapotranspiration and Heaving Clays in South Africa," *Geotechnique*, 23(2):141-150.

Wilson, C.R. and P.A. Witherspoon. 1970. "An Investigation of Laminar Flow in Fractured Porous Rocks," Pub. 70-6, Department of Civil Engineering, University of California, Berkeley, CA.

Wright, P.J. 1973. "Slurry Pressure Injection Tames Expansive Clays," ASCE, *Civil Engineering*, October.

Yoder, E.J., and M.W. Witczak. 1975. Principles of Pavement Design, 2nd ed., John Wiley and Sons, New York, NY.

Ziegler, T.W. 1976. "Determination of Rock Mass Permeability," Technical Report S-76-2, U.S. Army Corps of Engineers, Waterways Experiment Station, Vicksburg, MS.